Stony Brook University

Advanced Laser Patterning of a Cylindrical Sample

A Thesis Presented

by

David Hubert

to

The Graduate School

in Partial Fulfillment of the

Requirements

for the Degree of

Master of Science

in

Mechanical Engineering

Stony Brook University

May 2012

Stony Brook University

The Graduate School

David Hubert

We, the thesis committee for the above candidate for the
Master of Science degree, hereby recommend
acceptance of this thesis.

Dr. David J. Hwang
Assistant Professor, Department of Mechanical Engineering

Dr. Jon Longtin
Associate Professor, Department of Mechanical Engineering

Dr. John Kincaid
Professor, Department of Mechanical Engineering

This thesis is accepted by the Graduate School

Charles Taber
Interim Dean of the Graduate School

Abstract of the Thesis

Advanced Laser Patterning of a Cylindrical Sample

by

David Hubert

Master of Science

in

Mechanical Engineering

Stony Brook University

2012

The function of this thesis is the implementation of a four axis motion system to an Infrared Laser for micromachining applications. The ultimate goal of this project is to assemble a system that allows a user to create a two dimensional pattern that is then processed onto a cylindrical surface by means of a focused laser spot with adjustable speed and radiation source control. This generated system will then be used to examine the interaction between the laser and the material based on different laser powers, frequencies and processing speeds. This interaction will be examined on the surface of the cylinder.

This thesis is intended to provide some fundamental knowledge of various types of laser based processing utilizing a four axis motion control system. It will also convey the methodology used during the development of the controls system programming for various patterns.

The project began with a four axis motion system (X, Y, Z, and Theta axes) that is designed and manufactured by Rockwell Automation. Setting up the controllers and programming the system are outlined as well as the design specifications of the system. Modifications were made to facilitate laser processing and the methodology of patterning is discussed.

Parametric analysis of various frequencies, powers, processing speeds and feature transfer via roller printing to a soft polymer were examined as well as experimentation involving propelled gas to see if there is an improvement in surface patterning. Proprietary samples were also patterned to determine the best processing specifications. Spectrum analyses of various elemental samples were analyzing using laser induced breakdown spectroscopy and the direction of plasma generation based on the incident angle of the processing laser was examined.

1 Table of Contents

List of Figures

List of Abbreviations

I/O	Input/Output
ONS	One-shot
IR	Infrared
LIBS	Laser-Induced Breakdown Spectroscopy
m	Meters
mm	Millimeters
μm	Micron
nm	Nanometers
W	Watt
SEM	Scanning Electron Microscope

Acknowledgments

I acknowledge my thanks to the following professors for their help and guidance for my Master's Thesis

Thesis Advisor:

Dr. David J. Hwang- Department of Mechanical Engineering, Stony Brook University

Committee Members:

Dr. Jon Longtin- Department of Mechanical Engineering, Stony Brook University

Dr. John Kincaid- Department of Mechanical Engineering, Stony Brook University

I acknowledge my thanks to the following students for their help and guidance for my Master's Thesis

Di Liu

Tao Zhang

Michael Palazzolo

Matthew Quigley

Special Thanks to:

Rockwell Automation

Advanced Energy Research and Technology Center

Center for Thermal Spray Research

YucoOptics

Brookhaven National Laboratory

Dr. Noah D. Machtay- Department of Mechanical Engineering, Stony Brook University

Dr. Sanjay Sampath- Department of Material Science and Engineering, Stony Brook University

1. Introduction

This chapter is intended to introduce some concepts and systems that were used in the development in this paper as well as some background information as to why this research is useful.

1.1 Context

The phrase “four axis motion system” refers to the number of degrees of freedom the system is able to move. This arrangement allows for motion in the X-Direction, the length dimension; Y-Direction, the width dimension; Z-Direction, the height dimension; and the Theta-Direction, or rotational dimension. These degrees of freedom allow the programmer to create unique paths that can then be processed onto flat specimens, or using more clever programming, onto cylindrical or other three-dimensional shapes. The degrees of freedom for the system are shown below in Figure 1-1.

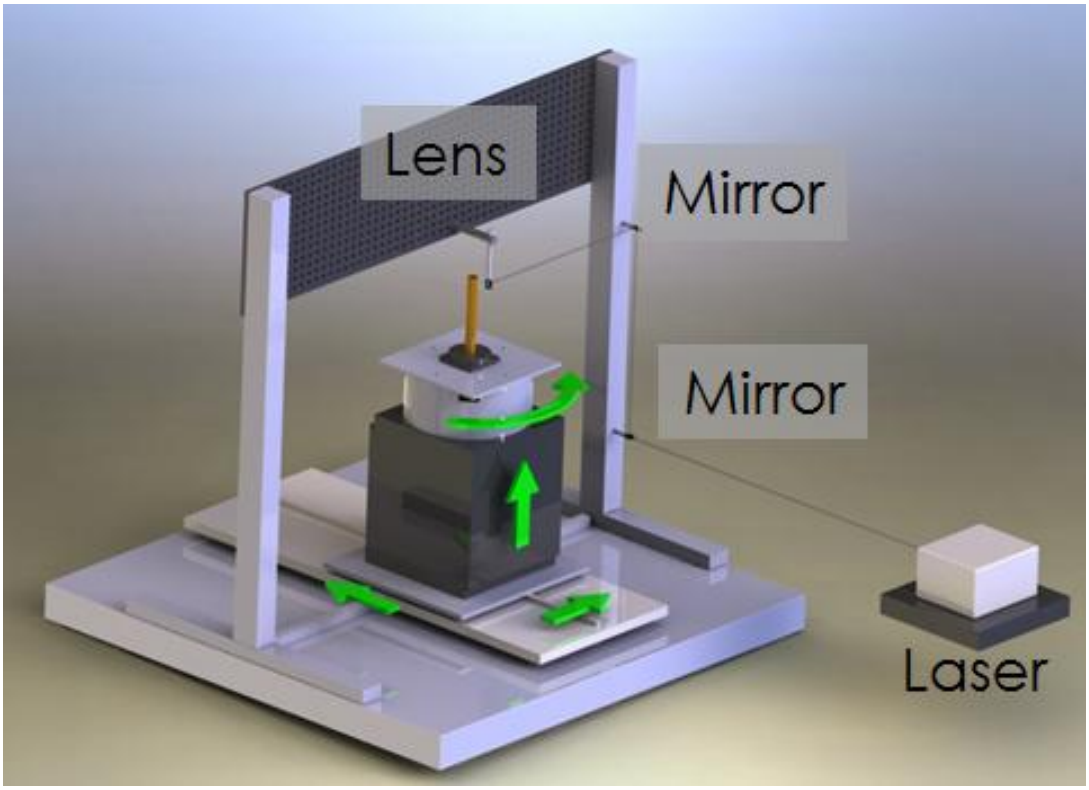

Figure 1-1: Motorized XYZΘ Stage

Two dimensional processing applications have been in use in hundreds of applications for years now. These applications include but are not limited to medical, military, industrial, and communications. A technique called “Galvanometric Scanning” is widely used in these processing applications but can be vastly improved. Currently, this technique processes the pattern in a step and repeat manner. A single, two-dimensional pattern will be created on a specimen, once completed, a new specimen is

loaded and the process beings again. This thesis intends to test the practicality of laser patterning on a cylinder. Potentially, this cylinder can be used as a roller to transfer the pattern onto a flat specimen. This would drastically cut down on the processing time and allow small scale patterning to be created on a much larger scale at a lower cost.

There is an intrinsic similarity between flat plate processing and the cylindrical processing to be described. Flat plate processing takes place in two dimensions; generally the x and y directions. Although a rounded surface is typically harder to machine due to the radius of curvature, this system allows for an ease of processing using the same concepts derived from flat plate processing. Figure shows the relationship between flat plate samples and cylindrical samples.

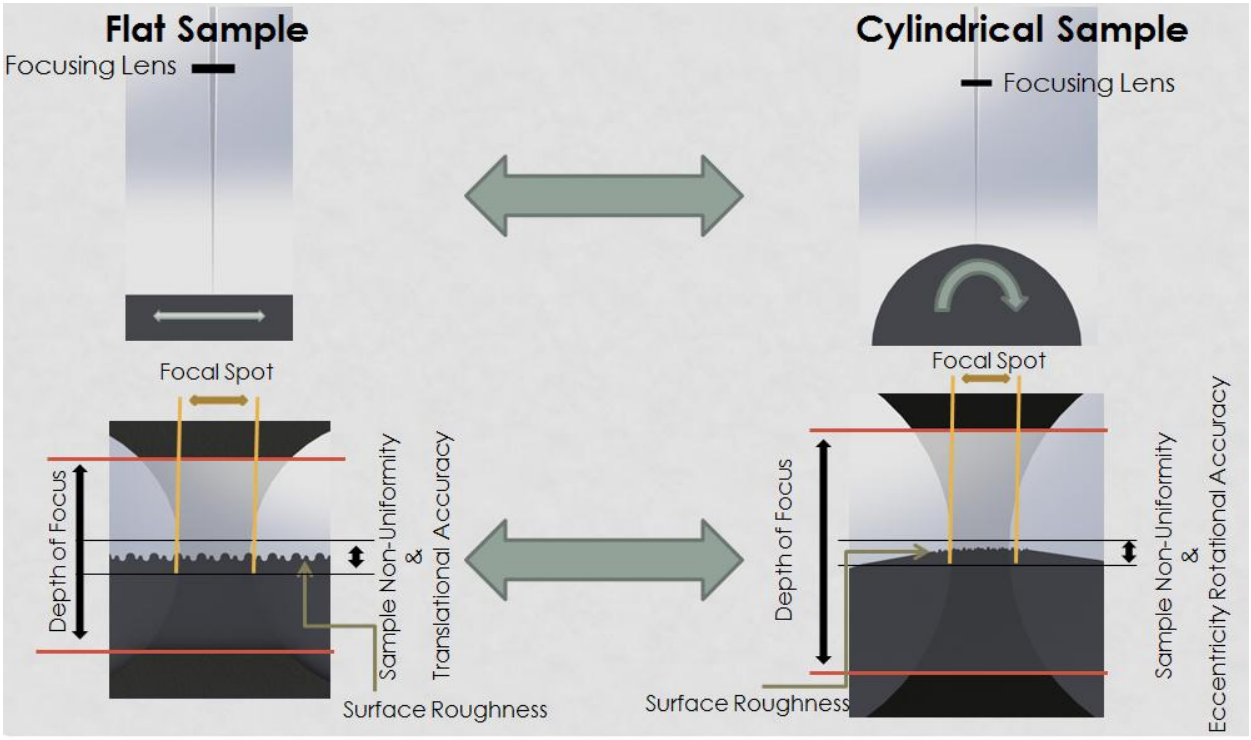

Figure 1-2: Flat Plate to Cylindrical Sample Relationship

Cylindrical processing can be accomplished by means of the same simple techniques used for flat plate processing, two axis motion. However; the difference is that the two axis of motion to be controlled for cylindrical processing will be the vertical axis, Z, and the rotational axis, theta as shown in Figure 1-3. With the system properly aligned, the processing on the rotational axis will essentially process a cylindrical sample as a flat sample provided the focal spot is small with respect to the radius of curvature. This allows for a point source assumption to be used provided the depth of focus is maintained with sample non-uniformity and surface variations. The process surface will always be perpendicular to the machining tool, in this case an IR Laser. This is a simple yet elegant solution to processing an unconventional specimen by means of a well know, practiced machining process.

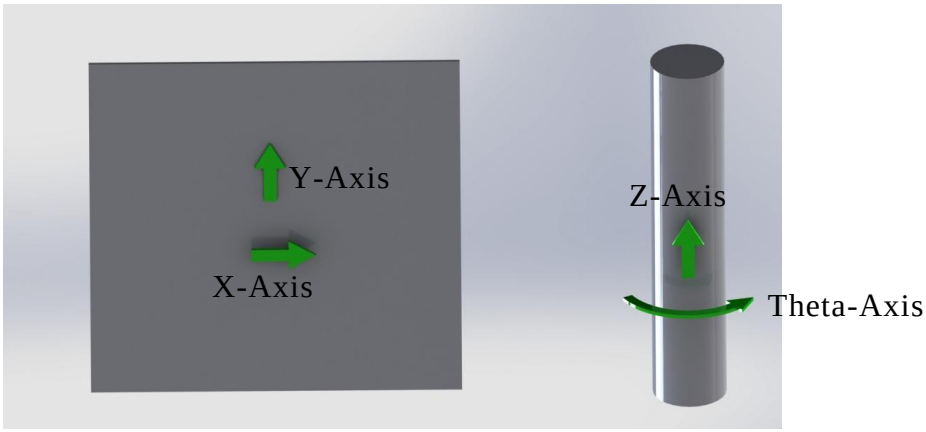

Figure 1-3: Two Axis Patterning; Flat Specimen to Cylindrical Specimen

This thesis utilizes an infrared laser to process a cylindrical surface by coupling it with a four axis precision motion system to test the validity of micro scale patterning at various speeds, frequencies and powers, and the transmission of patterns to a flat specimen. A proprietary thermal spray sample provided by the Center for Thermal Spray Research was also processed. Next, the spectrum of visible light emitted from the location of laser-material interaction was analyzed using a method called Laser-Induced Breakdown Spectroscopy. The direction of plasma generation based on the incident angle of the processing laser was also analyzed and finally, a flat sample was processed for imaging using a scanning electron microscope.

Chapter 2 begins with the basics of laser processing and scanning, the fundamentals of generating laser radiation, laser pulses, and the cardinal beam parameters. Laser beam induced material reactions as well as the concept of laser induced breakdown spectroscopy will be discussed. Chapter 3 discusses the architecture of the four axis motion system as well as the details of the motion system will be examined. This includes an overview of the system as well as all of the hardware it is comprised of. An overview of the radiation sources with details of their interaction will follow.

Chapter 4 describes setting up the control system and software will then be introduced. This includes information on the loading of the controllers and methodology used to create programs for a variety of patterns. System issues followed by a description and explanation of the patterning techniques that were explored were illustrated. Chapter 5 describes the preparation of the experimental setup and one of the most crucial processes, the indication of the cylinder. Indication of the cylinder ensured eccentricity which would guarantee the laser beam would be focused on the various surfaces to be machined.

A total of eleven separate experiments were performed, including parametric analysis on power, speed, and frequency variation. Testing the feasibility of a pattern transfer from a cylindrical sample to a soft polymer was explored next then followed by the processing of a proprietary coating. Experimentation concluded with LIBS analysis, plasma generation studies and SEM imaging of flat samples. Chapter 6 describes future applications whereas Chapter 7 summarizes the findings of this thesis.

1.2 Motivation/Objective

The motivation for this project was to overcome the conventional limitations of the current technology. Current technology such as Nano-imprint lithograph and soft lithography are very complex methods used to achieve features on a cylindrical surface. Soft lithography and 3D lithography are also limited in achievable resolutions.

The improvement of cylindrical patterning is the desirable outcome of this thesis. This includes but is not limited to an increase in quality, accuracy, resolution, and a decrease in complexity. Testing new applications such as thermo-electric devices and multi-layered thin film samples are also motivating factors in this research.

The objectives of this thesis are the establishment of the base test platform. This includes the programming of the motion system and the facilitation of laser processing. The next objective is an improvement strategy for ablative patterning. This includes parametric design and study of various laser parameters such as power, and frequency, in addition to variations in processing speed, the processed material and finally, the introduction of a compressed gas.

Another objective is to understand the relevant plasma physics for quality and accuracy improvement. This includes understanding the basics of plasma generation, and how laser-plasma interaction and the incident angle of the laser beam can affect the processing quality. This thesis would also test an application of cylindrical processing. This application will test pattern transfer via imprinting process. The final objective is to understand the requirements necessary for higher resolution processing.

2 Fundamentals

This chapter touches on the fundamentals of laser optics and the interaction between the laser and the material it is processing.

2.1 Principles of Laser Optics

This section provides an introduction to laser physics, the modes of operation of a laser, and finally, beam characteristics.

2.1.1 An Introduction to Laser Physics

LASER is an acronym for Light Amplification by Stimulated Emission of Radiation. The physical fundamentals of this phenomenon were found in 1916 by none other than Albert Einstein; however, the first laser was not built until 1960. A laser must be an intense source of electromagnetic radiation in order to separate the lasers inherent radiation from the normal sources of light. According to its design, a laser emits at one or more wavelength in the spectrum. However, it is essentially considered to be a monochromatic device meaning all of the colors produced are of a single hue. A lasers radiation is also intended to maintain a fixed phase relationship, or coherence, and show a small divergence. It is also possible to produce ultra-short pulses with Laser radiation sources.

We will consider light as electromagnetic radiation that is described as a wave. This wave consists of both an electric field vector and magnetic field vector as shown in Figure 2-1. The amplitudes of the electric field and magnetic field vectors are orthogonal to one another. The polarization or the orientation of oscillation of the electromagnetic wave is determined by their respective amplitudes as well as the phase of both components. To be linearly polarized requires that the magnetic and electric fields both be in phase. The direction of the resulting wave, which is the sum of both components, is conditioned by the amplitudes. If the phase difference between the electric and magnetic field equals ninety degrees and they are of equal amplitudes, the electromagnetic wave is said to be circularly polarized. In all other cases, it is elliptically polarized. Figure 2-1shows a linearly polarized electromagnetic wave.

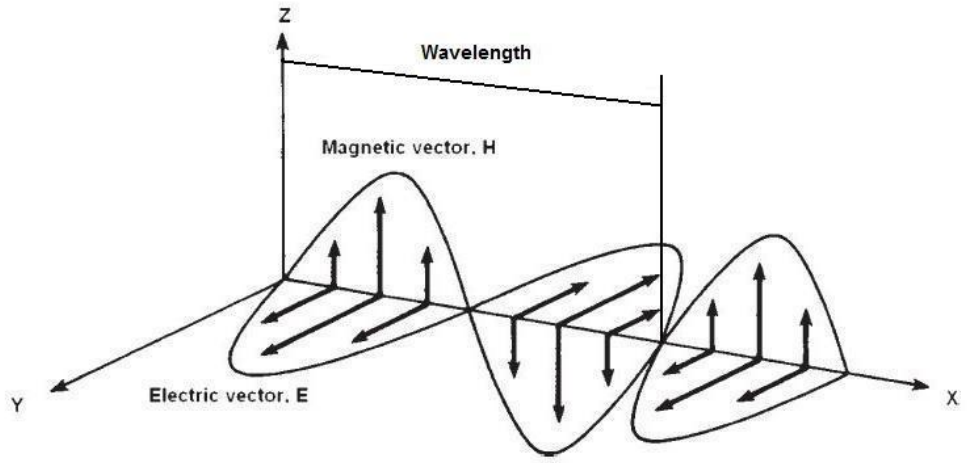

Figure 2-1: Electromagnetic Wave[1]

The speed of light, *c,* ($2.9979\times10^{8}\frac{m}{s}$ in a vacuum) links the frequency, *f,* and the wavelength, λ as illustrated in Equation 2-1.

Equation 2-1

$$c = f\lambda$$

However, quantum theory describes light as a stream of photons that are moving at light speed velocity. Without this interpretation, the wave theory fails to describe crucial physical phenomenon. This phenomenon is called the photoelectric effect which states each photon carries energy that is proportional to its frequency as shown in Equation 2-2 where *h* is the Planck factor ($h = 6.63\times10^{-34}\frac{J}{s}$.)

Equation 2-2

$$E = hf$$

As stated in the preceding paragraphs, electromagnetic radiation has been described as both a particle, and a wave. This is known as Wave-Particle duality which postulates that classical concepts such as a “Particle” and “Wave” are unable to sufficiently describe the behavior of quantum-scale objects.

Using quantum theoretical terminology for explaining material and atom interaction with light, photons can be absorbed, spontaneously emitted and emitted with stimulation which is the essential process of laser activity.

Assume a two energy level atom that follows the properties of the Bohr Model with the ground energy level being E_0 and the excited energy level being E_1. An interacting photon that interacts with the aforementioned two energy level atom can raise said atom to its excited level if it meets the Bohr Equation as given in Equation 2-3. This process is called absorption.

Equation 2-3

$$E_1 - E_0 = hf_{12}$$

Spontaneous emission occurs when an excited atom with energy level E_1 drops down to energy level E_0 by releasing a photon with frequency f_{12}. The emitted photons direction is stochastic or random. Just because an atom is excited does not necessarily mean it emits a photon in a stochastic process. It has the ability to do so in stimulated emission if a photon meeting the Bohr Equation hits the excited atom and triggers said atom to emit a photon with the same phase, frequency and direction. Hence, the desired process in a laser medium which amplifies incoming light, known as stimulated emission, is the reversal process of absorption.[1]

In a medium which consists of only two energy level atoms, stimulated emission will be the dominant process if the majority of these atoms are in energy level E_1. This condition, known as population inversion, is a necessary process for stimulated emission. In the case in which energy level E_0 accounts for the majority of the atoms, net absorption will be predominant and there would be no light amplification. For a material that is in thermal equilibrium, the distribution of atoms in various energy states is given by the Boltzmann Distribution law. This is shown in Equation 2-4.

Equation 2-4

$$N_1 = N_0 \exp\left[\frac{-(E_1 - E_0)}{kT}\right]$$

In Equation 2-4, N_1 and N_0 are the atom densities in the respective energy states E_1 and E_0. T is the absolute temperature and k is the Boltzmann Constant. The Boltzmann distribution law states that the higher energy level is less populated. The population of atoms in this higher energy state will decrease exponentially with increasing energy. As the temperature approaches infinity $(T \to \infty)$ the atom densities of the two energy states will be equal $(N_1 = N_0)$. For negative absolute temperatures, the excited energy levels density will be greater than the unexcited energy levels density $(N_1 > N_0)$. Therefore, it is practically impossible to utilize a two state system in thermal equilibrium as a laser medium due to the fact that population inversion cannot be achieved and without population inversion, it is impossible to achieve stimulated emission.

Generally, a three or four energy state levels is necessary to achieve population inversion. Therefore, we define E_2 and E_3 as the third and fourth energy levels. This means a three energy state will include energy levels E_0, E_1 and E_2 whereas a four energy state will include E_0, E_1, E_2 and E_3. Pumping is a technique used to reach population inversion in one of the aforementioned assumed systems. This method involves the insertion of energy into an unstable upper energy level which causes the upper level laser energy level to decay while emitting zero radiation. For this to work, the lifetime of the unstable upper energy level must be less than that of the excited upper laser level. A high ratio of the laser medium being excited into the upper laser level is possible with pumping. In a three energy state system, population inversion occurs between the first and second energy level (E_0 and E_1 respectively) by pumping the medium to the third energy level which is unstable (E_2.)

In a four state system, the laser activity occurs between energy level three to two (E_2 and E_1 respectively.) A radiation free transfer of energy occurs from the pump level, E_3, to energy level E_2. The lower laser energy level E_1 transitions in a radiation free process to the ground level E_0. A four energy state laser is advantageous because less

pump energy is required. This is because the lower laser energy level is less populated than in a three energy state laser.[2]Figure 2-2 shows the laser transition for both a three state system and a four state system.

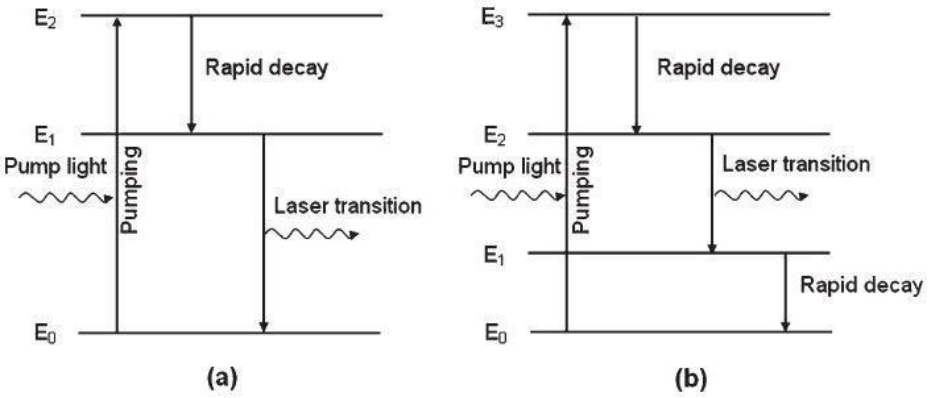

Figure 2-2: Laser Transition in a (a) Three State System and a (b) Four State System[1]

A typical simple laser contains a resonant cavity. This cavity consists of a set of well aligned, highly reflective mirrors at either end, oriented perpendicular to the cavity axis. The active laser material is then placed between these mirrors. Generally, one of the mirrors is fully reflective, with its reflectivity close to 100%. However, the other mirror, which is an output coupler, enables some transmission to allow the laser output to emerge. Pump energy is typically supplied as light at a different wavelength or as an electric current which can be provided by another laser, or a flash lamp. In an active laser, photons travel back and forth in the active laser medium in accordance with the Bohr Equation of laser transmission. These photons are amplified by triggering a stimulated emission and a certain amount emerges through the output coupler as laser radiation. A schematic of a resonant cavity is shown in Figure 2-3.

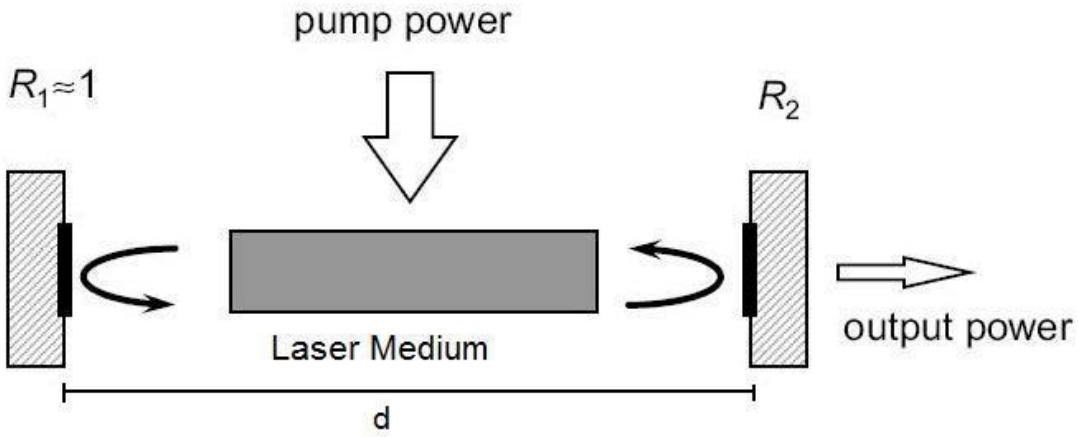

Figure 2-3: Laser Cavity[1]

The distance; *d*, between the two mirrors of the resonant cavity is a crucial parameter. This length determines which longitudinal modes can develop within the cavity. Longitudinal modes are standing waves, which meet Equation 2-5 where *n* is an integer.

Equation 2-5

$$d = \frac{n\lambda}{2}$$

These discrete frequencies are separated by $\frac{c}{2d}$. As previously stated, only photons that meet the Bohr equation of the laser medium are amplified during stimulated emission, this means that a laser only emits at one narrow wavelength. Realistically, the amplification of light within a laser is only possible at a specific bandwidth of frequencies. These frequencies relate to the particular laser medium. This bandwidth depends on the loss and gain characteristics of the resonant cavity in addition to the laser medium. Longitudinal modes and a gain characteristic example of a laser medium are shown below in Figure 2-4.

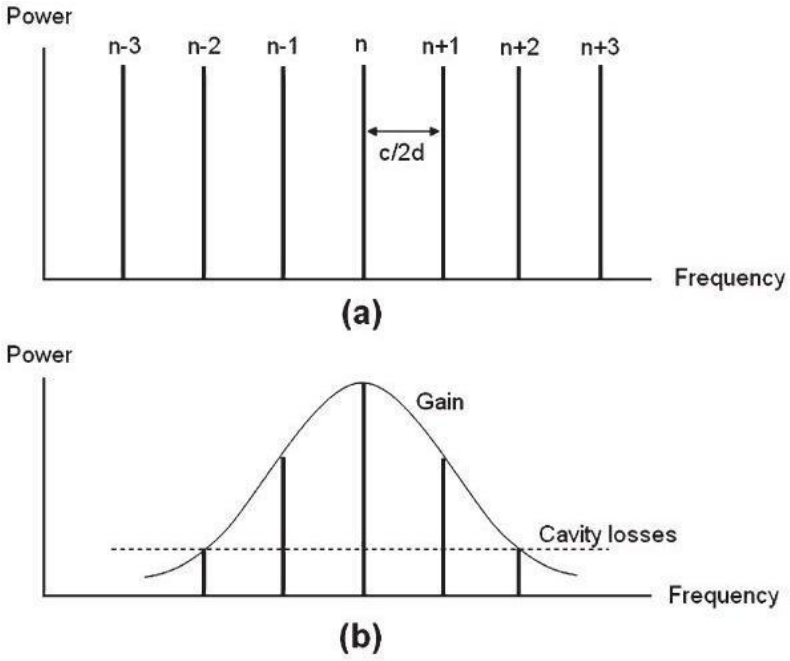

Figure 2-4: (a) Longitudinal Modes (b) Gain Characteristics[1]

2.1.2 Operational Modes

Laser output can be of two forms, one which has constant amplitude and is known as a continuous wave or CW, or one with periodic amplitude which is called pulse operation. In continuous mode, the pump source maintains a constant laser power over time. In pulsed mode operation, the output of a laser varies with respect to time. This results in periods in which the laser is either emitting radiation or it is not. Figure 2-5 shows a graph for pulsed laser operation mode with respect to time.

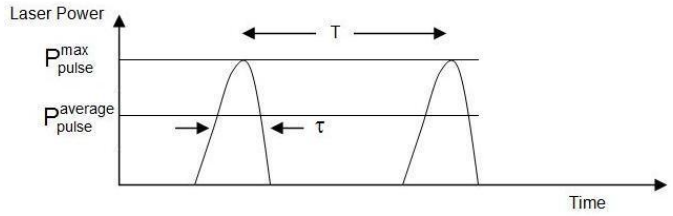

Figure 2-5: Pulsed Mode of Operation[1]

Important parameters of pulsed laser radiation are the peak power P^{Max}_{Pulse}, Average power P^{Avg}_{Pulse}, Pulse Length τ, repetition rate $\frac{1}{T}$, and the pulse energy. The first of many methods to achieve pulse laser radiation is called Pulsed Pumping. This is done by varying the pump energy over time. If the pump energy exceeds the laser activity threshold only for certain time periods, pulsed laser operation will occur. The time duration of the emitted laser pulses using this method are on the order of microseconds.

Pulse lengths on the order of picoseconds can be achieved via Q-Switching. Q-Switching changes the Q value of the cavity which results in short and intense pulses of laser radiation. The Q-Value of a cavity is indicative of the cavities ability to store radiation energy in the absence of laser activity. A high Q value leads to energy storage in the cavity without significant laser radiation. This leads to the development of a large population inversion. Changing the Q value from high to low results in the emergence of the stored energy as short and intense laser beam pulses, this occurs because the process of optical amplification is no longer prevented.

Essentially, Q-Switching involves "switching" the resonant Q value from a high Q, where the high energy is stored without the presence of laser radiation and once this energy reaches is maximum value, the Q value is dropped which allows for the creation of short, high intensity laser pulses. This emission of laser radiation decreases the population inversion within the cavity to a point in which the Q value will be re-adjusted to a high value, thus restarting the process. Electro-optical Q-Switching, Acousto-Optic Q-Switching, passive Q-Switching, and the rotating mirror method are some of the various methods of Q-Switching [1]

Mode locking technique can generate ultra-short laser pulses on the order of femtoseconds. By inducing a fixed phase relationship between longitudinal modes of lasers resonant cavity, the spectrum of frequency components of a laser radiation source can be used to create ultra-short laser pulses. Laser light is produced as pulses because the fixed phase relationship initiates controlled interference effects between the modes. Further pulse compression and amplification can be achieved by the chirped pulse amplification method, which is based on grooved surfaces called diffraction gratings. These diffraction gratings stretch the ultra-short laser pulses to pulses with a longer duration, which enables them to be amplified to a much higher energy because stretching avoids damaging the optics after the pulse is amplified, an optical compressor reverses the laser pulse, thus producing a high intensity, ultra short laser pulse. [2]

2.1.3 Beam Characteristics

There are many important characterizing features of a laser beam, a few of which are the transverse dimensions of the beam, the beam spot size and the beams propagation behavior. Lasers emit beams in a variety of characteristic patterns or transverse modes. These modes can occur as a pure, single mode, or as a mixture of several superposed pure modes. In a pure mode, the transverse irradiance distribution or beam profile is the square of the electric field amplitude. If this beam has rectangular symmetry, it can be mathematically described as a Hermite Gaussian function whereas if it has a circular symmetry it will be described as a Laguerre function. The simplest mode TEM_{00}, also known as the fundamental mode is the lowest order or Gaussian Beam which consists of a single spot that can be described with a Laguerre Gaussian Function (Equation 2-6) due to its cylindrical symmetry.

Equation 2-6

$$I\left(\frac{r}{w_0}\right) = I_0 \exp\left[-2\left(\frac{r}{w}\right)^2\right]$$

$I\left[\frac{W}{m^2}\right]$ is the irradiance or intensity, I_0 is the peak irradiance and w is defined as the distance transverse to the beam axis at which the value for irradiance falls to $\frac{1}{e^2}$ or 13.5%. This w term is a common definition for the beam spot referred to as the Gaussian diameter with 2w. Peak irradiance is found by integrating Equation 2-6 over the transverse plane and equating it to the beam power P. The result is

Equation 2-7

$$I_0 = \frac{2P}{\pi w^2}$$

Figure 2-6 shows the irradiance distribution and the associated schematic beam spot for the fundamental mode transverse to its beam direction.

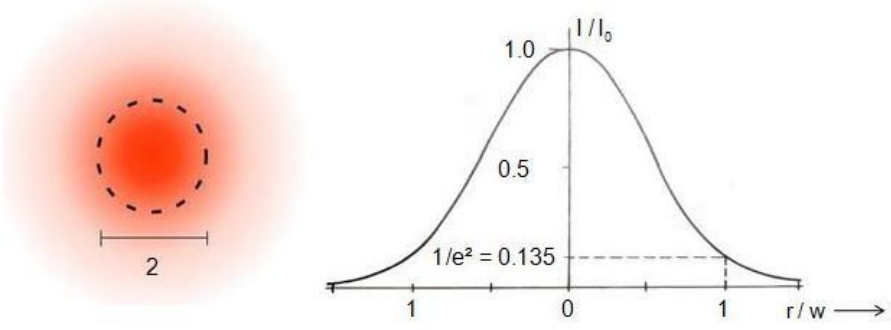

Figure 2-6: Fundamental Mode Distribution[1]

By solving the wave equation with diffraction, the propagation properties of this Gaussian beam can be outlined. However, since the calculation is difficult and extensive, the results will be presented without proof to aid in the characterization of the beam. The basic propagation property is that a laser beam which is a bundle of focused paraxial rays will converge to a finite minimum diameter w_0, the waist radius and diverges after passing its minimum radius. Figure 2-7 shows a schematic of a beam which is travelling through its minimum radius. The full angular spread Θ of the converging and diverging beam can be calculated using Equation 2-8.

Equation 2-8

$$\Theta = \frac{2\lambda}{\pi w_0}$$

The Rayleigh Length z_R, is another important parameter used in the characterization of laser beams. It is defined as the distance in beam direction from the waist radius to the beam radius of a width $\sqrt{2}w_0$. Equation 2-9 is the equation for the Rayleigh Length.

Equation 2-9

$$z_R = \frac{\pi w_0^2}{\lambda}$$

In Figure 2-7, the confocal parameter denoted by length *b* is twice the Rayleigh length. A Gaussian beam can be described by either the Rayleigh length or waist diameter because both parameters are in a fixed relationship for the Gaussian beam. [3]

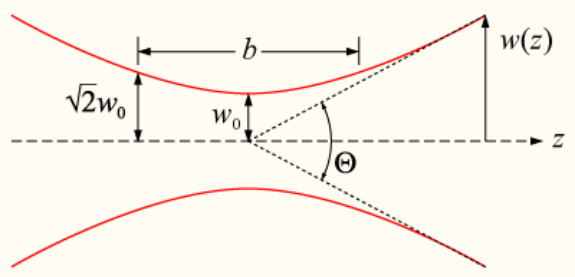

Figure 2-7: Beam Propagation and Rayleigh Length[1]

By passing the laser beam through a focusing lens, the waist diameter can be tightened. The resulting waist diameter is given by Equation 2-10.

Equation 2-10

$$w_1 = \frac{\lambda f}{\pi w_0}$$

w_1 is the smallest theoretically reachable waist diameter based on the incoming waist diameter w_0 , wavelength λ, and focal length *f*. Neglecting all other parameters, the smallest possible waist diameter is equal to the wavelength. Even though Equation 2-10 results in a theoretical value, this is still the most common approximation for the focused beam waist radius.

Most laser applications desire a small waist diameter and a long Rayleigh length. However, tight focusing of the waist diameter will lead to a decreasing value for the Rayleigh length. This creates a tradeoff. A small waist diameter will yield a high intensity and precision, a short Rayleigh length is disadvantageous in most real world applications. If a small Rayleigh length is assumed, improper focusing of the laser beam on a process surface will lead to a given displacement from the focus diameter. This focus diameter will lead to a bigger beam diameter and therefore to a bigger decrease of the beam intensity than what would occur given a larger Rayleigh length.

All of the aforementioned formulae are valid for the ideal Gaussian beam. However, each laser source in all real applications suffers from a variety of imperfections which means the theoretical modes are not reached. This defect can be accounted for with the factor "times diffraction limit" which is also called an M^2-Factor. This factor is an indicator for the quality of the beam. When this factor is equal to one is indicative of a beam in its fundamental mode. Generally, this value will be given by the lasers manufacturer; however, it can also be calculated using Equation 2-11 after measuring the waist radius and full angular spread.

Equation 2-11

$$M^2 = \frac{w_0 \Theta \pi}{2\lambda}$$

As the M^2value increases past one, the beam qualities are worse than that of the fundamental mode. Accounting for the beam quality, the formulas for the Rayleigh length and waist radius are given by Equation 2-12 and Equation 2-13.

Equation 2-12

$$z_R = \frac{\pi w_0^2}{\lambda M^2}$$

Equation 2-13

$$w_1 = \frac{\lambda f M^2}{\pi w_0}$$

A decrease in beam quality is caused by a bigger waist radius, bigger angular spread, and a shorter Rayleigh length. This will lead to an M^2-Factor greater than one.

2.2 Laser-Materials Interaction

This section discusses the interaction between the laser and materials to be processed. This includes energy transfer via absorption, the physical effects of irradiated materials and the benefits of ultra-short laser pulses for material processing.

2.2.1 Energy Transmission by means of Absorption

When a laser beam is incident on a materials surface, the electromagnetic radiation interacts with the electrons of the materials atoms. This is due to the fact that the frequency of said electromagnetic radiation in the ranges of laser light is too high to excite any other components of an atom. An electron that is excited by electromagnetic radiation is affected by a force F, v as the speed of the electron, c as the speed of light, E which is the amplitude of the electric field, and finally, H as the amplitude of the magnetic field. This relationship is given by Equation 2-14.

Equation 2-14

$$F = eE + \left(\frac{v}{c} H \right)$$

Since the speed of light is the fastest speed any object can travel, it is given that the velocity of the electron will be less than the speed of light, making $\frac{v}{c} < 1$. Assuming the magnitudes of the amplitudes of the electric and magnetic field vectors are equal, it is apparent that the electric field component is the more critical value in the examination of electromagnetic radiations interaction with electrons. The radiative energy transforms into kinetic energy of free electrons and into the excitation of bound electrons within the material. Over time, the degradation of these excited electrons leads to heat generation. Figure 2-8 is a schematic of various physical processes such as reflection, absorption, transmission and scattering caused by incident radiation on the macro scale.

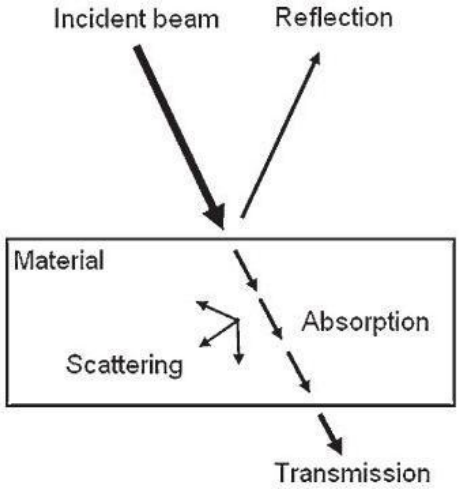

Figure 2-8: Reflection, Absorption, Scattering and Transmission[1]

The absorption of radiation is one of the most important and desirable phenomena that occur in the laser processing of materials. Absorption is basically the transmission of energy from the laser beam to the material. This can result in various effects such as plasma formation, heating, melting, and photo-ablation. These effects form the basis of a number of laser materials processing techniques.[4] The characterization of the electromagnetic radiation and the thermo-physical properties of the material are critical in describing the effects these processes. The Beer Lambert law describes absorption as the intensity attenuation of light travelling inside a material with I_0 as the incident intensity, I(z) as the intensity at a depth *z* and an absorption coefficient of μ. This relationship is given by Equation 2-15 below.

Equation 2-15

$$I(z) = I_0 e^{-\mu z}$$

The Beer Lambert law states that the intensity of laser radiation decreases exponentially inside of the material. The attenuation length or the depth of significant absorption is the reciprocal of the absorption coefficient. For materials that are highly absorbent, μ is in the range of $10^5 - 10^6 cm^{-1}$. Since the attenuation rate is the reciprocal of the absorption coefficient, this rate is within the range of $10^{-5} - 10^{-6} cm$.[5] Absorption, transmission and reflection are related such that when all three fractions are added together, they will always equal one. However; For opaque materials, transmission can be disregarded so the fraction of the incident beam intensity which get absorbed and reflected are given in Equation 2-16 where *A* and *R* are the values for absorptivity and reflectivity, respectively.

Equation 2-16

$$A + R = 1$$

Both the absorptivity and reflectivity are strong functions of temperature and wavelength. The factors complicate the calculation or estimation of these terms. The reflectivity of different medals with respect to wavelength and temperature are given below in Figure 2-9.

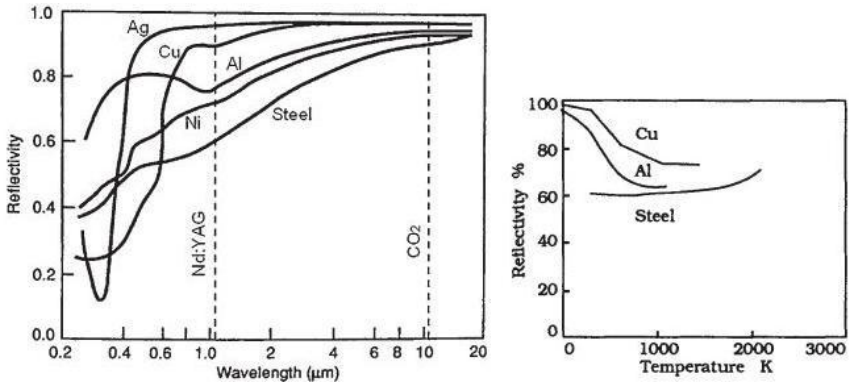

Figure 2-9: Reflectivity as a Function of Wavelength and Temperature[1]

Even though each metal has differing values for absorptivity and reflectivity based on their respective crystal and atomic structure, there is a general trend. As the wavelength increases, the reflectivity also increases, whereas when the temperature rises, the reflectivity will fall.

2.2.2 Physical Effects of Irradiated Material

A temperature distribution within the material is created when light energy is converted into heat energy and is subsequently conducted throughout the material. Based on the magnitude of the rise in temperature, various physical effects can occur. These include but are not limited to material heating, melting and vaporization. Furthermore, the ionization of vapor during the laser irradiation may lead to plasma generation and in addition to the thermal effects, the interaction between the laser and material can be associated with the photochemical processes such as photo-ablation. The aforementioned radiation induced material reactions are shown in Figure 2-10.

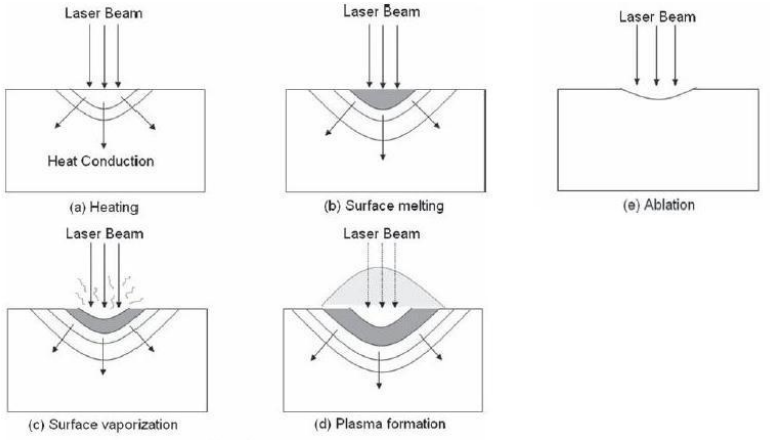

Figure 2-10: Various Laser Material Interactions[1]

A one dimensional equation for heat conduction can be used to approximate the temperature distribution on the laser irradiated process surface during heating. The assumptions are that the initial temperature is constant, the energy input is constant during irradiation, the material is uniform with temperature independent thermo physical properties, and energy losses from the surface are considered to be negligible. Following the stated assumptions, the equation for one dimensional heat transfer is given by Equation 2-17 where T is the temperature at a depth z after a time t with a thermal diffusivity α .

Equation 2-17

$$\frac{\delta T(z,t)}{\delta t} = \alpha \frac{\delta^2 T(z,t)}{\delta z^2}$$

With the initial temperature defined as T_0 the energy transfer from the laser beam at the material surface can be modeled as shown in Equation 2-18 below.

Equation 2-18

$$-k\frac{\delta T(0,t)}{\delta z} = \delta A I_0$$

The absorptivity *A* multiplied with the incident laser radiation I_0 is the absorbed laser energy. δ is a factor for either the time $0 \le t \le t_p$ where radiation hits the surface with t_p as the laser pulse length or zero for $t > t_p$ with no incident radiation, whereas *k* from the above equation is the coefficient of thermal conductivity. In solving these equations, formulae for the temperature with respect to time and depth (T(z,t)) during the time of radiation ($0 \le t \le t_p$) and after ($t > t_p$) are obtained. The proof of these formulae will be omitted; however, they can be viewed in the source.[1]

To investigate phase transformations, we will now utilize the basic discussion of laser induced heating. If the temperature of a beam with high intensity is incident on a materials surface and it exceeds the materials melting point, the material will transform to a liquid state. Determining the depth to which liquefaction occurs is an interesting prospect. Using the equations for one-dimension heat conduction where temperature is a function of depth and time, we will add the melting temperature as T_m. Figure 2-11 shows the surface temperature for a process in which the melting point is exceeded.

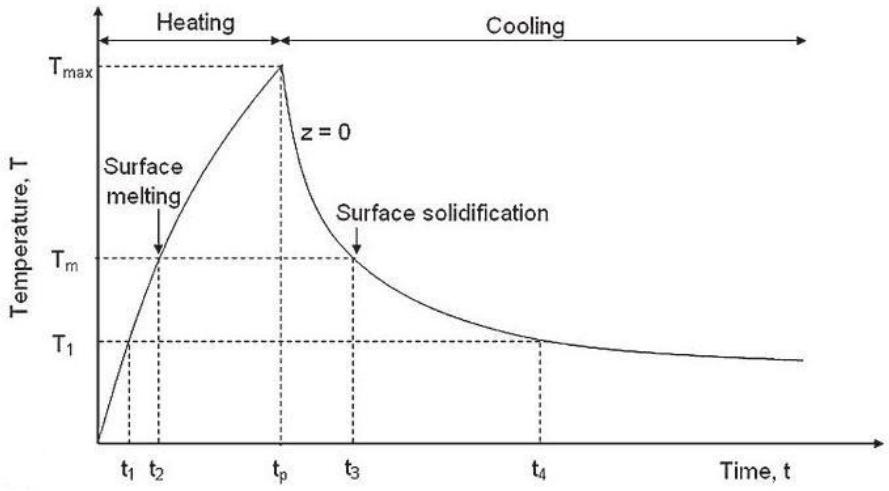

Figure 2-11: Surface Temperature Exceeding the Melting Point with Respect to Time[1]

For the case in which there is no phase change, the materials surface is irradiated for a pulse length t_p. The path of the temperature with respect to time will be similar to the temperature difference from time t_2 to t_3. Figure 2-12 shows the depth of liquefaction with respect to time by finding the depth z_m for each time in which the melting temperature is equal to the temperature at a depth z_m and time *t* ($T_m = T(z_m, t)$)

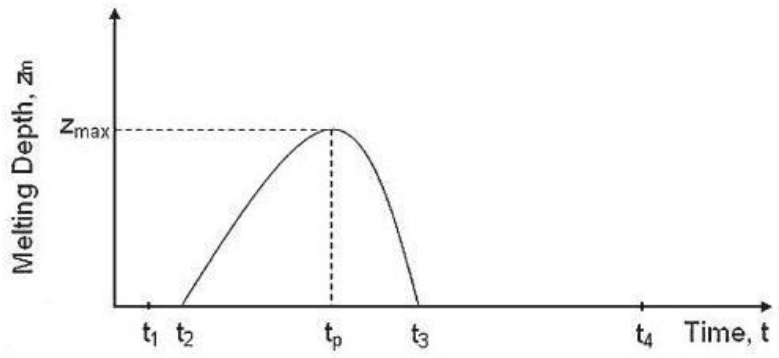

Figure 2-12: Depth of Liquefaction with Respect to Time[1]

The melting phase develops at the process surface at a time t_2 and will increase to its maximum depth z_{max} until time t_p in which case it begins to solidify until time t_3 where the material no longer has melted parts. Figure 2-12 not only illustrates the melting depth, it also indicates how long each depth will stay in a liquid state.

However, the depth of melting is limited by the vaporization of the material at the boiling point temperature. Evaporative material removal will occur before the depth of melting increases, this will occur before the surface temperature exceeds the boiling point. The depth consideration is useful for a laser welding process. Once the vaporization begins on the surface of the material, continuing laser irradiation will cause the liquid-vapor interface to move within the material. Also, it is accompanied by the evaporative material removal for the surface above this liquid-vapor interface. Assuming the energy transmitted via the laser beam is equal to the absorbed energy by the material, the speed of the liquid-vapor interface is given in Equation 2-19 where H_v is the latent heat of vaporization of the material, T_b is the boiling temperature of the material, ρ is the materials density and c_t is the specific heat capacity.

Equation 2-19

$$v_s = \frac{AI_0}{\rho(c_t T_b + H_v)}$$

The depth to which vaporization occurs can be calculated by multiplying the pulse length t_p with the speed v_s. The vapor plume that evolves on the surface consists of ions, molecules, clusters, atoms and electrons. This plume develops a recoil pressure on the materials surface which exceeds the maximum surface tension pressure. This leads to melt expulsion in the molten part. This means there are two processes in which material can be removed, either melt expulsion or surface evaporation. Both types of material removal are shown in Figure 2-13.At a low laser power, the dominating material removal process is melt expulsion, whereas at higher powers, melt expulsion rates decrease and surface evaporation continuously increases.

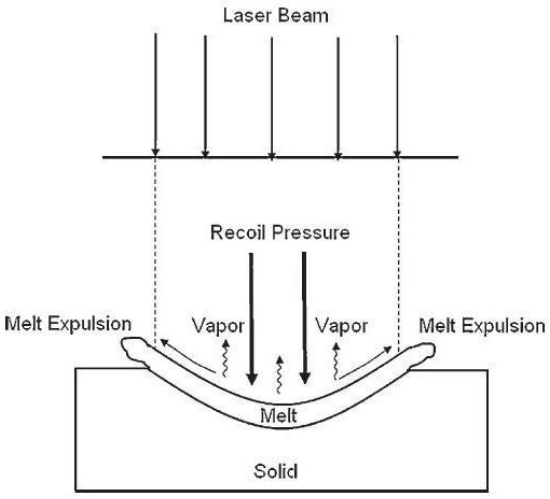

Figure 2-13: Material Removal as Melt Expulsion and Evaporation[1]

For high laser beam intensities, there is another factor that must be accounted for. The high intensity beam will cause a significant amount of surface evaporation which can interfere with the laser beam, so this laser beam-vapor interaction must be analyzed. At high power, the surface evaporate will itself be ionized by the beam. This ionized vapor is also known as plasma and near the surface; it will affect the laser irradiation on the materials. Therefore, it is crucial to define a laser power density in which the majority of the ionization of the vapor, resulting in plasma formation, will take place.

Laser induced vapor ionization can occur by two mechanisms, Multi-photon absorption and avalanche ionization. In multi-photon absorption, incident photons are directly absorbed via molecules in the vapor. The photon energy then excites bound electrons which then exit the molecules and ionize the vapor.

In order for avalanche ionization to occur, the vapor has to contain free electrons. These free electrons must absorb the laser energy by inverse bremsstrahlung. In this process, excited electrons ionize the molecules of the vapor though collisions. These collisions will lead to more electrons in the vapor, which then start to absorb energy and interact with other molecules of the vapor which results in a so called avalanche breakdown of molecules in the focal area. This breakdown process essentially consists of cascade ionization and electron generation. The generation of plasma via optical breakdown is a threshold phenomenon that is reached when the free electron density in the plasma is around $10^{18} cm^{-3}$. Generally, the avalanche ionization process is the major contributor to ionized electrons to plasma.

The method in which the plasma develops on the processes surface has great implications on the laser radiation-material interaction. For intensities that just exceed the intensity necessary for plasma generation, the plasma will form close to the evaporating process surface and stay attached to said surface. The confinement of stationary plasma close to the evaporating surface is referred to as plasma coupling. When the intensity of the laser significantly exceeds the plasma generating intensity,

the high laser power will trigger rapid expansion and propagation of the plasma away from the surface and toward the laser beam. This will eventually lead to the separation of plasma and the process surface which is termed as plasma decoupling.

The preferred process in laser material processing is plasma coupling because it results in an increase in absorptivity of the material. This supports the energy transfer from the laser beam to the materials surface. Particularly for applications in which a highly reflective material is used with infrared radiation where the radiation absorption from the laser is relatively small, plasma coupling increases the efficiency of the energy transfer. On the other hand, Plasma decoupling creates a shielding effect because the radiation is absorbed by the detached plasma. This causes a sharp decrease in transmitted energy to the target surface which is an undesirable effect for most laser processing applications.

Ablation is a term that can be understood in two different ways. Ablation is a material removal process by either photo thermal or photo chemical means. Like vaporization, ablations via photo thermal stresses are achieved via a rapid temperature increase on the process surface and vaporization of the material. Ablation via thermal stresses in inhomogeneous targets such as a coated material results in explosive ablation of the thin film. In contrast, photo-ablative material removal via chemical means ablates the material by breaking bonds in molecular chains. A requirement for this type of ablation is that the energy of one or more simultaneously absorbed photons must exceed the bond energy of the molecule. For ceramics and metals, thermal ablative mechanisms dominate the material removal during processing. Although photochemical ablation is the dominant process used for the machining of polymers, said polymers can also be effectively machined via thermal ablative mechanisms. Efficient ablation will take place if the timescale for energy transfer from the electrons to the lattice is greater than the pulse length of the radiation, also known as the thermal relaxation time. The thermal relaxation can be approximated by Equation 2-20 where d is the absorption depth and k is the thermal diffusivity. This minimizes the thermal damage through heat transfer.

Equation 2-20

$$\tau = \frac{d^2}{4k}$$

Additionally, the ablation process is characterized by the ablation threshold that corresponds to the laser flux in which ablation will begin. Based on the materials optical and thermal properties, the ablation threshold may differ. [1]

The heat accumulation effect is another important aspect of laser-material interaction. To more accurately explain this phenomenon, we will first explain the average intensity by example. The average intensity is given by Equation 2-21

Equation 2-21

$$I_0 = \frac{P}{A}$$

For a given power of 25W and a spot size of 50 microns, we can compute what the average intensity will be on the order of ten megawatts per square centimeter. Figure 2-14 shows the schematic of a laser pulse where $\frac{1}{R}$ is the repetition rate or frequency and t is the pulse duration.

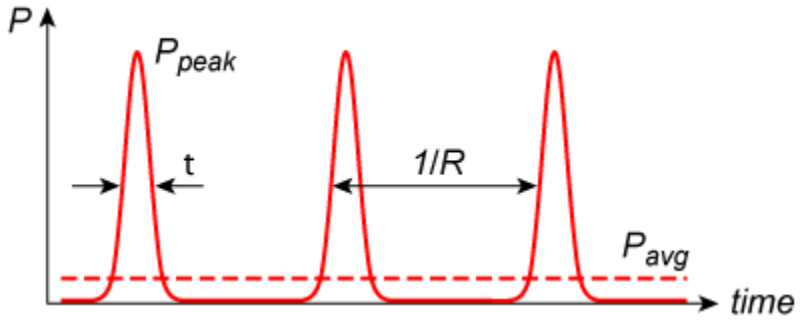

Figure 2-14: Laser Pulse Schematic[1]

For a 100 kHz Laser, there are 100,000 pulses per second. With an average power of 25watts, the pulse energy will be given as the power generated in one second, divided by the number of pulses per second, or 250 micro joules. For pulse duration of 10 nanoseconds, it is also possible to calculate the peak intensity. This is given as the peak power divided by the area of the spot size. This value is approximately ten gigawatts per square centimeter.

Now, let's analyze another laser with a lower frequency to see how this will affect the peak intensity. Again, we will use an average power of 25 watts and a spot size area of $25x10^{-6} cm^2$, and we will lower the frequency to 10 kHz. The pulse energy becomes 2,500 micro joules, a factor of ten larger. Inserting this value into the peak intensity equation yields a value of 100 gigawatts per square centimeter.

By decreasing the frequency of the beam, but maintaining all other parameters will result in an increase in the peak intensity. In order to keep the same average power, each pulse must be more intense for a lower frequency range. In terms of material processing, the frequency is not the most important aspect for high speed applications. With higher frequencies, it is possible to cover more area while maintaining a good pulse overlap, however, the intensity of each pulse may not be large enough to actually process the surface.

Increasing both the power and the frequency of the pulses would transmit a large amount of energy to the target material. A longer pulse duration results in a larger amount of energy transfer to the material, resulting in a higher temperature gain as shown in Figure 2-15. This increase in temperature results in a longer cooling time. However, if the material is not cooled back to its original temperature before the next

pulse arrives, there is a temperature runaway effect. Each subsequent pulse will further increase the temperature of the material. This effect is shown in Figure 2-16where as the peak energy and frequency are increased, the visible damage to the surface increases.

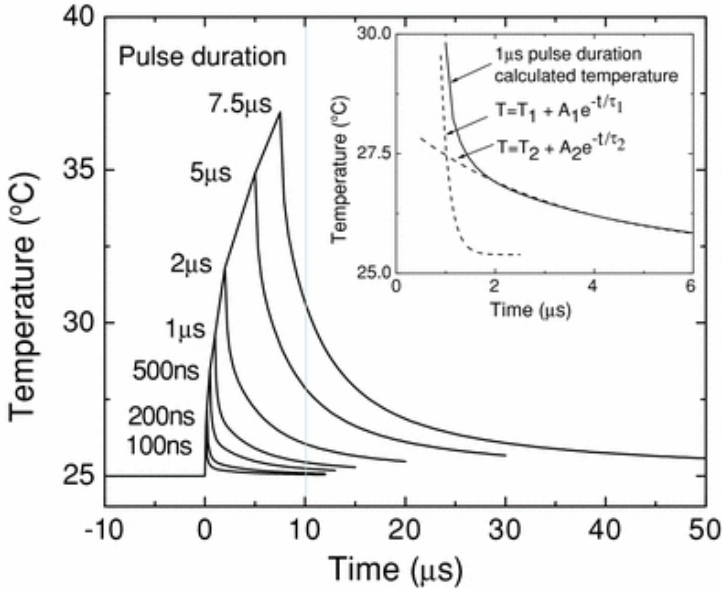

Figure 2-15: Heat Accumulation Effect[6]

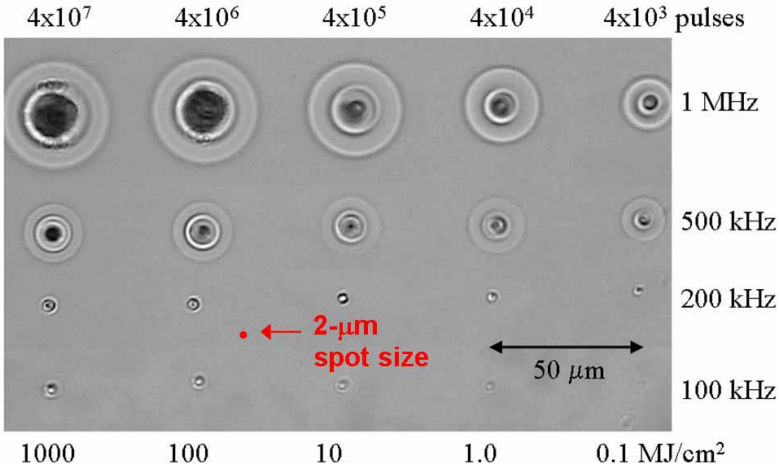

Figure 2-16: Heat Accumulation Effect Example[7]

2.2.3 Benefits of Ultra-Short Laser Pulses for Material Processing

Ultra short laser pulses in the range of femtoseconds are used for micromachining applications where the feature size transitions into the sub-micron level. Due to the short time of energy transfer, a femtosecond laser emits laser pulses with very high intensities. Since the time duration of femtosecond pulses are smaller than the relaxation times in which the electrons transfer energy to the lattice, a reduction of heat and shock wave influence on areas in the immediate vicinity of the processing occurs. This allows for ablation without any thermal influence on the remaining surface. This is referred to as cold machining. Another reason why ultra-short laser pulses are advantageous compared to longer pulses are that the threshold of the ablation lies at a lower energy level and is better defined. Figure 2-17 shows the results of machining for a femtosecond, picosecond and nanosecond pulse.

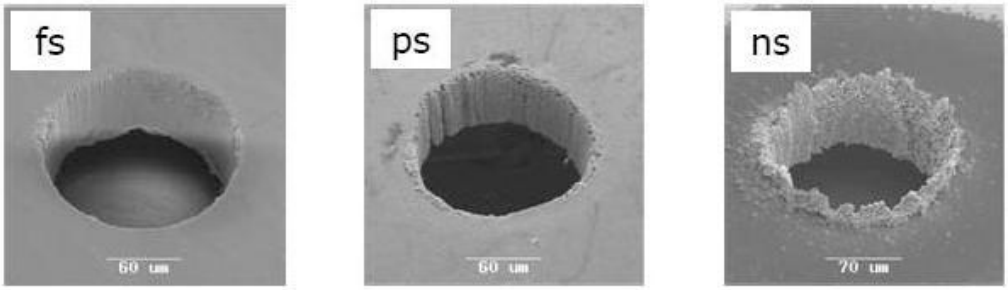

Figure 2-17: Machining Results for Different Pulse Lengths[8]

Figure 2-17 shows that as the pulse length decreases, the machining precision that can be obtained increases. The femtosecond pulse machining yielded a hole with perfectly machined edges whereas the longer pulse durations clearly show melt expulsion at the edges. This is more apparent in the nanosecond pulse than in the picosecond pulse. The results back up the relationship between relaxation time and pulse length where the energy from a longer pulse will diffuse into the material which leads to thermal penetration resulting in melt expulsion.

2.3 Laser-Induced Breakdown Spectroscopy (LIBS)[9,10] and Laser Process Monitoring

LIBS is a rapid chemical analysis technology that uses a short laser pulse to create a micro-plasma on the sample surface. This analytical technique offers many compelling advantages compared to other elemental analysis techniques. A typical detection limit of LIBS for heavy metallic elements is in the low-PPM range. LIBS is applicable to a wide range of sample matrices that include metals, semiconductors, glasses, biological tissues, insulators, plastics, soils, plants, soils, thin-paint coating, and electronic materials.

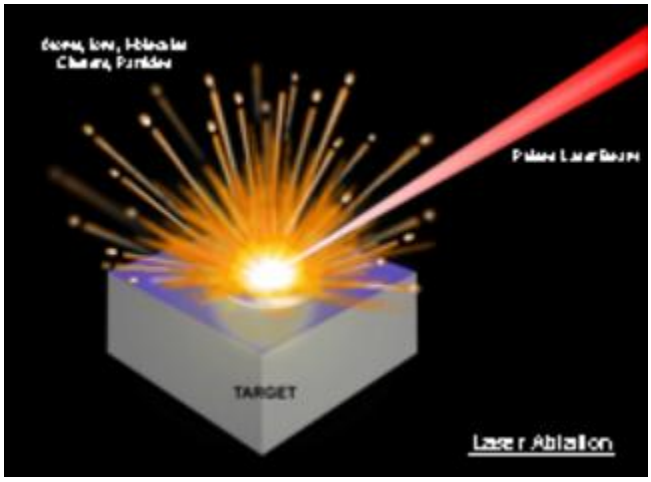

Figure 2-18: Laser Ablation[11]

The main physical process that forms the essence of LIBS technology is the formation of high-temperature plasma, induced by a short laser pulse. When the short-pulse laser beam is focused onto the sample surface, a small volume of the sample mass is removed in a process known as Laser Ablation. This ablated mass further interacts with a trailing portion of the laser pulse to form highly energetic plasma that contains free electrons, excited atoms and ions. Many fundamental research projects have shown that the plasma temperature can exceed 30,000K in its early life time phase.[12]

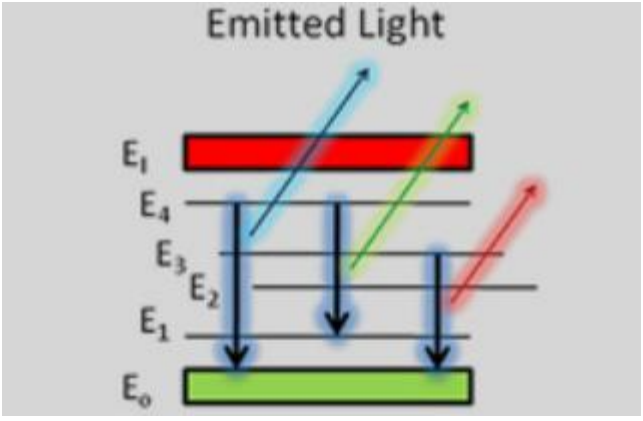

Figure 2-19: Emitted Light[11]

When the laser pulse terminates, the plasma starts to cool. During the plasma cooling process, the electrons of the atoms and ions at the excited electronic states fall down into natural ground states, causing the plasma to emit light with discrete spectral peaks. The emitted light from the plasma is collected and coupled with an ICCD/spectrograph detector module for LIBS spectral analysis. Each element in the periodic table is associated with unique LIBS spectral peaks. By identifying different peaks for the analyzed samples, its chemical composition can be rapidly determined. Often, information on LIBS peak intensities can be used to quantify the concentration of trace and major elements in the sample.

3 Experimental Setup for Cylindrical Patterning

This chapter discusses the hardware setup for my experimentation. This includes a general overview of the system, the controls hardware, precision stages, custom parts, and the optical sources.

3.1 System Overview

This system was designed and manufactured by Rockwell Automation of Shirley, New York. It is a motion control system that is capable of executing precise movements in four directions. The axis convention was determined by standing in front of the system and describing the motion. Left to right motion was defined as the x-direction or axis 1. This plane has the ability to move a total of 18 inches (457.2mm) at speeds around $500\,\frac{mm}{s}$ ($19.2\,\frac{in}{s}$) before vibration in the system becomes too large. Front to back motion was defined as the y-direction (axis 2) and has the ability to move a total of 16.5 inches (406.4mm) at the same speed as the x-axis. Vertical movement was defined as the z-direction (axis 3) and can move a total of 3 inches (76.2mm) at a speed of approximately $15\,\frac{mm}{s}$ ($0.6\,\frac{in}{s}$). Finally, the rotational axis was defined as axis 4 and has the ability to rotate 20º and can rotate at approximately $200\,\frac{\text{deg}}{s}$ ($3.48\,\frac{rad}{s}$.)Figure 3-1 is an unmodified image of the motion system.

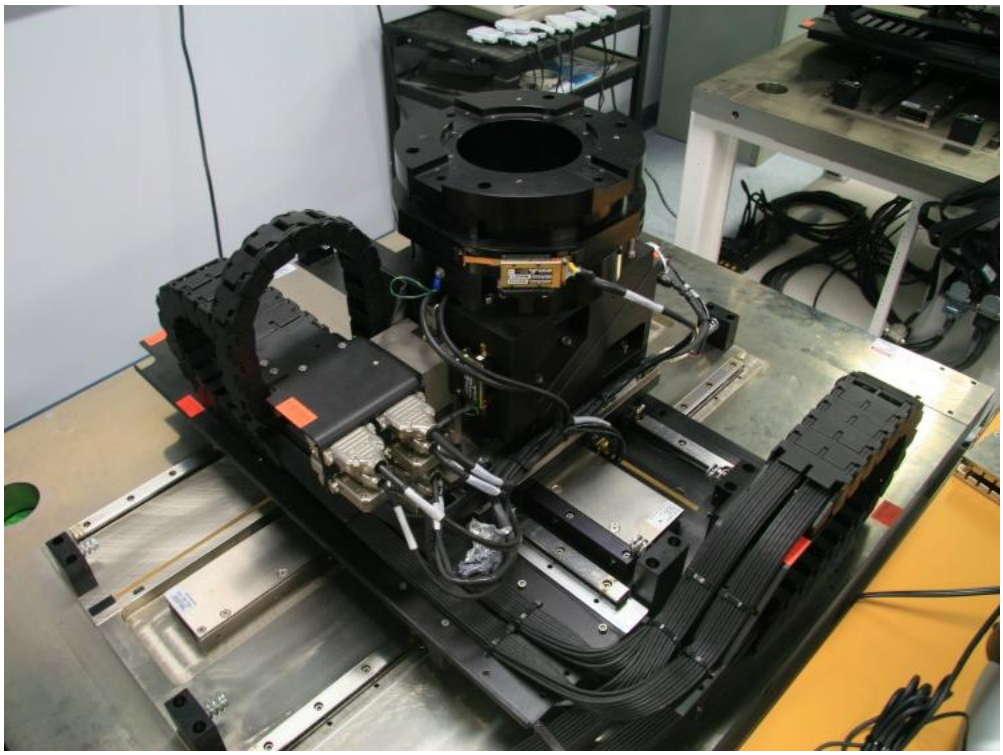

Figure 3-1: Unmodified System

3.2 Controls System

This system requires a number of components in order to achieve precise motion. This section identifies these components and provides a description of their capabilities.

3.2.1 MERS-50 Linear Encoder System

The MERS-50 Linear Encoder System is a high precision position feedback transducer for machinery or other equipment control systems. As a non-contact, optical encoder the system is comprised of a profile scale strip that is attached to the substrate axis and a scanning readhead. Figure 3-2 shows the typical MERS-50 layout. This system obtains resolutions of one tenth of one micron $(0.1\mu m)$

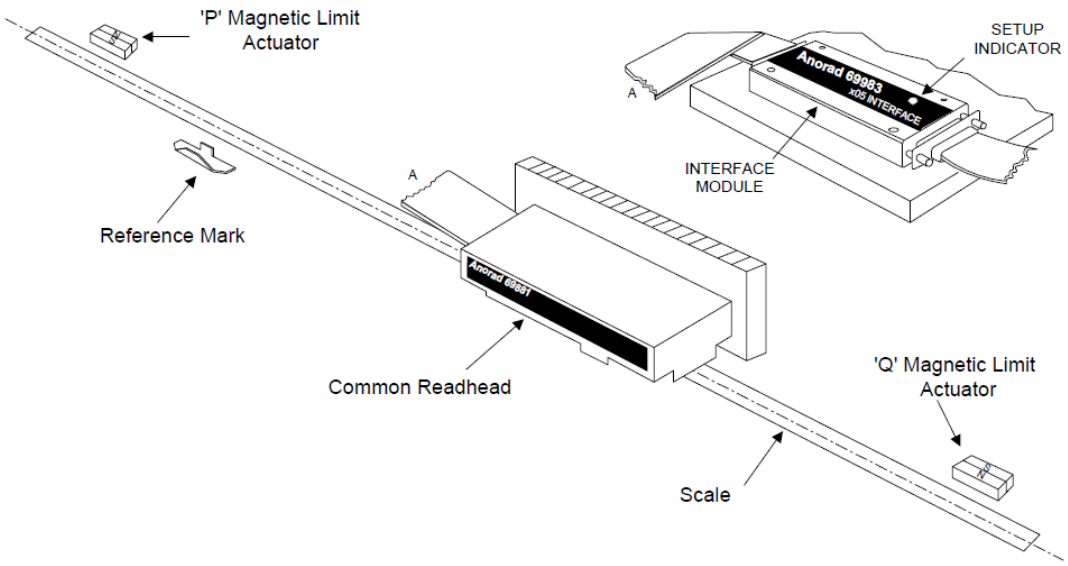

Figure 3-2: Typical MERS-50 Layout[13]

The scale used is a 6mm wide, protective coated strip which is mounted directly on the axis substrate material. The self-adhering ribbon scale is gold plated and coated with a polyurethane lacquer. The common readhead provides two sinusoidal analog signals in quadrature and outputs signals for reference marks and limits. The unit's maximum read velocity is $5\frac{m}{s}$.

3.2.2 Motion Control

The servo drives used for this experimental setup are Allen-Bradley Ultra Series Model 1398-DDM-009. They are brushless analog drives with a 15 amp peak. There are a total of four of these drives, one for each axis of motion the system attains.

The controllers are also Allen-Bradley. This ControlLogix 1756 system includes a network connect to allow communication with the control computer, Power supply, and a pair of two axis servo controllers. The first controller communicates with the X and Y axes on, one on each channel, and the second controller communicates with the Z and Theta axes. Figure 3-3 below is an image of the controller setup on the system.

Figure 3-3: Servo and Controller Setup

3.3 System Design and Modifications for Cylindrical Patterning

Although this system was excellently designed for precision, there were some modifications that had to be made in order to enable processing. This subsection describes the modifications that were applied to the system.

3.3.1 Overhead Bracket

This system performs precise movements on four axes; however, all four axes cannot be utilized to their potential without a method to hold a processing tool. In this case, the processing tool will be a laser or other optical components that will be used to redirect the laser onto the processing surface. To fix this problem, an overhanging apparatus was designed.

The motion system has a large thick plate of steel in which the rails for the motion system is mounted. This plate also had a number of extra holes tapped in each of the four corners which provided a location for mounting. It was desired that this mounting apparatus would be adjustable. In order to accomplish this, an aluminum plate was designed, fabricated and attached to the table. This plate was necessary in order to maintain the full range of motion of the x-axis. If vertical rails were attached to the table base, the system would crash. This mounting plate also had tapped holes which were utilized to attach a system of rails to the table. Figure is an image of the attached plate and rail.

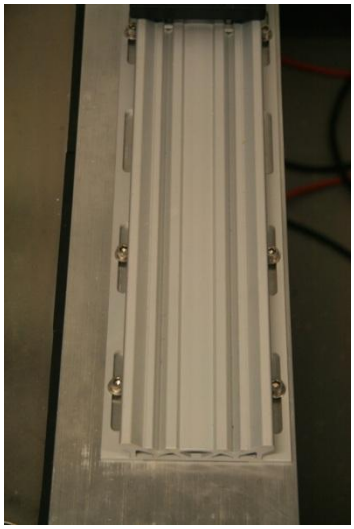

Figure 3-4: Rail System

Another system of rails was attached vertically to provide adjustable heights. The plates and rails were attached on either side of the motion top. Next, a two foot by four foot section of one inch square equally spaced ¼-20 tapped holes was attached over the top of the motion stage. This plate facilitates the mounting of various optical components which will allow the full use of the motion stage. Figure 3-5 is the final modified setup in which experimentation will occur.

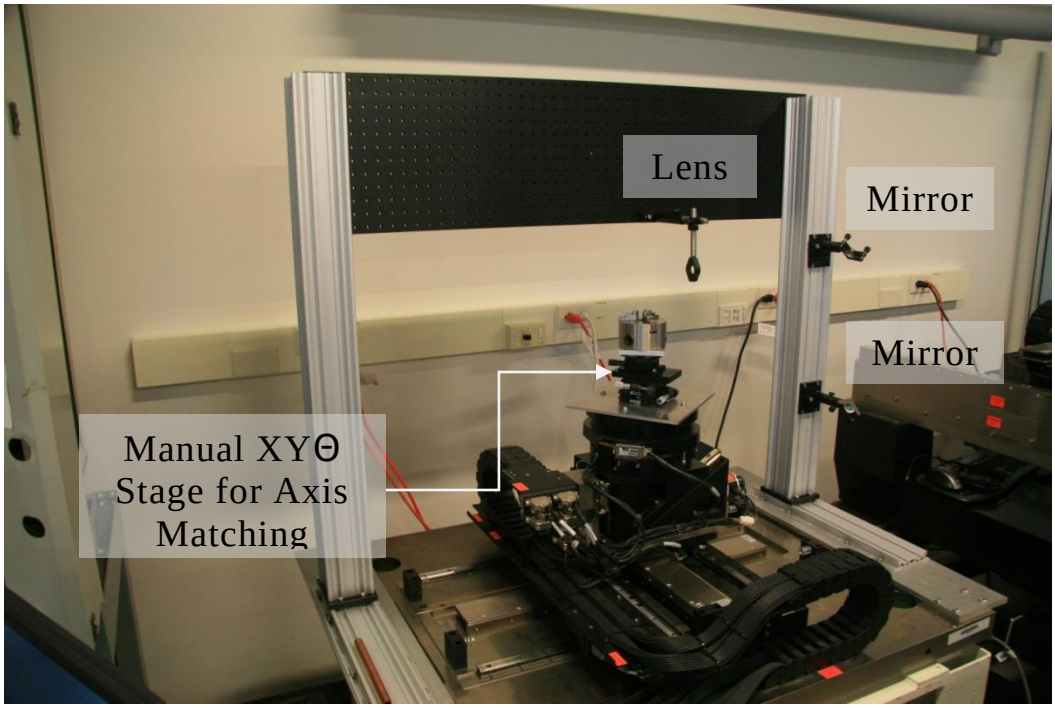

Figure 3-5: Modified Setup

3.3.2 Mounting Cover

The next modification was required to provide a surface for the specimen to be processed. The top of the motion system in its current state does not allow for specimen mounting (Figure 3-6), however it did have an array of tapped holes. A plate was designed and fabricated to cover the gap on the top of the motion system. A three by three pattern of 1 inch spaced ¼ -20 threaded holes was machined into the center of this cover. This allowed for a variety of components to be mounted to the cover. Figure 3-7 is a dimensioned drawing for the custom designed mounting cover.

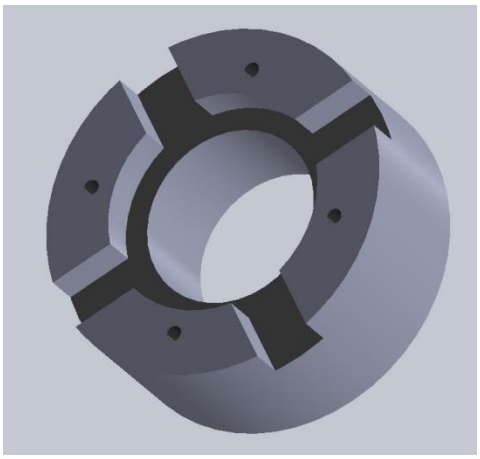

Figure 3-6: Motion System Top

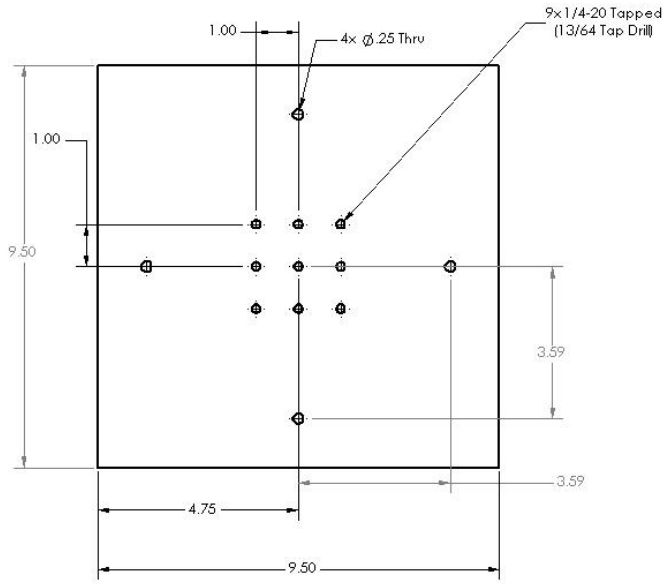

Figure 3-7: Mounting Cover Drawing

3.3.3 Chuck Plate

Another plate was required to allow the three-jaw chuck to be mounted to the motion system. The pattern on the rotary axis could not be used for two reasons. First, the hole pattern on the chuck was a larger diameter than any of the mounting holes on the rotary axis, and secondly, even if the holes were of the correct dimension, it would not be possible to attach them to one another since the two components to be joined were both tapped holes. Since the hole patterns were similar, it was necessary to counter bore the mounting holes and to us spacers to provide clearance for rotation. Figure 3-8 is a dimensioned drawing for the custom designed chuck plate.

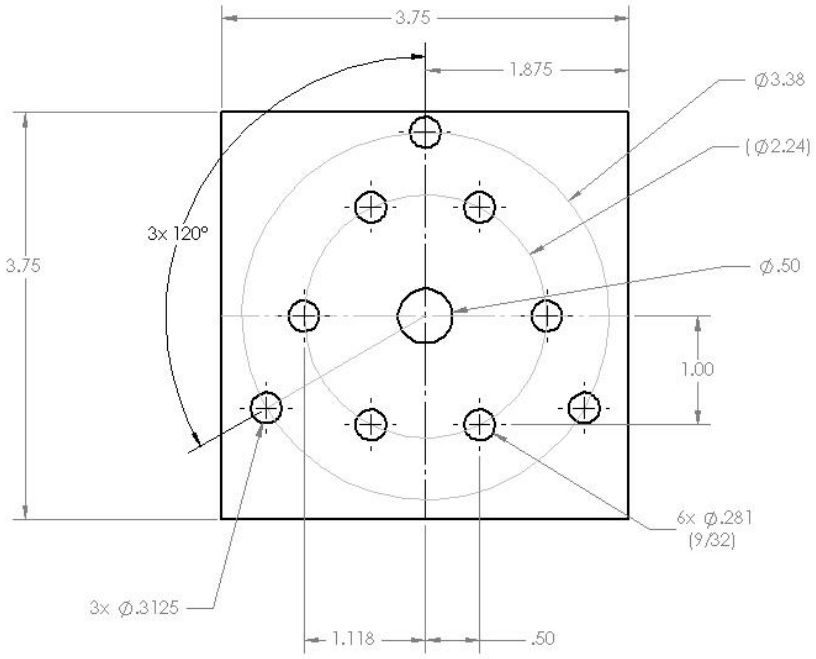

Figure 3-8: Chuck Plate Drawing

3.3.4 Other Modifications

In addition to these custom designed parts, there were some more modifications that needed to be added in order to ensure accurate processing. Since this thesis entails micromachining, precision is crucial, if the laser loses focus, the results will be very poor. The problem would arise during cylindrical processing. If the cylinder was not perfectly centered, it would create a wobble as the specimen rotated potentially dropping the laser out of focus. To ensure central alignment, two linear precision stages were added. These stages were attached at 90º to one another so changes could be made in both the x and y directions. The linear stage is shown below in Figure 3-9

Figure 3-9: Linear Stage[14]

In addition to the two linear stages, a rotary axis was also added. Since the motion system was limited to 20º of motion, it was necessary to include this product in order to index the specimen. The program would process the 20º that it could on the first pass, the rotary axis would be increased by 20º providing a new surface and then the program would restart. This process would need to be repeated 18 times to pattern the entire surface of the cylinder. Figure 3-10 below shows the chuck mounted to the chuck plate, rotary stage, two linear stages and finally the mounting cover.

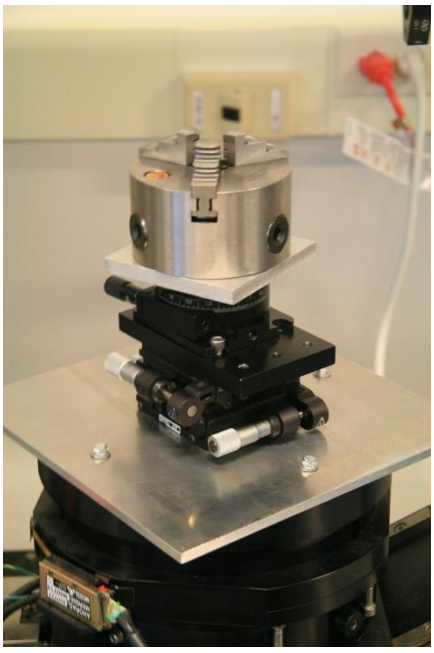

Figure 3-10: Adjustment Stages

3.4 Laser and Optical Components

This subsection describes all optical components and other systems required to perform micromachining using a laser beam. A 100mm focal length lens was used to focus the beam.

3.4.1 Radiation Source

The radiation source is a Q-Switched IR Laser manufactured by YucoOptics of Bohemia, New York. This source performs at a wavelength of 1,064 nanometers with a pulse repetition rate in the range of a manually triggered single shot up to 150 kHz. It has a pulse width of 15 Nano-seconds and is capable of pulse energies up to 12 mJ. The pulse to pulse stability is less than two percent of the root mean square of the pulse energy. It is horizontally polarized with a polarization ratio in excess of 100:1 with an average power in excess of sixteen watts. The long term stability is less than or equal to three percent over a twelve hour run period with a beam roundness greater than 90%. Finally, the spatial mode is $TEM_{00}\left(M^2 < 1.2\right)$ which is very good.

To justify the selection of this radiation source, we look to Equation 2-16 and Figure 2-9. From Equation 2-9, we know A=1-R. Figure 2-9 shows the reflectivity for various wavelengths. The Infrared Laser performs at a wavelength of 1064 nanometers. For copper processing, the approximate value for reflectivity is 0.85 which results in an absorption value of 0.15. For a green laser with a wavelength of approximately 500 nanometers, the reflectivity value is approximately 0.4, which results in an absorption value of 0.6, a factor of two larger than that of the Infrared Laser.

This factor would lead many to assume that the green laser would be a better selection due to its higher value for absorption. However, the power of the green laser is limited to approximately 3 watts, whereas the IR Laser is capable of powers in excess of 27 watts. Although less of the IR lasers energy is being absorbed by the sample, it still provides a better radiation source due to its larger power output.

3.4.2 Cooling Unit

A cooling unit is a requirement for laser processing. The system gets so hot that it could detrimentally affect the unit, so in order to keep it from overheating; a Neslab RTE-111 cooling unit was utilized.

This unit has an analog temperature range of -25ºC to +100ºC (-13ºF to 212ºF) with a temperature stability of ±0.01ºC. The cooling capacity at 20ºC is 500 watts and has a bath volume of 1.9gallons or 7 liters.

3.4.3 Thermal Head

In order to measure the power output of the laser, the beam had to be directed to a thermal head. This thermal head can record the power output of the laser. In this experiment, an Ophir 30(150)A/30(150)A-LP1 was used. This unit's recommended use is for short term measurements up to a power of 150Watts. It absorbs high energy, long pulses and is convection cooled. The manufacturer specifications are given below in Figure 3-11.

Absorber:	Broadband: 0.19 - 20µm, LP1: 0.25-2.2µm	
Aperture:	Ø17mm	
Digital Power Scales:	150W / 30W for BB, 150W/30W/3W for LPI	
Maximum Power:	150W for 50s, 100W for 90s 30W continuous	
Maximum Average Power Density:	BB: 20KW/cm², LP1: 35KW/cm²	
Power Noise Level:	3mW	
Power Accuracy:	±3%[a]	
Maximum Energy Density J/cm²	Broadband	LP1
<100ns	0.3	0.05
1µs	0.5	0.3
0.5ms	5	20
2ms	10	50
10ms	30	250
Response Time with Display (0-95%):	1.2s	
Linearity with Power:	± 1%	
Energy Scales:	300J / 30J / 3J	
Energy Threshold:	20mJ	
Cooling:	Convection	

Note a: LP1 heads have relatively large spectral variation in absorption and have a calibrated spectral curve at all wavelengths in their spectral range. When used with the Nova II (software v 1.59 and above) or USBI (V 1.17 or above) supporting this feature, accuracy is ±3% for any wavelength from 250 to 2200nm. When used with displays not supporting this feature, accuracy will be ±3% for wavelengths 532nm, 755nm, 1064nm and 2100nm and ±6% for other wavelengths in the spectral range 400 – 1100nm.

Figure 3-11: Thermal Head Specifications

Used in conjunction with the thermal head is a digital display. The Orion-TH display was also manufactured by Opir.

3.4.4 Infrared Viewer

Infrared light is not visible to the naked eye, so in order to ensure alignment of the beam with the optical components and finally the processing surface, it was necessary to use an Infrared viewer. The ElectroViewer 7215 is a high performance, hand-held IR viewer which enables the user to view in the near IR wavelength range.

4 Detailed Control Strategy

4.1 RSLogix 5000 Software

RSLogix offers a unique approach to automation. This software is a single control platform with a common control engine and developmental environment expressly designed to deliver world-class capabilities for any automation discipline.

This technology offers an easy to use, compliant interface, symbolic programming with structures and arrays and a comprehensive set of instructions whether you are using discrete, process, batch, motion, safety, or drive based applications. It provides ladder logic, structured text, function block diagram and sequential function chart editors for program development as well as support for machine control applications.[15]

RSLogix 5000 allows the user to have one intuitive design and configuration and software package that can be used to simplify the development of complex control solutions. It also allows greater access to real-time information or to develop localized applications in a single control platform. This leads to optimized productivity and the ability to quickly react to market and business demands with faster startups, reduced commissioning time, maintenance and training costs and an overall lower total cost of ownership.

4.2 Controller Implementation

This subsection describes how to create the controller files, add I/O modules and communicate with the system via the LogixPro5000 Software.[16], [17], [18], [19], [20]

4.2.1 Creating a Controller

To implement a controller, there were a number of steps that had to be followed. From the new controller dialog box, the controller type had to be selected as show below in Figure 4-1. A name, chassis type, slot number and location were also given to the controller at this time.

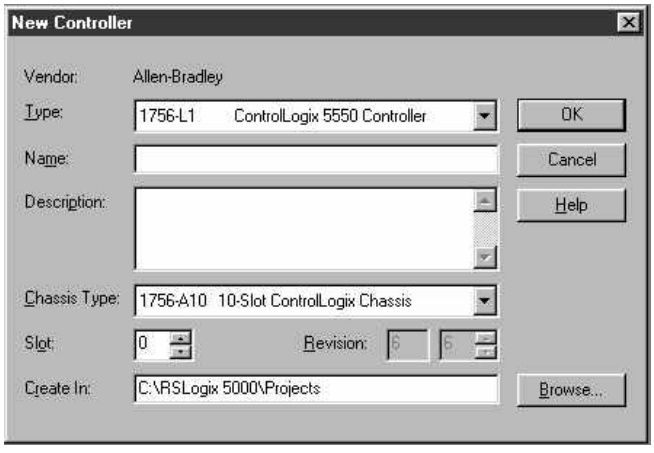

Figure 4-1: Controller Setup

At this time, the controller file has been created; however, there is no input output, tag database, or associated programs. The controller organized is a graphical

representation of your controller file. The display consists of a tree of folders and files that contain all of the information about the programs and data in the current controller file. This tree contains five folders as shown below in Figure 4-2.

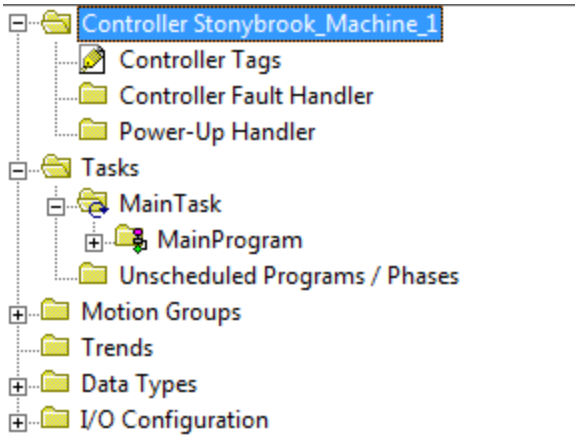

Figure 4-2: Folder Tree

The controller file name contains subfolders most notably for the controller tags. These tags are the unique names given to various commands used later on in the programming process. The task folder contains the tasks for your controller file. Underneath each task are the associated programs and ladder routines. The trends folder contains any trends you are running in the controller file. This allows you to view a graphical display of data sampled over a period of time. This will not be utilized in our experimentation. Data type's folder shows user defined, predefined, and module defined data types. Finally, the I/O configuration folder contains information about the hardware configuration of the controller file. It holds a hierarchy of modules with which the controller is configured to communicate. Currently, there are no I/O modules in the controller organizer.

4.2.2 Adding Input/Output Modules

To add an I/O Module, it was necessary to right click on the I/O configuration and select "New Module." A window will appear with a list of available modules, as shown below in Figure 4-3.

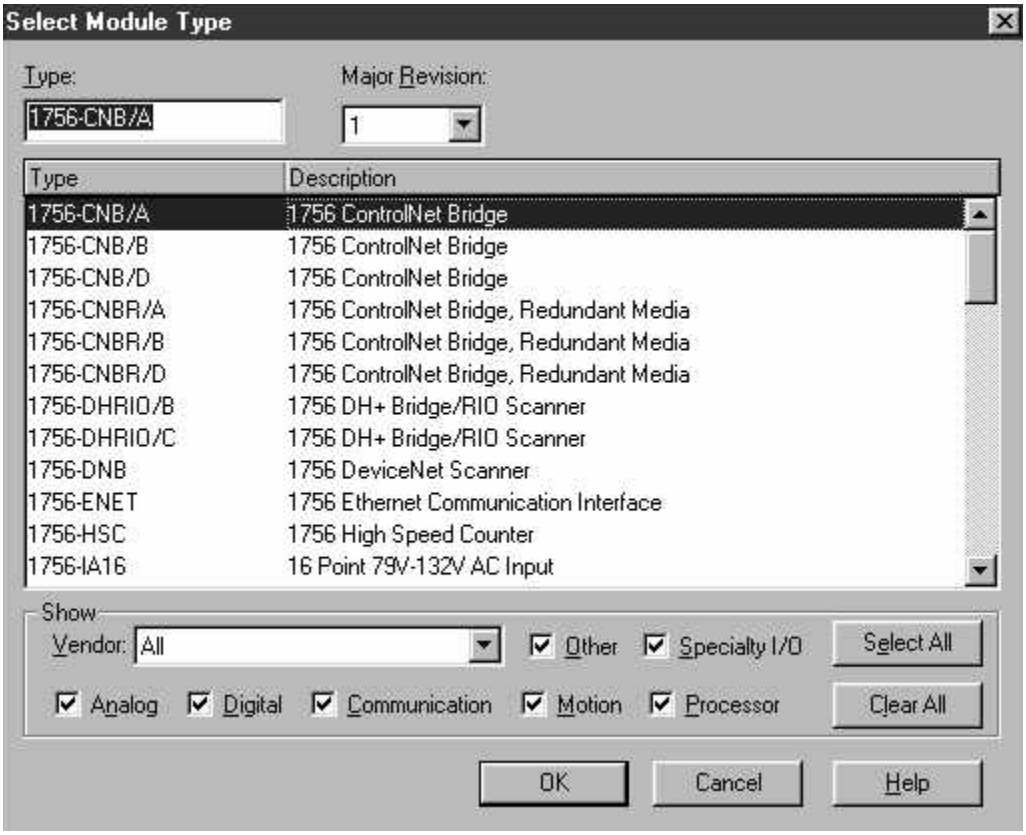

Figure 4-3: Module Selection

After selecting the correct module, and naming at accordingly, the new module will appear in the controller organizer under the I/O Configuration folder. This process was to be repeated for all controllers. The next step was creating a discrete tag for the Input/Output module that was just created. These tags will vary for each specific type of module depending on the communication format that was to be chosen.

From the controller organizer, double click on the controller tags icon. The data monitor appears with three entries in the tag name column, this is the tag structure. Figure 4-4 below shows the tag name that appears. “Local” signifies that the module is housed within the same chassis as the controller. The following number, in this case, “0” is the slot number within the module. Each module has two slots, denoted as “slot 0” and “slot 1.”

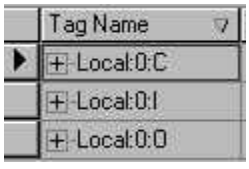

Figure 4-4: Tag Name

4.2.3 Creating a Motion Group

Once the process of configuring the Input/Output devices is completed, the next step is to set up a motion group. This is accomplished by right clicking on the motion group's folder in the controller organizer and selecting new motion group. This motion group is created as a unique tag, as shown in Figure 4-5, the Data Type is called Motion_Group. The scope is designated to the controller and any naming convention can be followed. Four axes were set up, two on each controller on modules zero and one.

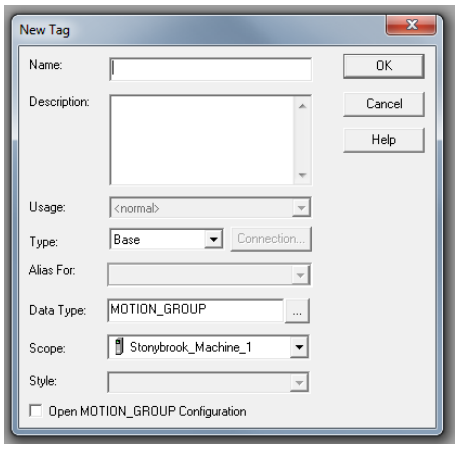

Figure 4-5: Adding a Motion Group

Once each axis was completed, the axis properties must be added. The properties contain a total of 16 tabs each. These tabs were populated with information provided by Rockwell Automation with information such as the maximum speed, range of motion and so on. The axis properties window is shown below in Figure 4-6.

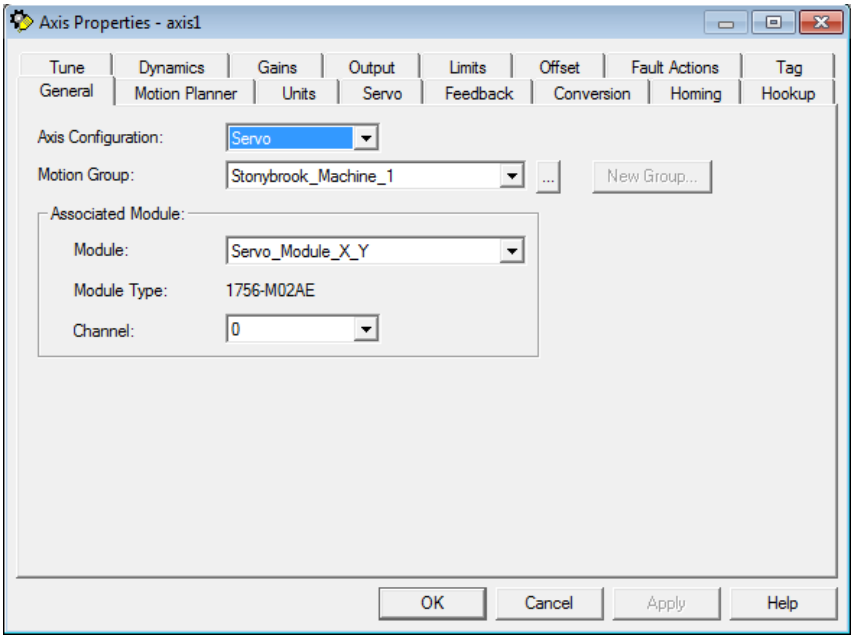

Figure 4-6: Axis Properties

Once all four axes have been created and the associated information has all been populated, the programming process can begin. Figure 4-7 below is an image of the final controller organization sidebar. This now includes all of the controller and motion groups necessary for programming to begin.

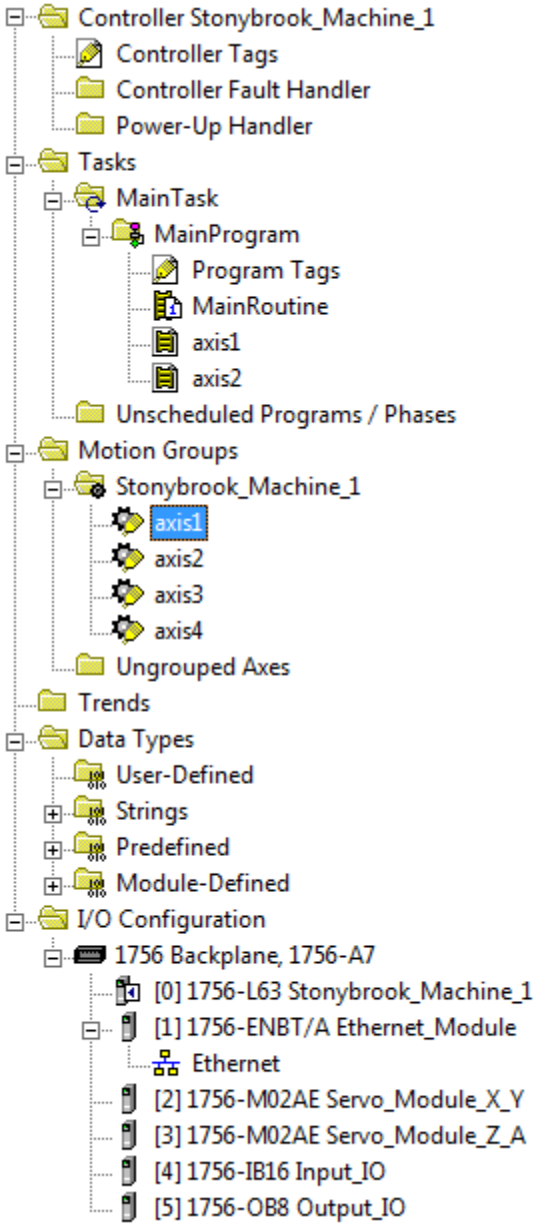

Figure 4-7: Final Controller Organizer

4.3 Programming Breakdown

After communication has been established between the controllers and the computer, the next step is programming. For this thesis, there are a variety of patterns that were programmed. I will explain the process and logic behind the programming for one pattern, which can then be applied to all other patterns. Every process requires a unique tag to be designated. These tags were named in conjunction with what task they were created to complete.

The first critical element of every program is ending the program, either when it is completed or if there is an error. The first two rungs of each program will complete this task. A bit is the smallest storage location in memory that contains either a 1, meaning it is on, or a 0, meaning it is off. This first bit is connected to the Input/Output of the controllers and will allow all of the subsequent coding to be processed. One Shot (ONS) is an instruction that will either enable or disable the remainder of the rung based on the status of the storage bit. Once this process is completed, the Motion Axis Stop commands will be executed, stopping movement of all axes. Having these commands in a parallel orientation means they will all stop at once, whereas a series orientation would execute one at a time and take longer.

Another important tag that was created was "Sequence." This tag is essentially an index variable that changes based on the Move (MOV) command. This command changes the value of the sequencer and when used in conjunction with the "Equal To" (EQU) command, enables rungs to be either skipped if the value is dissimilar or processed if it is the same. This unique tag also allows for loops to be easily executed by moving the sequence to a value that was designated earlier in the programming. Without this sequence, the program would run from the first rung to the final rung with no possibility of selecting a procedure.

Before proceeding, it is necessary to have some background information on some of the commands. As shown below in Figure 4-8, commands have various inherent bits. Whenever the bit is highlighted green, the bit has a value of 1 meaning it is active. *.EN* is the enable bit which, as the name implies, is active when that particular instruction is enabled. Next *.DNis* the done bit which indicates that all calculations and messaging are completed. *.ER* is the error bit which indicates when the instruction is used illegally. The In Process bit *.IP* is indicative of a process being executed and the final bit *.PC* is the process complete bit which indicates the operation is complete. The differences between the *.DN* and *.PC* bits are that the *.DN* bit sets after an instruction has completed execution whereas the *.PC* bit sets when the initiated process has completed.

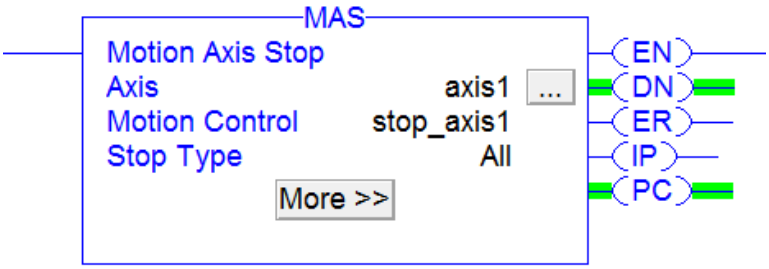

Figure 4-8: Bit Mnemonics Example

With that being said, over the program there are a large number of bits that simply check if a process has been completed. This double check ensures that the program will not advance prior to any steps completion. So wherever a command is run, the next line will ensure that it was completed correctly. Once the motion stop has been verified, the run proceeds to turn off the servos for each and every axis, this concludes the stop. Figure 4-9 shows the logic to stop motion for a three axis program. Many programs utilize all four axes.

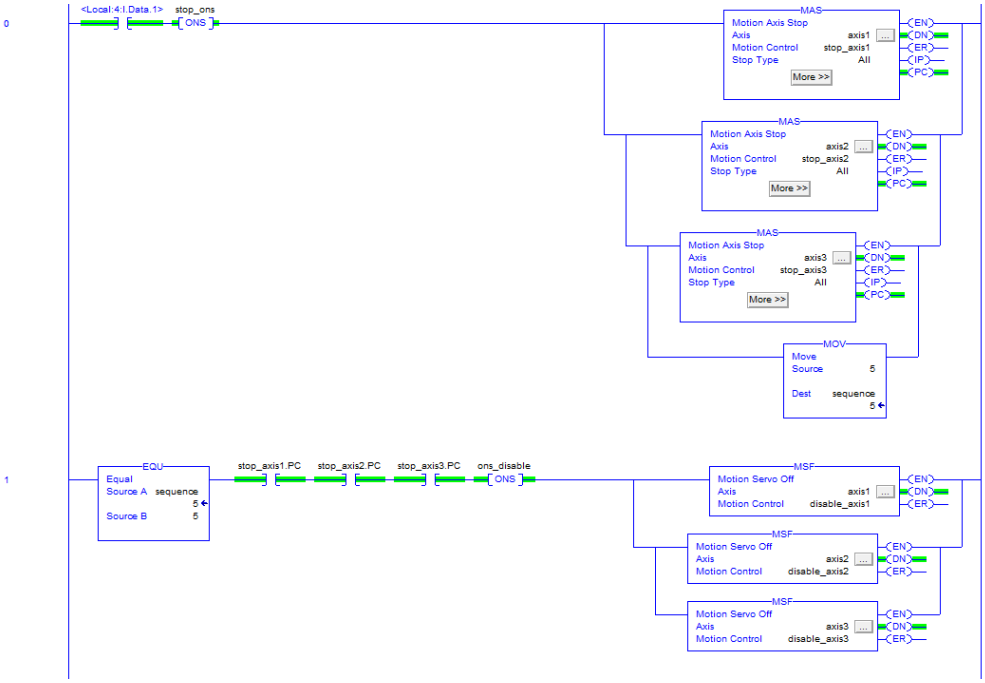

Figure 4-9: Stop Motion Logic

To start motion, a similar process is followed as the stop motion. A bit is created that connects with the I/O of the controller. Following the logic described above, these commands will all have the *.DN* or *.PC* bits following the commands to ensure proper completion of the task as well as the Move and Equal to commands that index the program through its various steps. All axes are shutdown using the Motion Axis Shutdown Reset (MASR) command and then the motion servos are enabled with the MSO command. This rung also contained a variety of computations. These computations are used to define variable that are used later on in the programming, such

as feature sizes, processing speed, processed feature count, and the number of loops that will be executed. This simply provides a centralized location that allows for easy manipulation of the code without having to scroll through some of the longer programs and make the changes in a large number of locations.

The next critical step is the Motion Axis Home command. In order to ensure reproducibility as well as precision, each and every program must begin from the same absolute position. This command makes every axis move to its extremes in order to reestablish its position relative to the table. Without this command, the program would start at a location in which it had either ended at previously, or a location it was moved to by hand when the program was not running.

After this step, the system will always be at the same location. From here, it is moved to a generic location that is derived from the means of processing. This means all axes are moved to an absolute position that will allow the laser to be focused on the specimen to be processed. These values will change based on the size of the specimen, and whether or not is a flat plate or cylindrical specimen.

The next rungs are used to lay out the feature that is to be processed. For features with a greater number of sides, this loop will be longer, whereas simple patterns will be short. Figure 4-10 is an example of the logic that is followed to achieve motion. It begins with an Equal to bit which will execute the rung if Source A is equal to Source B. MAM is the motion axis move command which will execute for whichever axis is selected and based on the motion type, position, and speed. The source will then be indexed, checked at the onset of the next rung, continue once the motion has been confirmed complete. For each motion command, I've built in a timer. This timer is in the units of milliseconds and is used so there is not an instantaneous change in direction which would put unnecessary stresses on the system. Once the timer is completed, the sequence will be indexed and the logic will repeat itself until a single feature is completed.

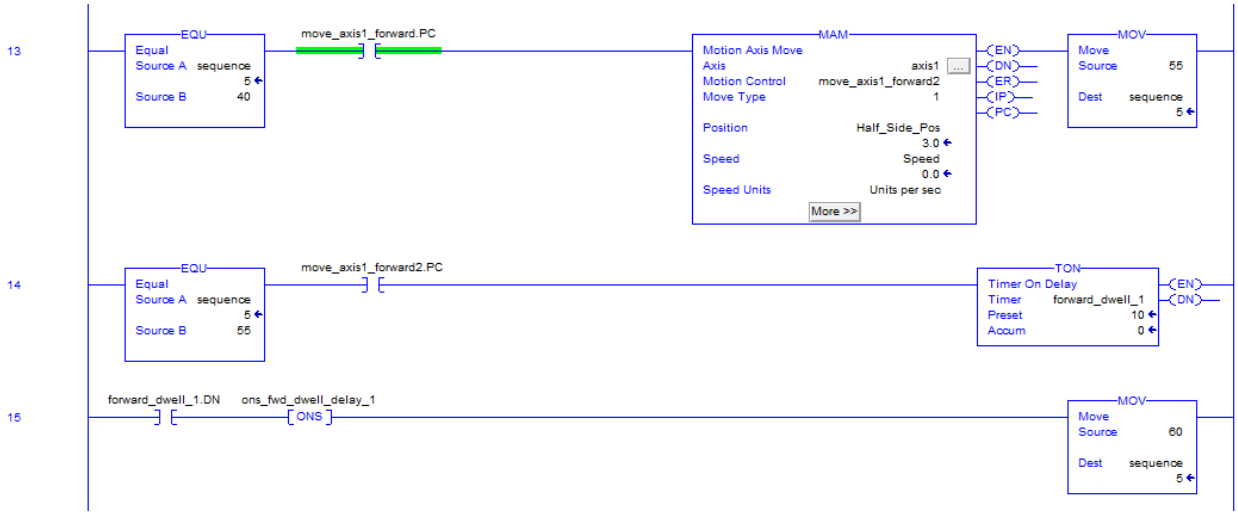

Figure 4-10: Motion Logic

In order to loop this feature creation, a variety of index variables were completed. Every time the feature was created, a value of one was added to this index variable, and once it reached a value that was obtained based on the feature and specimen sizes, the program would advance. Figure 4-11 is an example of the logic used to create a loop in the program. For this example, there were 9 required movements to create the feature which explains the forward_dwell command. Next is the addition of one to the index variable every time the program reaches this point. The move command brings the loop back to the start of the feature and repeats until the desired value is achieved. This is done using the Greater than or Equal To (GEQ) command. In this example, when the *Indexer* is larger than the *Square Count* it will proceed to reset the indexer and move to the next step.

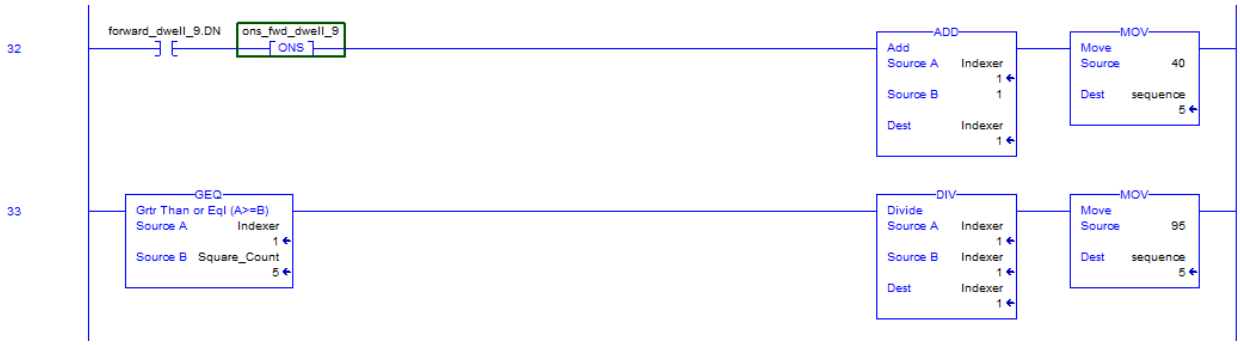

Figure 4-11: Loop Logic

Most programs have four loops built in. The first loop will repeat to process a pre-designated number of features along a given axis. The next loop will index the height of the motion stage. This is useful because it allows the user to repeat the machining process along a given path until the desired depth has been reached. Without this loop, whatever depth the feature is processed to on the first pass would be the maximum achievable depth. The next loop is created to save time. As opposed to processing in one direction; for example left to right on a flat plate, this loop creates the same feature moving from right to left, directly over the previous pattern. Once the desired number of features has been processed, the height will index again and the process will repeat. The next loop executes once the desired number of features and depth have been reached. At this point, the system will re-orient itself, providing a new, unprocessed surface for the patterning to restart. During this process, the height will also be reset to its default value to ensure the correct focusing on the new surface. The process then restarts at the first loop and continue until the processing has been completed. Figure 4-12 is a flowchart that shows the program structure. At the culmination of the program, a final motion command is executed. This command will bring the motion stage to the front of the table allowing for ease of examination or removal of the processed specimen.

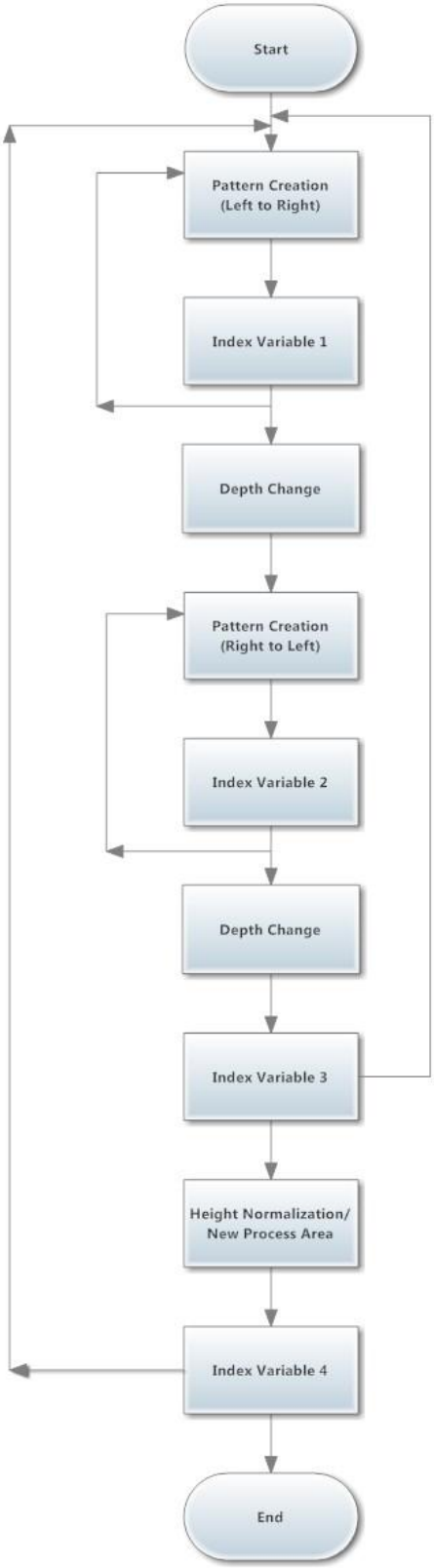

Figure 4-12: Motion Flowchart

Figure 4-13 below shows the types of patterns that were coded. These patterns were coded for both flat plate processing as well as cylindrical processing. The increase in thickness of some line segments signifies the opposite direction of motion. This means that half of the pattern would be processed as the system was moving upwards, and the other half would be created as it was moving downward. After both passes, the pattern would be complete. This two directional patterning meant that the connecting lines between the features would be processed twice.

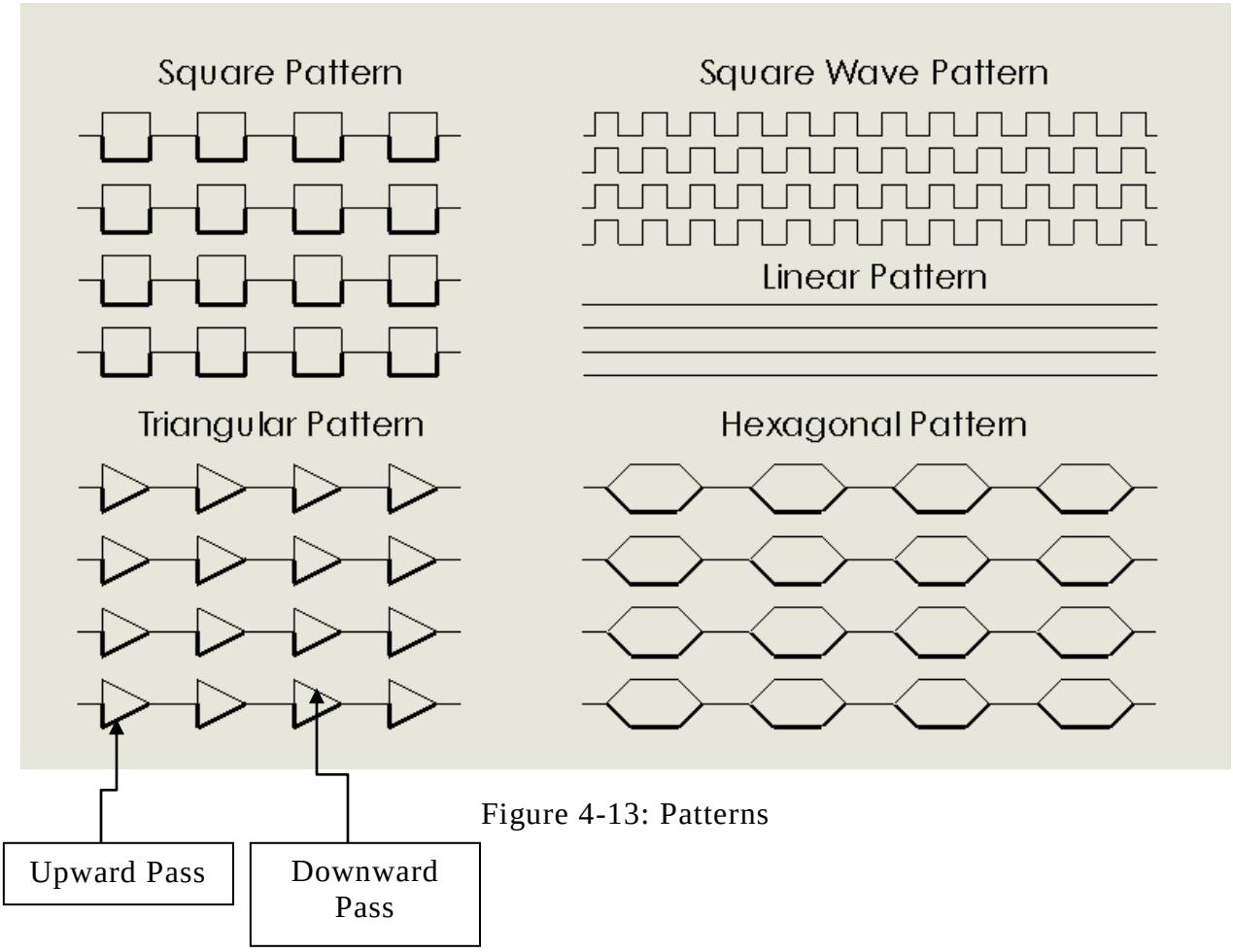

Figure 4-13: Patterns

4.4 System Issues

This chapter discusses a number of issues with the motion system and overall processing applications. Due to the issues outlined in this chapter, the more elegant patterns such as the hexagon and triangle were unable to be processed. These patterns require the simultaneous movement of two axes and with the feedback feature not functioning properly; the patterns would be misaligned and uneven.

4.4.1 The Z-Axis

A number of solutions have been attempted with no success. These issues are related to motion in the Z direction. This motion is crucial because all cylindrical patterning is done primarily in the Z and Theta directions.

As previously stated in 0: Programming Breakdown, the way the process is should work is a motion command will begin, the motion will execute and upon completion of said command, the process complete bit will trigger and the next step will commence. In reality, the feedback system is not working properly and as soon as the motion begins, the process complete bit will trigger and move on to the next step. After contacting the manufacturer about this issue, they pointed me to a few options in the axis properties. None of these options successfully resolved the problem.

In order to still perform processing, a solution needed to be found. Albeit a band aid on the larger issue, delays were built in at the end of each motion command during the programming process. This would allow the user to increase the delay based on the distance to be moved in the Z direction in order to allow the motion to be finished before proceeding to the next step.

Another issue relating to the Z-Axis is its motion speed. This issue corresponds with the feedback issue that was just explained. This axis has the ability to move up to 15mm per second, however, due to its lack of feedback, any increase in speed in the axis properties will result in a crash of the axis and a subsequent cancellation of the active program. Therefore, the default homing speed of 1mm per second must be utilized throughout the processing.

The final issue with the Z-Axis is related to one of the modifications. The addition of the cover plate, two linear stages, rotary stage, chuck plate, and the three jaw chuck have added a significant amount of weight to the top of the motion system. This extra weight makes the motion in the z-axis harder when it is increases, and easier when it is decreasing. This will result in a difference in processing speeds based on the direction of motion.

The manufacturer has been looking into the feedback issue, since that solution of that problem will result in the solution of the other two problems. With the feedback working correctly, it is possible to adjust the maximum speed of the axis and increase the overall processing speed. The solution to the weight issue is also easily fixed once the feedback is working correctly. In the axis properties there is a torque scaling option. This option scales the motion speed between the forward and reverse directions. This would cause the system to work harder when the z-axis is moving upward, but this would enable the system to process at the same speed in either direction.

4.4.2 Shutter Control

Due to the issue with the feedback of the z-axis, that created an issue with the shutter control. Since it was unknown precisely when a motion would finish, there was no way to incorporate the control of the shutter via the program. In doing so, it would be possible that the shutter would close too soon, which would create a gap in the pattern, or, it would close to late, in which case the pattern would be over-processed. Outputting a signal at given times from within the program is possible, but as previously stated, it would case more of an issue. At the beginning and end of the program, a manual shutter would be opened or closed to allow for processing. This would prevent the issues that would arise from the computer controlled shutter.

Shutter control was necessary to create more elegant patterns such as the hexagon, square, or triangle because without it, the laser would have to move from one end of the pattern to the other without altering it. The solution to this problem can be seen in Figure 4-13 with the increase in line thickness. To prevent a new line to be processed in moving from one end of the pattern to the other, the pattern was overlapped in some locations.

4.5 Strategy for Cylindrical Patterning

There are a number of different programming techniques that could be used to achieve the same processed pattern. For ease of visualization, various patterning steps will be outlined for the triangle wave. Four options were conceived and illustrated in Figure 4-15. Arrows indicate the order in which the segments are processed. Options that involved having step two move upwards as opposed to downwards were not considered because in essence, it is the same pattern.

Option one required seven steps and entailed processing the lower portion of the pattern twice. The program would complete the entire triangle, and then begin to overlap the processing in order to move onto the next feature. Option two was also seven steps and portrays the processing of the lower section before the upper section. The pattern would move from the lower corner, up to the peak, and then turn around and retrace its path. Following this step, the other half of the triangle was processed, completing the feature.

Option three was a nine step option. This option included shutter control, which as explained in 4.4.2:Shutter Control was not a viable option at this point. Regardless, this option patterned the triangle; the shutter would close, preventing processing from continuing, and indexing up to the peak of the triangle. Once this location was reached, the shutter would open and the processing would resume.

Option four was an eight step process that involved two separate patterning times. For this option, the z-axis would pattern up the cylinder, processing half of the feature. Figure 4-14 will aid in describing the process. First, the entire lower half of the pattern would be processed from left to right in accordance with the visual aid; this is shown by the bold lines, and the solid lines on the lower half of the feature. After this portion of all features has been patterned, the direction of motion would reverse, becoming right to left. The adjoining lines will be reprocessed, and then the dashed lines will be the path that is followed to complete the pattern.

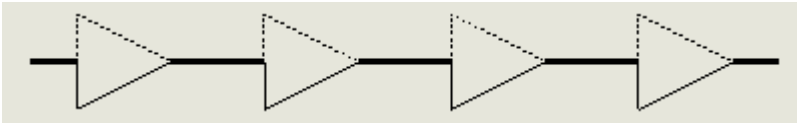

Figure 4-14: Option Four

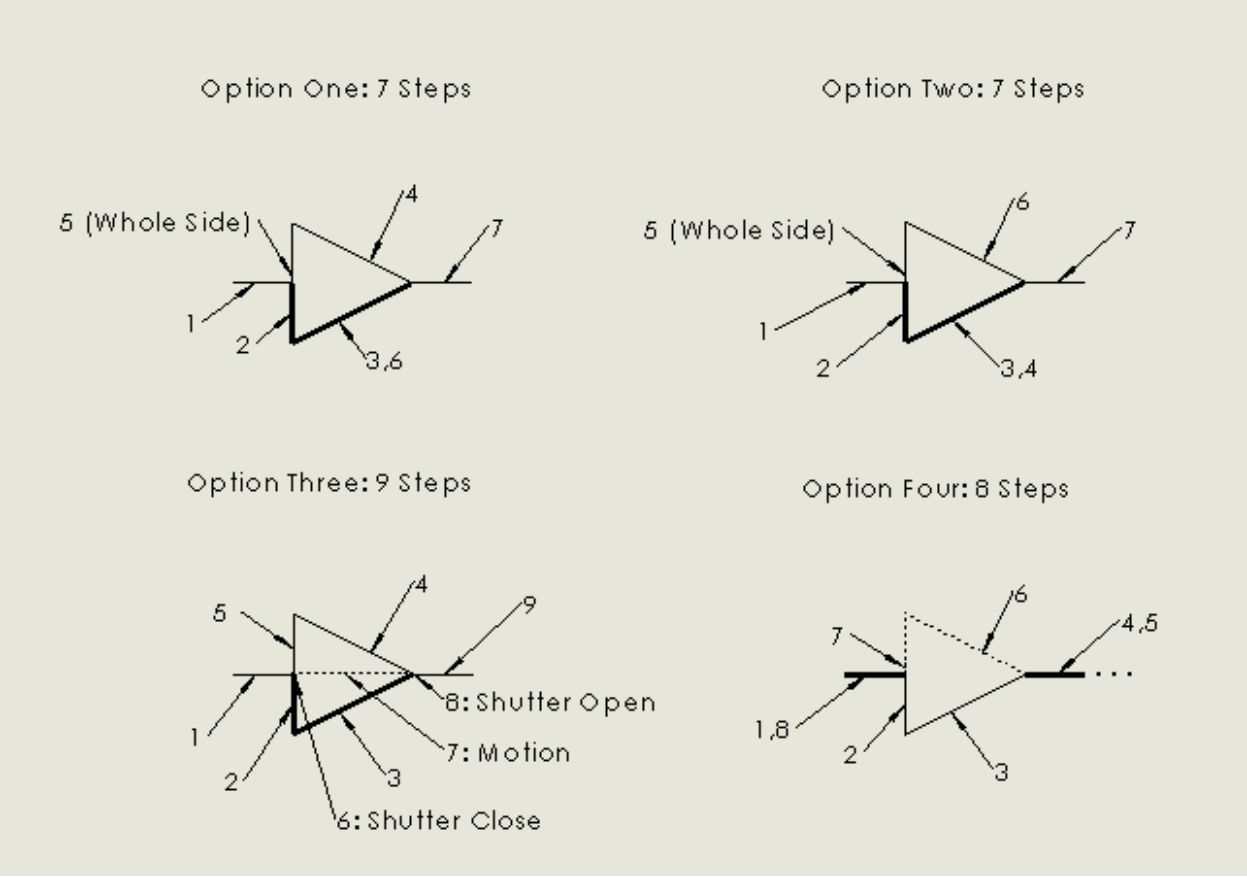

Figure 4-15: Patterning Options

Ultimately, option four was the selected method of processing. The ideal method would be option three but the possibility of shutter control but as previously mentioned, this was not a viable option at this point. Although option four required more steps than options one and two, it had other benefits. First, the sections that were to be processed twice would reside on one axis. This singular movement ensured accuracy in the reprocessing of the feature. The next and more important benefit was that of direction change. For each axis, there is a time required for acceleration and deceleration to occur. Constantly changing the direction of motion is inefficient and potentially damaging to the axes.

5 Demonstration of Cylindrical Patterning Via Laser Ablative Processing

This chapter discusses the experiments that were performed. There were a number of critical factors in each experiment, such as the laser power, current supplied to the laser, processing speed, material type, and the pattern chosen. The dimensions of each pattern processed will also be provided as a side by side comparison of what was expected, and what was the actual result. Each experiment done will describe each of these factors and then images of the results.

5.1 Experimental Procedure

This chapter discusses the steps required to prepare for the experiments. This includes arranging the radiation source and its optical components, and focusing the beam on the cylindrical surface.

5.1.1 Optical Arrangement

Since the system being utilized is a standalone system, it was necessary to redirect the laser beam from the source which was located on an optical table; over to the specimen. This was accomplished using three Thor-Labs mirrors that were precisely mounted and angled to direct the beam to its desired location. A fourth optical component was used to focus the beam; this was a 100mm lens.

5.1.2 Focusing the Beam

The final pre-experimental step was focusing the beam. This tedious task was accomplished utilizing two programs that were written to focus in the x-direction and y-direction. First the system was manually focused without being active to determine the approximate location. Then, the system was activated and moved to this approximate location, when a loop would then take over and, upon input from the user, slowly index the axis until the beam was focused.

This process took quite some time because the focusing program can only move the system incrementally in one direction. Once the focus location was surpassed, the program had to be re-run in order to adjust in the opposite direction. Also, the incident beam was not approaching the surface of the cylinder perpendicularly. This meant that each time you refocused the beam on one axis; a slight modification would be required on the other axis as well. Focus is obtained at the position in which the spark created by the beam hitting the specimen is the brightest. Figure 5-1 is a representation of an unfocused position. Although the laser is comprised of Infrared light, a beam was created in order to aid in the visualization of this concept. Figure 5-2 shows the beam when it is in focus where the green emission from the surface is the generated plasma.

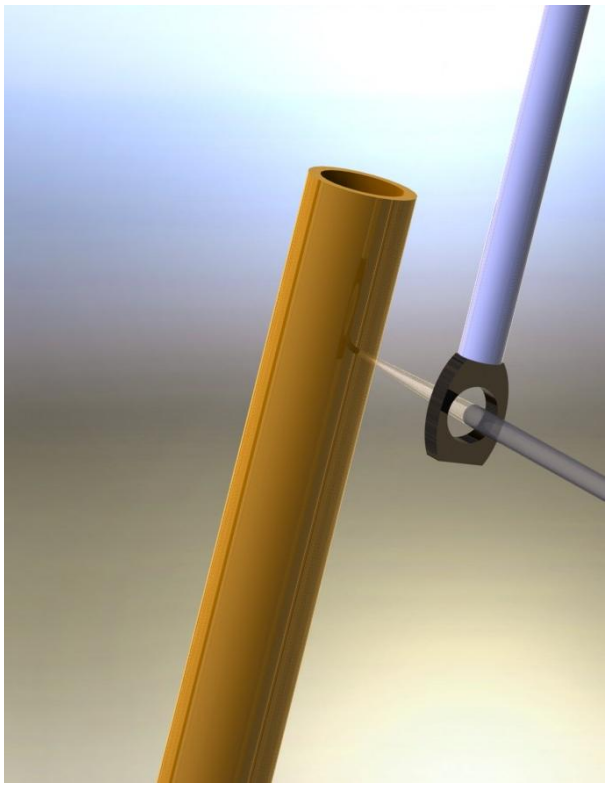

Figure 5-1: Unfocused Beam

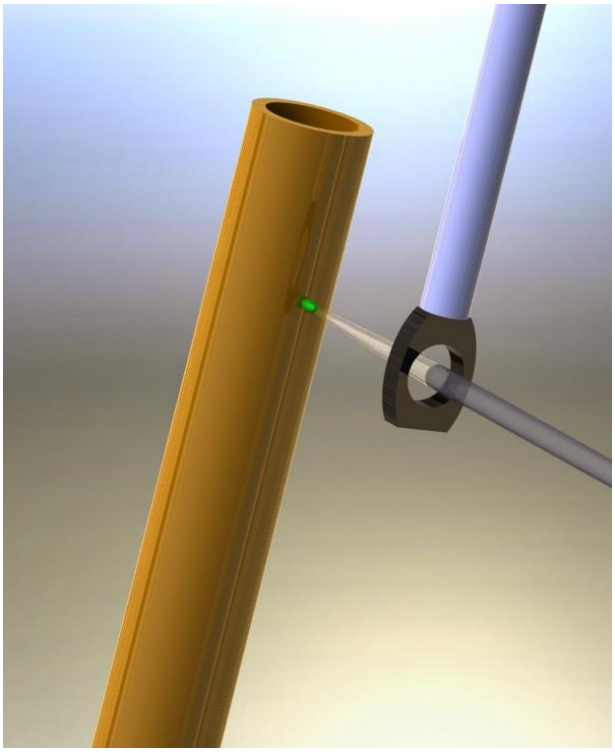

Figure 5-2: Focused Beam

5.2 Indicating the Cylinder

This chapter includes details on the purpose of indicating the cylindrical sample, why it is necessary, the method used to accomplish this task, and a further investigation of why precision is so vital for scaling analysis.

5.2.1 The Indication Process

Indicating the cylinder is a method utilized to ensure concentricity between the axis of rotation, and the specimen mounted to the stages. To explain why this step was so crucial, we will refer back to Equation 2-12, Equation 2-13, and Figure 2-7. The laser we are using for processing has a wavelength of $\lambda = 1{,}064\,x10^{-9}\,m$, initial beam radius of $w_0 = 1.5mm = 1.5x10^{-3}\,m$, a times diffraction limit of $M^2 = 1.2$, the focal length of the lens is known to be 100mm or 0.1m. Inserting these values into Equation 2-13 yields the waist radius.

$$w_1 = \frac{\lambda f m^2}{\pi w_0} = \frac{(1{,}064x10^{-9})(0.1)(1.2)}{\pi(1.5x10^{-3})} = 27.1\mu m$$

Doubling this radius will give us the waist diameter which is 54.2microns. Plugging this value for the waist radius into Equation 2-12 will give us the Rayleigh Length.

$$z_r = \frac{\pi(27.1x10^{-6})^2}{(1{,}064x10^{-9})(1.2)} = 0.00018m = 0.18mm$$

Doubling the Rayleigh Length yields the focal length which is 0.36mm. This means that in order to maintain beam focus, the axis of rotation must be within 0.36mm of perfect center or the beam will go out of focus.

As previous stated in3.3.4:Other Modifications, it was necessary to include two linear stages to ensure that the eccentricity of the rotating specimen was precise. A non-concentric cylinder will display a wobble while rotating and a point on the surface will trace out an ellipse as opposed to a circle. Figure 5-3 below illustrates the concept of eccentricity. The center of rotation is designated by the black dot, located in the center of the circle with the value e=0. This is designated a circle because it is perfectly centered about the point of rotation. As the values for eccentricity increases, the center of the curve is further away from the center of rotation, so as a single point revolves around the center of rotation, it follows an elliptical path. The further away from the point of rotation, the more elliptical the orbit will become.

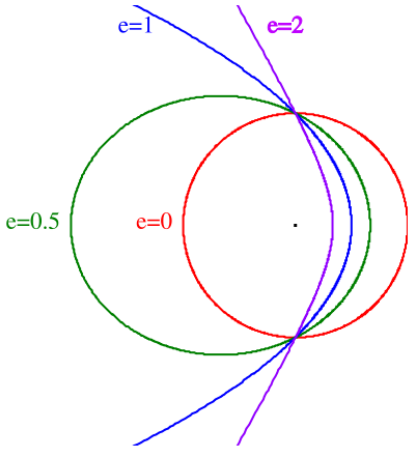

Figure 5-3: Eccentricity

To prevent this elliptical rotation, a dial indicator was temporarily mounted to the system and used to center the cylinder. While slowly rotating the specimen, the indicator would show which direction the cylinder needed to be moved in order to attain the correct center of rotation. The two linear stages were precisely adjusted and ultimately, the cylinder was centered to within five ten thousandths of an inch (±0.0005”) for the twenty degree rotation the system was capable of. An image of the indication process is shown below in Figure 5-4.

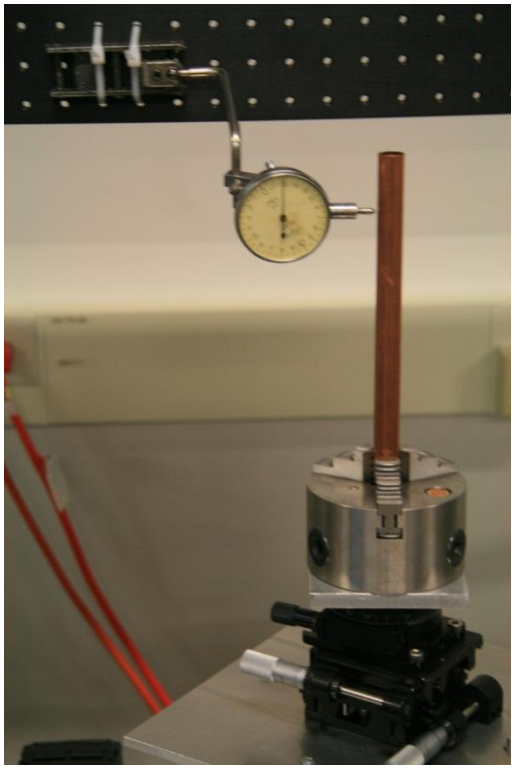

Figure 5-4: Indication Process

5.2.2 Further Analysis

In expanding upon the ideas shown in 5.2.1:The Indication Process, we will now examine what would happen to the Rayleigh length if changes were made to the experiment. First we will touch on what would be the result if the focal length of the lens was altered. Equation 2-13 calculates the waist diameter, since the focal length is in the numerator, an increase in this value would result in an increase in the spot size. Conversely, a decrease in this value will result in a decrease in the spot size. For example, doubling the focal length would double the waist diameter, and halving it would halve the waist diameter.

Now, examine what would happen to the Rayleigh Length. As previously stated, increasing the focal length increases the waist diameter. Equation 2-12 has the square of the waist diameter in the numerator, so this increase in the waist diameter will lead to an increase in the Rayleigh length by a squared factor, increasing its value rapidly. Conversely, decreasing the diameter would drastically reduce the focal length, making it very difficult to focus.

In an example for micro-scale patterning, we will take a focal length of 10mm or 0.01m. This yields a waist radius of 2.7microns which is a factor of ten smaller than that of our 100mm focal length lens. However, in computing the Rayleigh length, we obtain a value of 1.8 microns, a factor of one hundred smaller than the Rayleigh length of 100mm. It is evident that as the spot size is scaled down to sizes that would enable the processing of Nano-scale features, the focal length will be so miniscule that an auto-focusing device would be necessary to keep the beam in focus. A device of this nature could potentially utilize a piezoelectric to dynamically make adjustments to compensate for the variation in the surface.[21] Without this device, variations in the surface would cause the beam to lose focus and thus hindering the lasers ability to process. Figure is a visual representation of the decreasing focal length as spot size decreases.

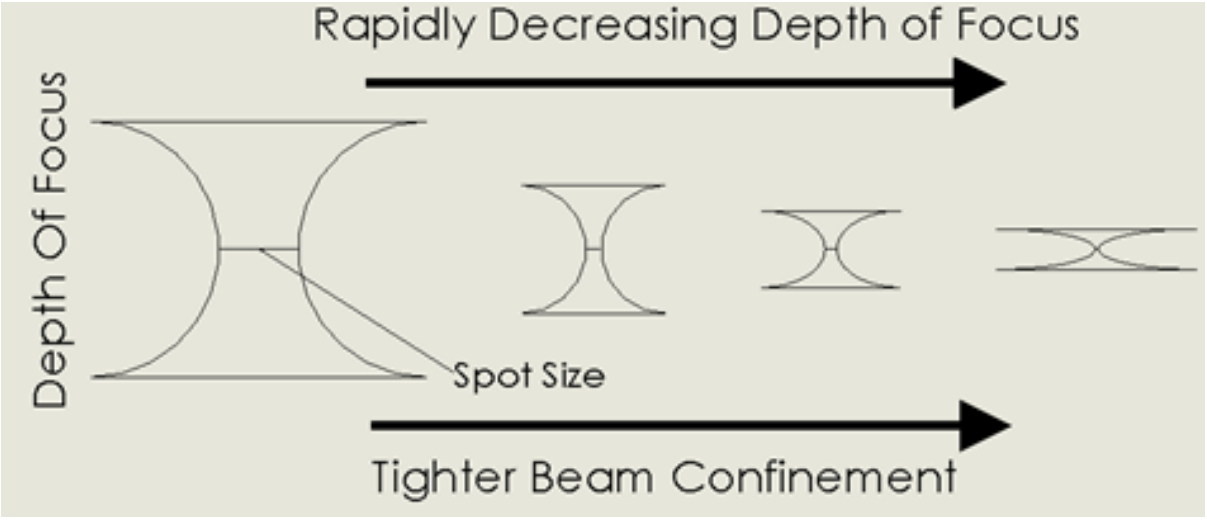

Figure 5-5: Improving Resolution

5.3 Ablative Patterning for a Copper Tube

This subsection illustrates various examples of laser ablative patterning on cylindrical copper samples.

5.3.1 Proof of Concept: Similarity between Flat and Cylindrical Samples

This experiment is a proof of concept of the similarity between flat plate samples and cylindrical samples. A simple raster motion was used to illustrate the similarity between the processing of two samples with different geometry. Figure shows a generated pattern on a cylindrical surface whereas Figure 5-7 shows flat sample processing. These patterns show excellent similarity, overall uniformity and a very close threshold for black copper generation.

Figure 5-6: Cylindrical Sample Processing

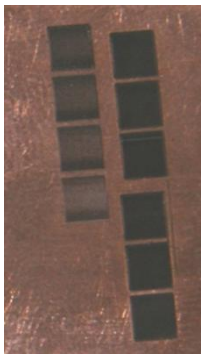

Figure 5-7: Flat Sample Processing[22]

5.3.2 Parametric Analysis of Processing Speed and Power Variations

This experiment is a study of processing speed in relation to laser power. A variety of linear patterns were created on a cylindrical copper surface for varying rotational speeds. The power would then be increased, and the patterns would be recreated using the same speeds to see what the differences are. Figure 5-8 shows the pulse overlap of various scan speeds. The faster the processing speed at a given frequency, the less pulse overlap there is, whereas a very slow speed yields an abundance of pulse overlap. Figure 5-10 illustrates the direction in which the process data was analyzed. Due to the fact that the rotary axis could be more readily controlled, this was the data that was analyzed, whereas the z direction of motion was used to provide a clear processing surface.

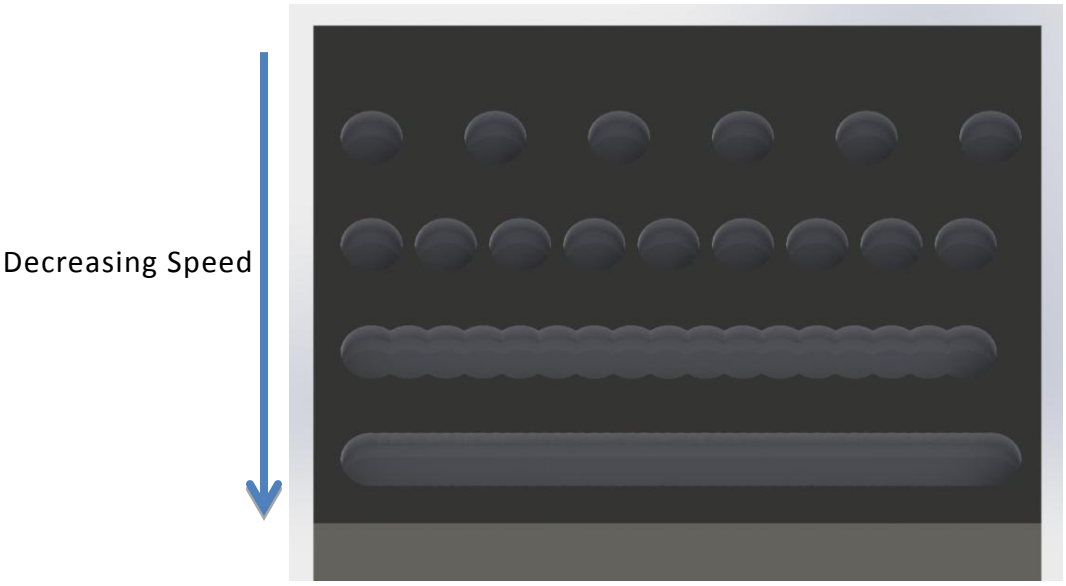

Figure 5-8: Processing Speed

Trial No.	Rotational Velocity [Deg/Sec]	Tangential Velocity [mm/Sec]	Test 1		Test 2		Test 3		Test 4	
			Power [W]	Current [A]	Power [W]	Current [A]	Power [W]	Current [A]	Power [W]	Current [A]
1	15	2.91	9.95	37.9	15.45	38.9	19.95	39.6	25.22	40.5
2	30	5.82	9.95	37.9	15.39	38.9	20.11	39.6	25.19	40.5
3	45	8.73	9.97	37.9	15.4	38.9	19.87	39.6	25.04	40.5
4	60	11.64	10.02	37.9	15.36	38.9	19.96	39.6	25.17	40.5
5	90	17.46	9.99	37.9	15.42	38.9	20.24	39.6	24.85	40.5
6	120	23.28	9.97	37.9	15.32	38.9	20.08	39.6	24.97	40.5
7	150	29.09	9.98	37.9	15.33	38.9	19.95	39.6	24.9	40.5
8	180	34.91	10.01	37.9	15.26	38.9	19.86	39.6	25.15	40.5
9	200	38.79	9.98	37.9	15.22	38.9	20.07	39.6	24.92	40.5

Figure 5-9: Velocity, Power, and Current Values

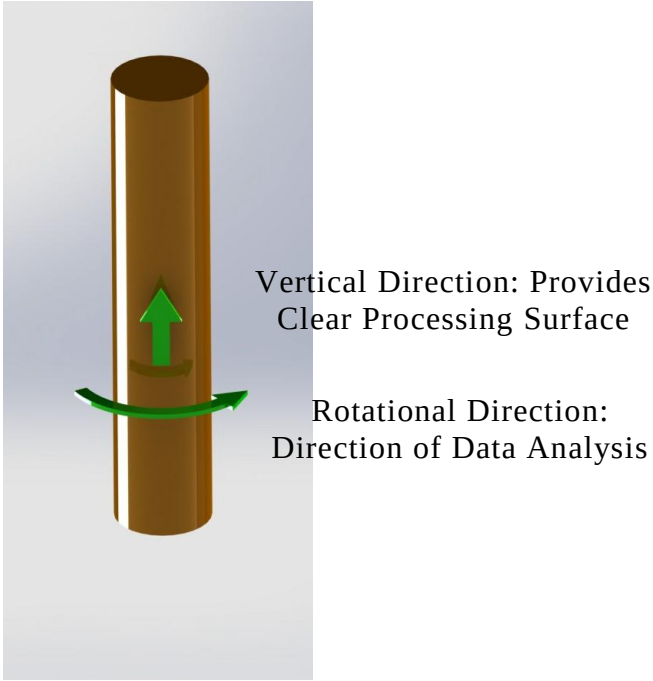

Figure 5-10: Data Analysis Schematic

The radial variation in the cylinder was ±0.23mm which led to a potential velocity variation of ±0.06mm/s. The molten width was the measured dimension and the results based on processing power and speeds are illustrated in Figure 5-19. Figure 5-11through Figure 5-18illustrate the patterns created at varying powers, and magnifications. Images were taken using a scanning electron microscope and an optical microscope in reflection mode. In order to give some perspective of depth, the SEM images were tilted and rotated.

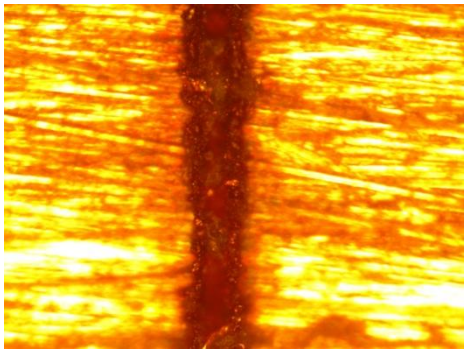

Figure 5-11: 10 Watts 20x Magnification

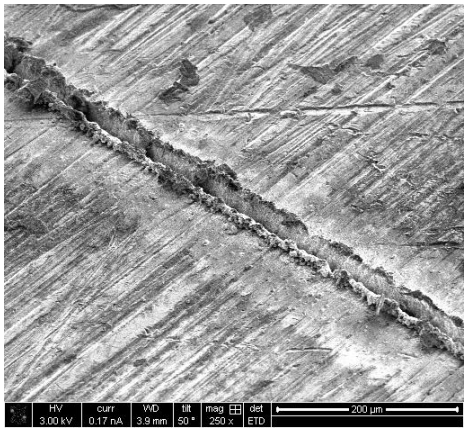

Figure 5-12:10 Watts 250x Magnification

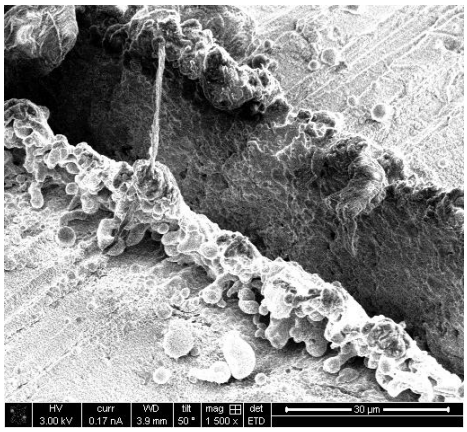

Figure 5-13: 10 Watts 5,000x Magnification

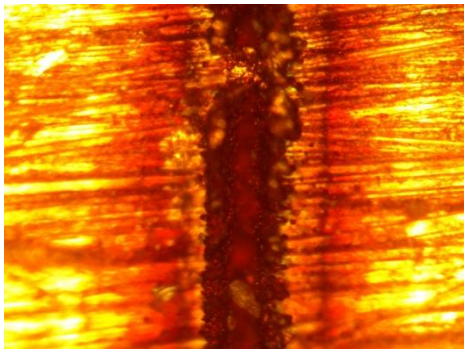

Figure 5-14: 20 Watts 20x Magnification

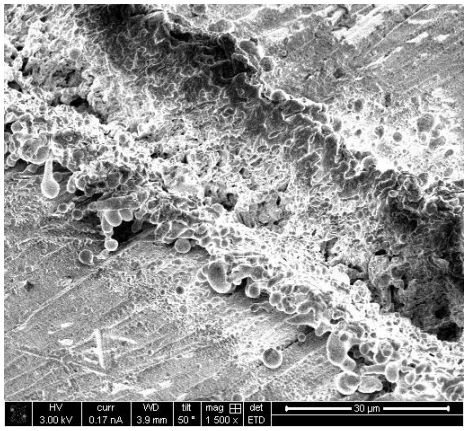

Figure 5-15: 20 Watts 5,000x Magnification

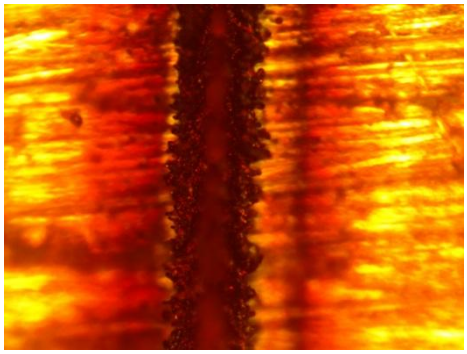

Figure 5-16: 25 Watts 20x Magnification

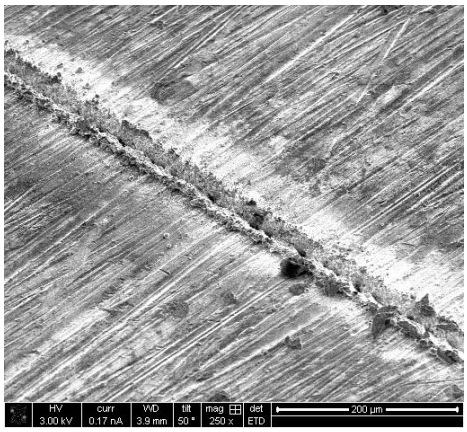

Figure 5-17: 25 Watts 250x Magnification

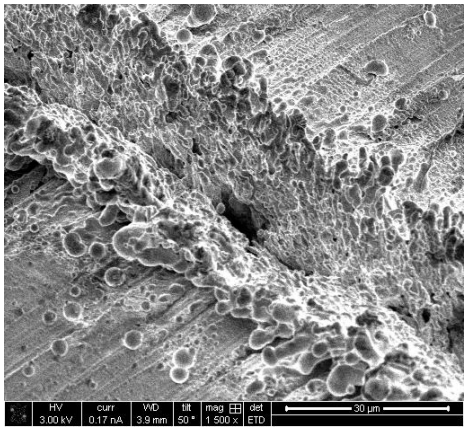

Figure 5-18: 25 Watts 5,000x Magnification

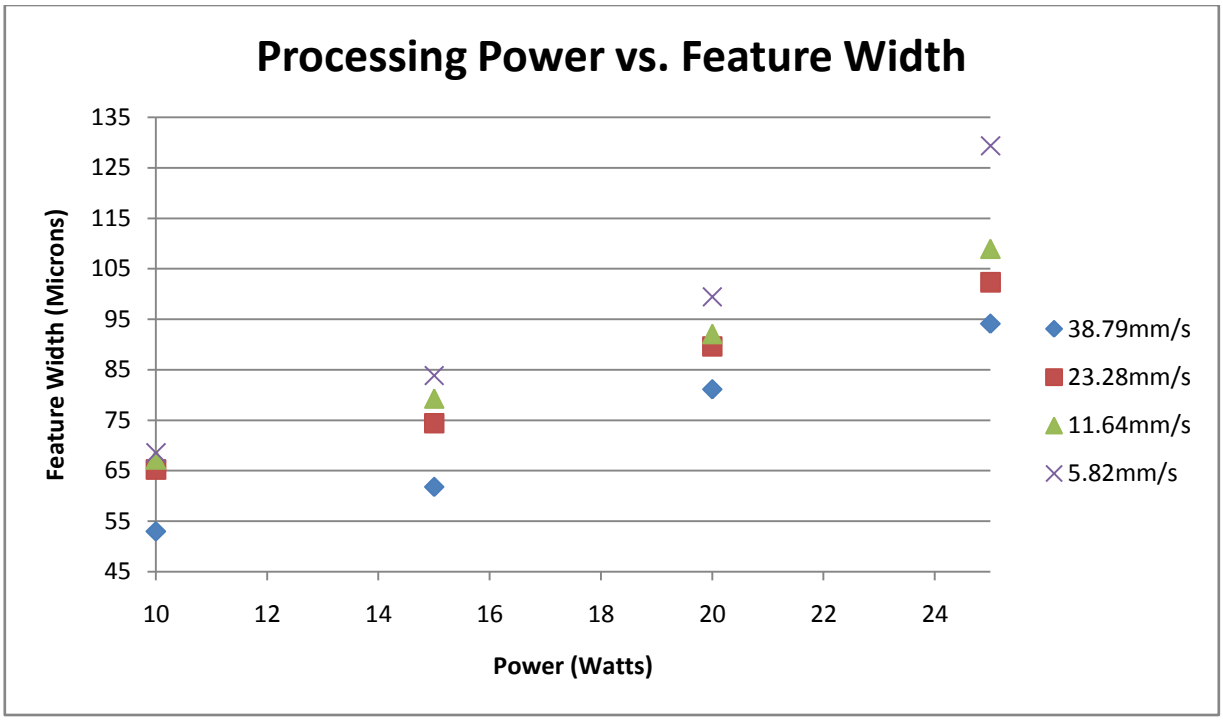

Figure 5-19: Processing Power vs. Feature Width

In analyzing the results, it is evident that for slower speeds, there is more ablation due to a larger number of pulses striking the specimen per unit length. Increasing the power will also increase the ablation rate because higher energies are being applied to the materials surface. It is clearly visible that the slowest speed and the highest power results in the highest rate of ablation, whereas the lowest power at the highest processing speed will result in the lowest ablative rate. As the speeds increase, the thickness of the processed pattern decreases and the visible blackening of the surface will also decrease.

The width versus power has Gaussian profile dependence. In examining the depth versus power relationship, it is evident that as power increases, the depth will not follow the exponential decay as defined in Beer's Law. Plasma interaction must be considered for feature quality. The generated plasma causes the re-deposition of material and as the power increases, the depth of the pattern will decrease. Speed versus power is related to the number of pulses per unit length. For fast speeds, there are less pulses, which results in a lower amount of energy transfer, whereas slow speeds increases the energy transfer. Either extreme of low speed and high power, or high speed and low power will result in poor processing quality as shown in Figure 5-20 and Figure 5-21 below.

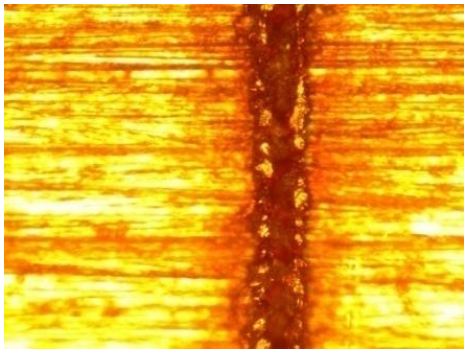

Figure 5-20: 10 Watts 38.79mm/s

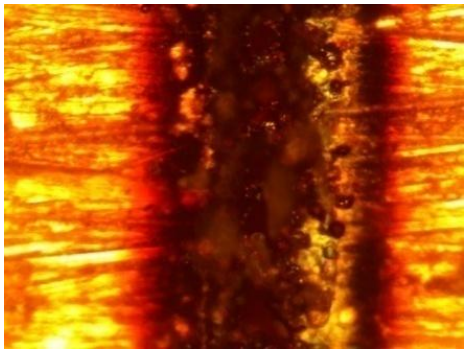

Figure 5-21: 25 Watts 5.82mm/s

5.3.3 Parametric Analysis of Power and Frequency Variations

In this experiment, patterns were processed at a variation of powers and frequencies. Adjusting the frequency would change the pulse energy and potentially result in a change in the appearance of the processed pattern. Figure 5-22 below tabulates the frequencies, power, current, and pulse energy for each pattern created. The processing speed remained constant for this experiment.

Pattern	Frequency [kHz]	Power [W]	Current [A]	Pulse Energy [µJ]
1	70	20.12	39.4	287.43
2	35	20.02	39.4	572.00
3	35	9.96	38.1	284.57

Figure 5-22: Process Data

For a frequency of 70 kilohertz and a power of 20 watts, the pattern created had smooth edges and was not burned as shown in Figure 5-23. Next, the frequency was halved to 35 kilohertz while maintaining power. This resulted in a doubling of the pulse energy. This increased energy at the same processing speed resulted in a severe blackening of the specimen as well as a degradation of the edges as shown in Figure 5-25.Figure 5-24 and Figure 5-26show the pulses per unit time based on the power and frequency. The same amount of energy is delivered to the surface, however the pulse energy changed.

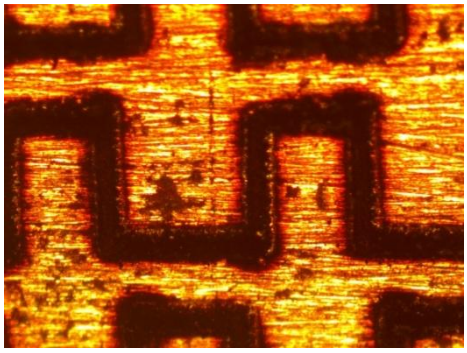

Figure 5-23:70kHz – 20W - 287µJ – 2.91mm/s

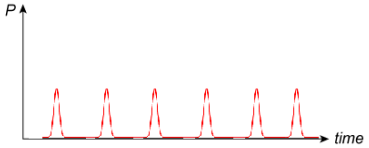

Figure 5-24: Pulses per unit Time

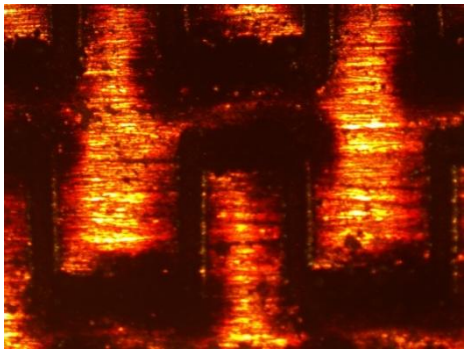

Figure 5-25: 35kHz – 20 W – 572 µJ – 2.91mm/s

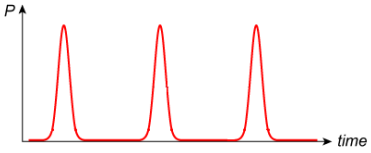

Figure 5-26: Pulses per unit Time

Lastly, the frequency was held at 35 kilohertz and the power was decreased to 10 watts. This led to pulse energy to within 3 micro joules of the initial processed pattern. This pattern was then compared with a processed pattern with the frequency, speed and power doubled. This led to the same number of pulses per unit length, and the same pulse energy. However, this shows process scalability by achieving the same processing parameters at different processing speeds.

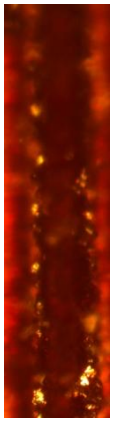

Figure 5-27: 70kHz – 20W - 287µJ – 5.82mm/s

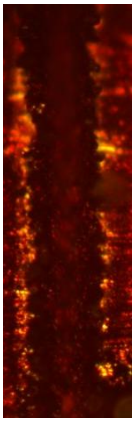

Figure 5-28:35kHz – 10W - 287µJ – 2.91mm/s

With the same pulse energy and pulse rate, the two features were not completely similar. These results can be attributed to a phenomenon known as pulse broadening. As the frequency of a laser increases, the pulse duration will slightly expand, which will change the heat flux onto the surface. This change in heat flux will result in a differing of processing quality.

5.3.4 Relationship between Compressed Gas Injection and Processing Efficiency

This experiment utilizes gas injection in an attempt to increase the efficiency of the laser processing. The experimental setup is shown below in Figure 5-29 with a zoomed in view in Figure 5-30. The same pattern, speeds, and power were utilized to see if there was an improvement.

The results for the patterns are given below in Figure 5-30. The pattern is visibly cleaner and less burned. During laser processing, the laser-material interaction point will cause a plasma generation. As the plasma expands, it interacts with the beam and this interaction will hinder the machining process. By introducing a propelled gas, provided it has enough momentum, will push the plasma away from the surface, thus providing a clear processing path and therefore improving the patterned feature. Practically, it would improve scribing performance and reduce the laser power cost and fundamentally it makes a difference in ablation plasma physics in practical scribing conditions. [23]

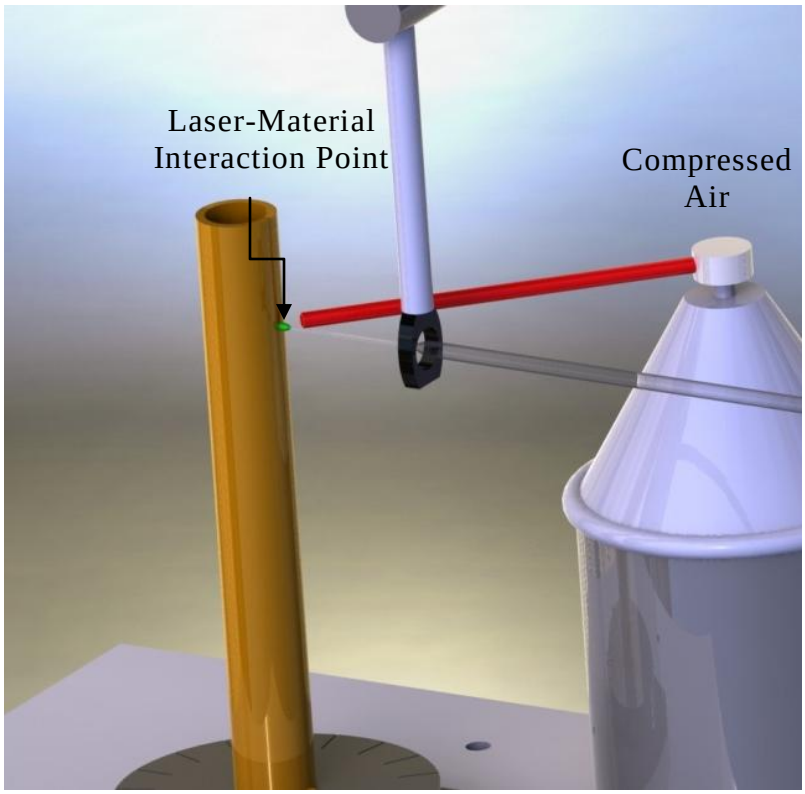

Figure 5-29: Compressed Gas Injection Schematic

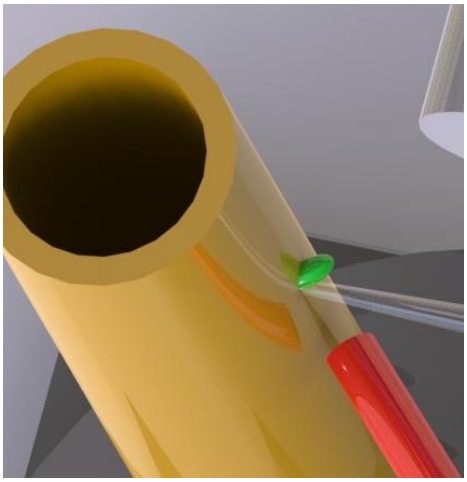

Figure 5-30: Plasma Removal

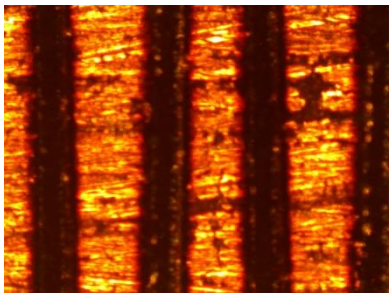

Figure 5-31: 25 Watts – No Gas

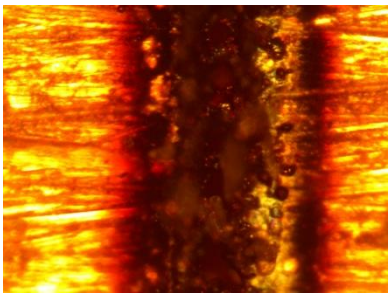

Figure 5-33: 25 Watts – No Gas

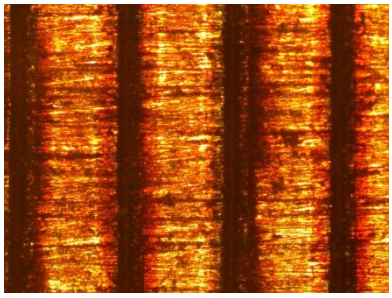

Figure 5-32: 25 Watts - Gas

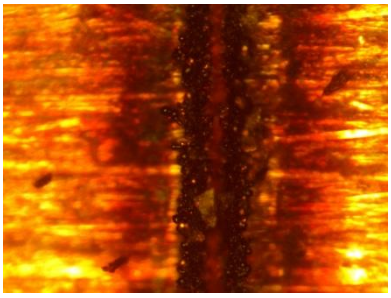

Figure 5-34: 25 Watts - Gas

Figure 5-31 and Figure 5-32 show the processed feature without compress gas injection whereas Figure 5-33 and Figure 5-34 show the results with compressed gas injection. The width of the processed feature without gas injection was measured as 208.38 microns whereas with gas injection it was just 93.66 microns. This shows that under practical scribing conditions, there is an evident increase in processing efficiency with the introduction of a compressed gas.

5.3.5 Proof of Concept: Full Surface Patterning

This experiment was performed to test the validity of processing a full 360º of a cylindrical surface. This experiment required indexing a manual rotary axis 19 times to attain full feature patterning. Although the motion system has the ability to process a twenty degree range, which would require 18 total passes, the features did not take up the full range. Instead, each iteration processed close to 19º which led to the nineteenth manual index. Figure 5-35 is a schematic of the processing concept. Each hash mark on the rotary stage represents a 20º change in angle. To better visualize the rotation, a small extrusion was added at the base of the cylinder as well as displaying an index of more than 20º in the figure.

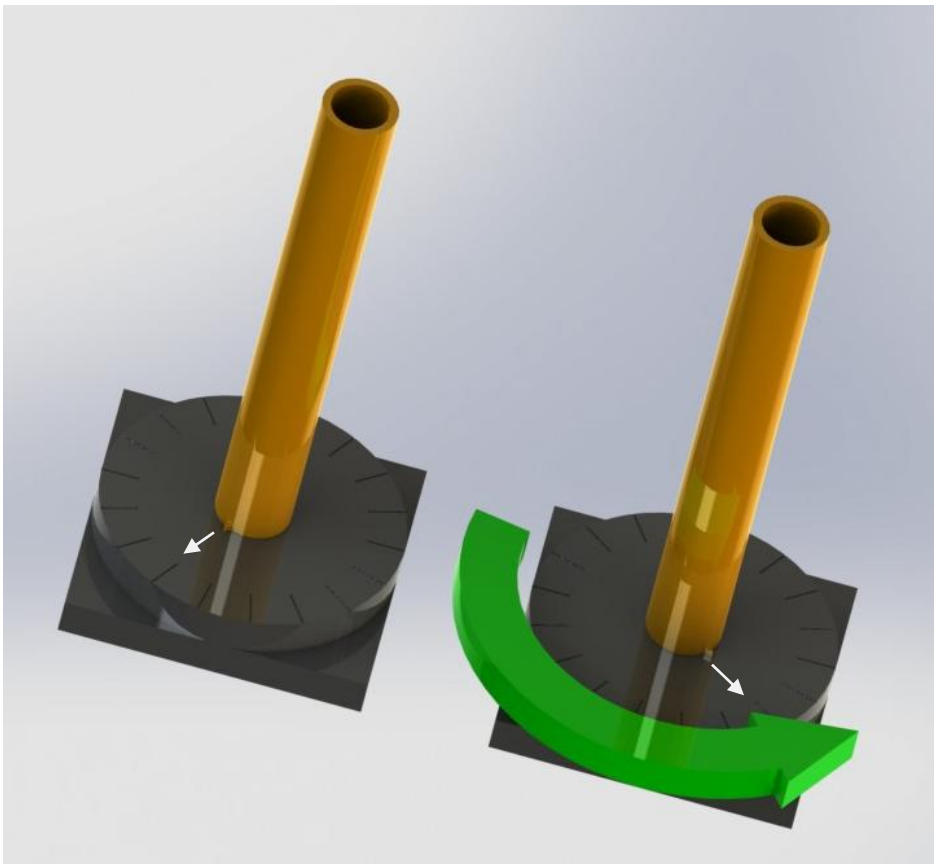

Figure 5-35: Full Surface Patterning Schematic

Beginning with an unprocessed copper tube, a square wave pattern with side lengths of 0.25mm was patterned. A total of 30 squares were made per vertical pass, with six vertical passes being processed per program iteration. This was run at a power of 10 watts and a speed of 1mm per second. Initially, at the conclusion of the program, the stage would be manually rotated 20 degrees. However, this left a small gap between program iterations. To fix this issue, the stage was rotated approximately 20 degrees, the shutter was opened to locate the spot, and then stage was reposition to restart the feature where the previous iteration had ended. This process drastically reduced the processing gap and in some sections portrays what the patterning would look like if the motion system had a larger range of motion.

Each iteration of the program took approximately 20 minutes to complete. This included 17 minutes of actual processing time, plus an addition three minutes for manual indexing and the re-initialization of the system. Figure 5-36 is an image of the final feature which was comprised of 3,420 square waves. Figure 5-37 shows the pattern dimensions.

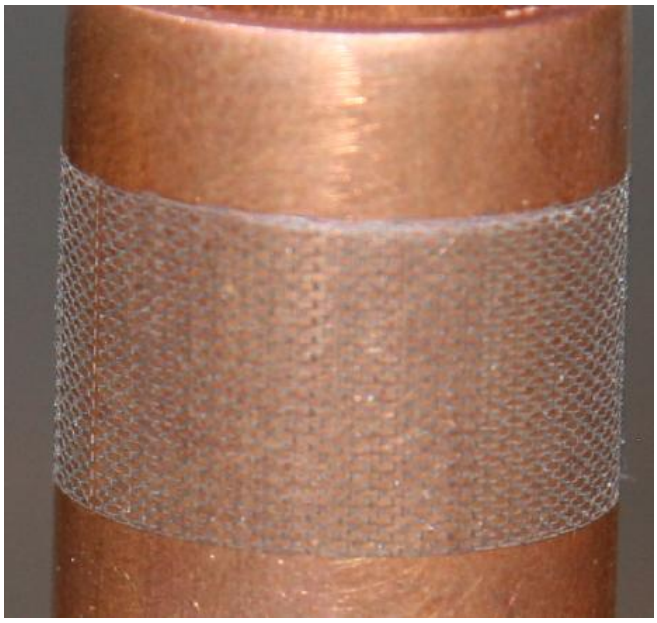

Figure 5-36: Full Patterning

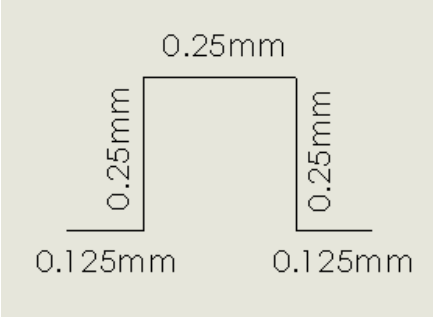

Figure 5-37: Pattern Dimensions

5.4 Cylindrical Patterning of a Thermal Spray Sample

This experiment entailed processing a proprietary thermal spray coating. This coating was designed a process in the Center for Thermal Spray Research at Stony Brook University. The sample was 20mm in diameter and 37mm tall with a wall thickness of almost 2mm. The purpose of this experiment was to test the feasibility of laser processing this specimen and see if it was possible to pattern. The specimen was too short to be mounted in the chuck jaws and be processed, so it was affixed to another sample to enable processing, the setup is shown below in Figure 5-38.

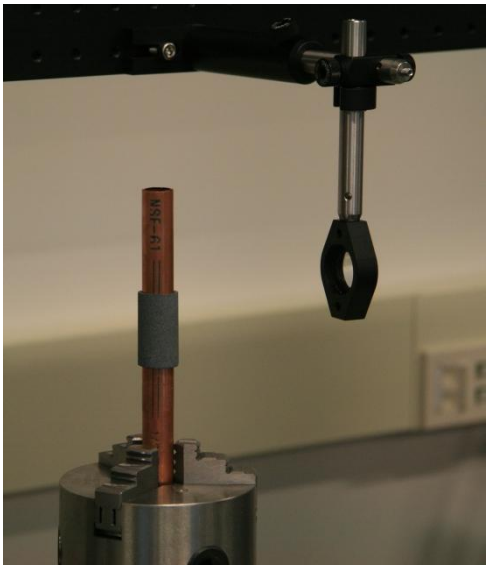

Figure 5-38: Thermal Spray Sample

All previous experiments were conducted on copper samples which were highly reflective. Due to this fact, the starting power level for processing was decreased from 25watts to 10watts. Even at ten watts, the power was too great. A large spark (Figure 5-39) was created on the surface of the sample and when processing was completed, the pattern was unrecognizable. The same case was present when the power was decreased to five watts. The power was then halved again to 2.5 watts and was more successful; however, the features were too small (0.25mm sides) to be visible. These three trials are shown below in Figure 5-40.

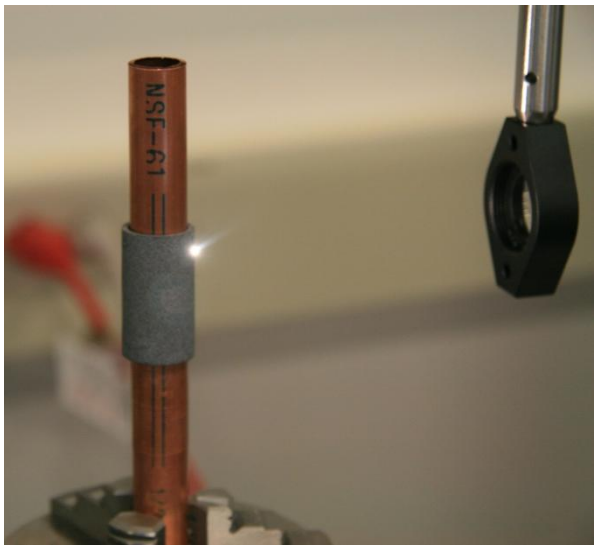

Figure 5-39: 10 Watt Spark

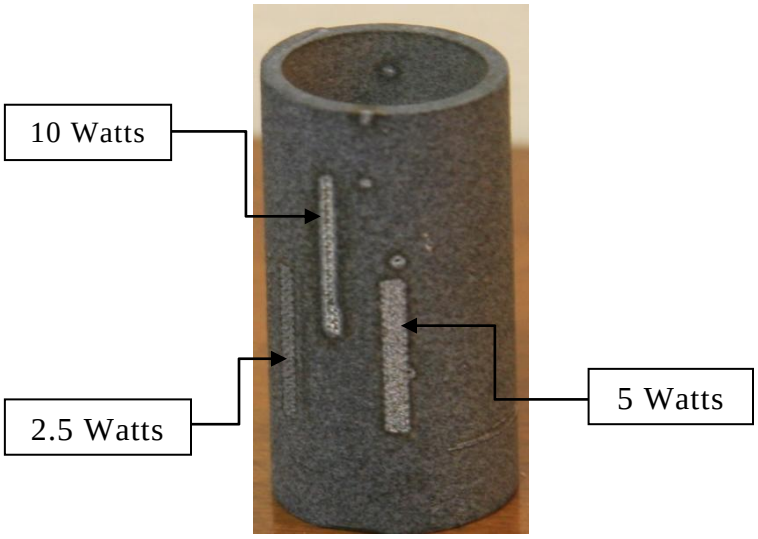

Figure 5-40: Trials 1-3

The next set of trials doubled the feature size from 0.25mm sides to 0.5mm sides. The power of 2.5 watts was re-examined, as well as new powers of 3.15, 3.75 and 4.1 watts. The clearest pattern was obtained at power of 3.75 watts. The pattern was then expanded, and repeated as a means of improved visualization. Figure 5-41shows trials four through seven with their respective powers and Figure 5-42 shows the expanded pattern for the 3.75 watt case.

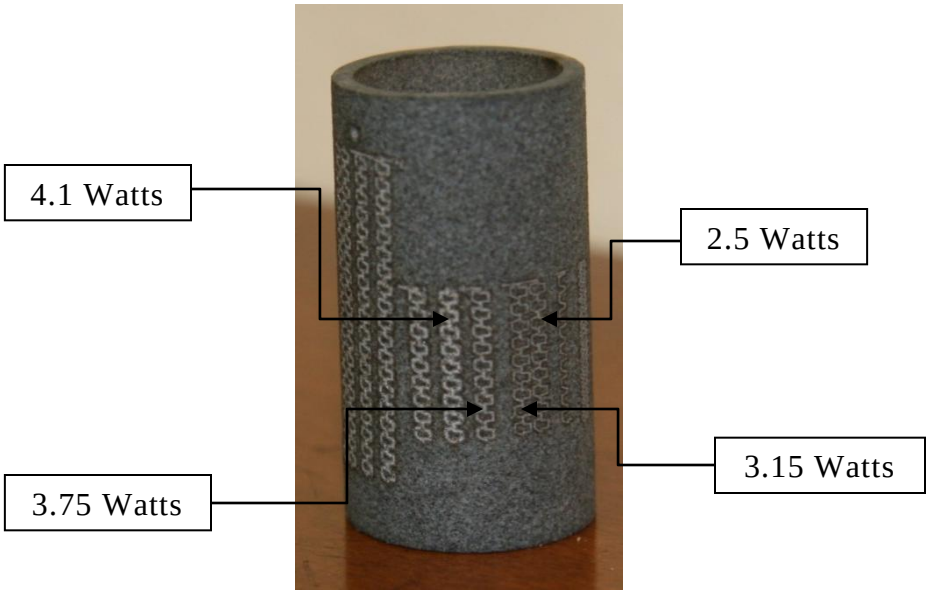

Figure 5-41: Trials 4-7

Figure 5-42: 3.75Watt Expanded Pattern

It was determined that high power levels were far too destructive in machining this specimen. Any power above 4 watts would melt the surface and degrade feature recognition, at higher powers such as five or ten watts, the material appears melted and is unrecognizable. For a power of ten watts, there was a slight darkening of the interior surface but for lower powers there was no visible change. A focusing pulse was used at 25 watts and that left a visible mark on the cylinders interior as seen in Figure 5-40.

5.5 In Situ Process Monitoring from Laser Induced Plasma Emission

This experiment examines the theory of Laser Induced Breakdown Spectroscopy that was outlined in Chapter 2.3. During the processing of the copper samples, a distinct green emission was visible as shown below in Figure 5-43.

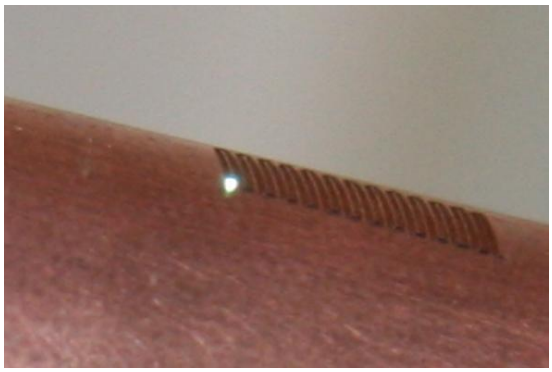

Figure 5-43: Visible Green Emission

Using a fiber optic cable to collect light from the laser-material interaction location as shown below in Figure 5-45, the emitted light was transmitted to a spectral analyzer that could accurately determine the wavelength of said light. This spectral analyzer was not as precise as the measurements we compared to; however this system has the ability to scan a much wider range of wavelengths. Figure 5-44 is a computer model of the LIBS experiment whereas Figure 5-45 is an image of the actual setup.

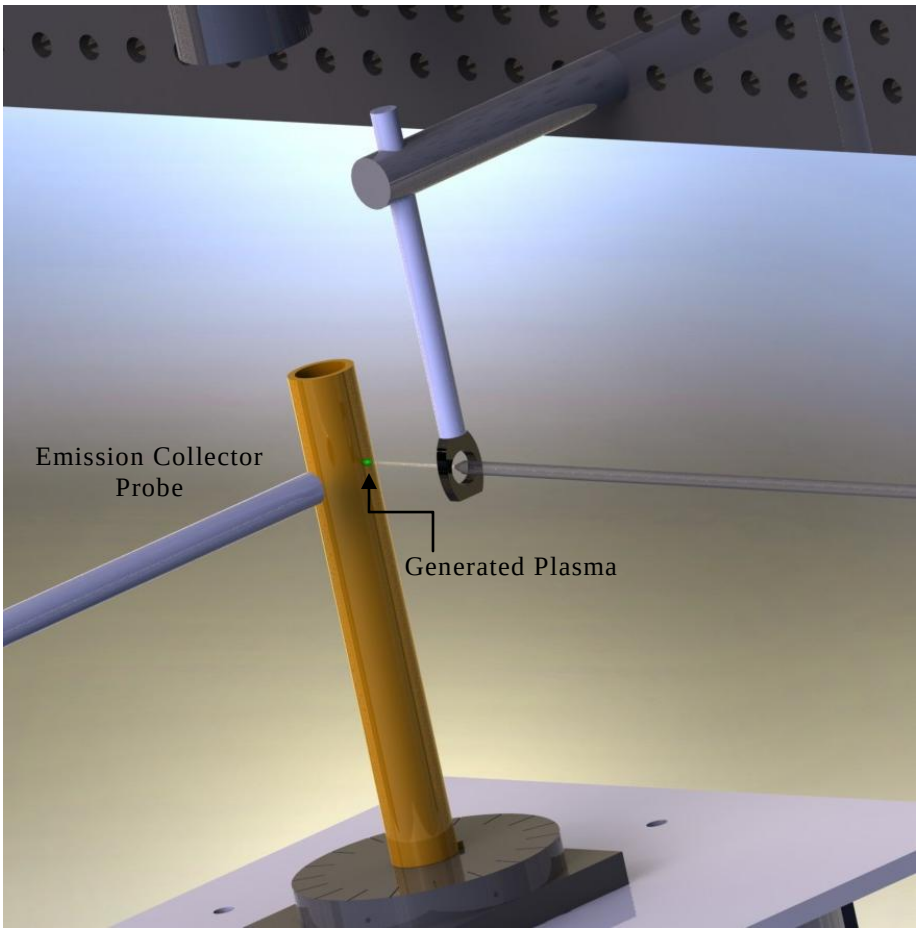

Figure 5-44: LIBS Model

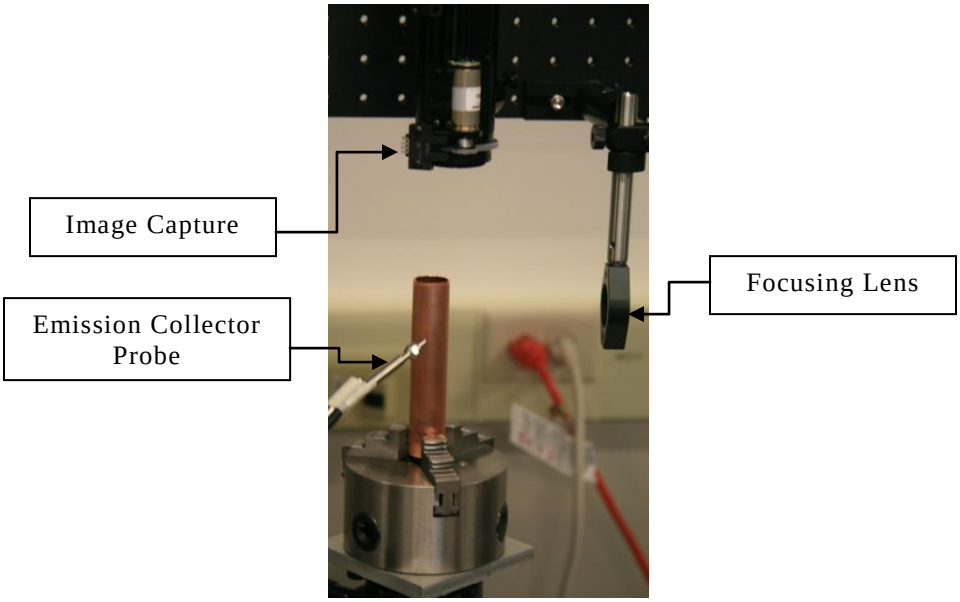

Figure 5-45: LIBS Setup

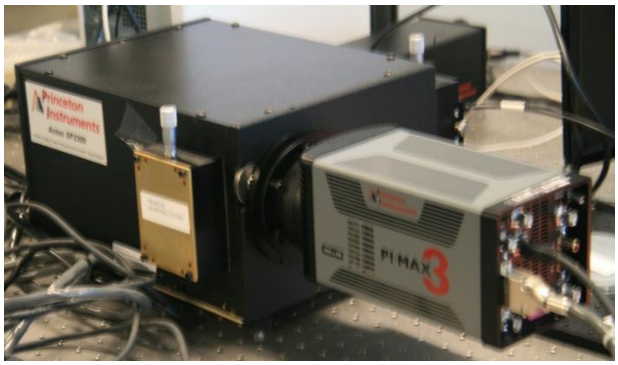

Figure 5-46: Spectral Analyzer

As shown in Figure 5-47, the spectrum of emission for copper is between 500 and 560 nanometers with peaks located at around 330 and 520 nanometers. These wavelengths correspond to green light. Figure 5-48 shows the results obtained from our spectral analysis. There are peaks located at wavelengths of 326.86, 514.73, 521.39 and 654.59 nanometers. This verifies that the material being processed is indeed copper. In addition to Figure 5-47, Peax 2.0 which is a database software that enables a user to search, identify and plot elements and molecules in a spectrum. The element database is the atomic spectra database from the National Institute of Standards and Technology (NIST.) [24] This software produces peaks located at wavelengths of 324.75, 327.39, 515.32, 521.82 and 647.02 nanometers in addition to a large number of other peaks we were unable to measure with the accuracy of our system.

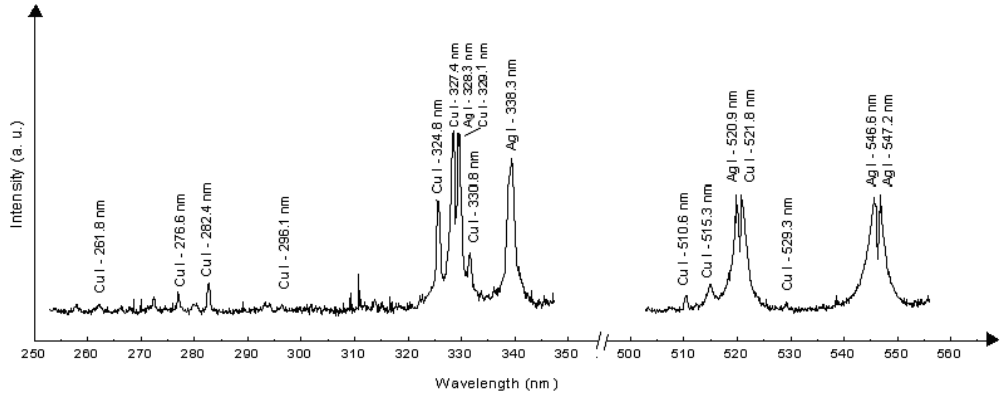

Figure 5-47: LIBS Spectra of Copper[25]

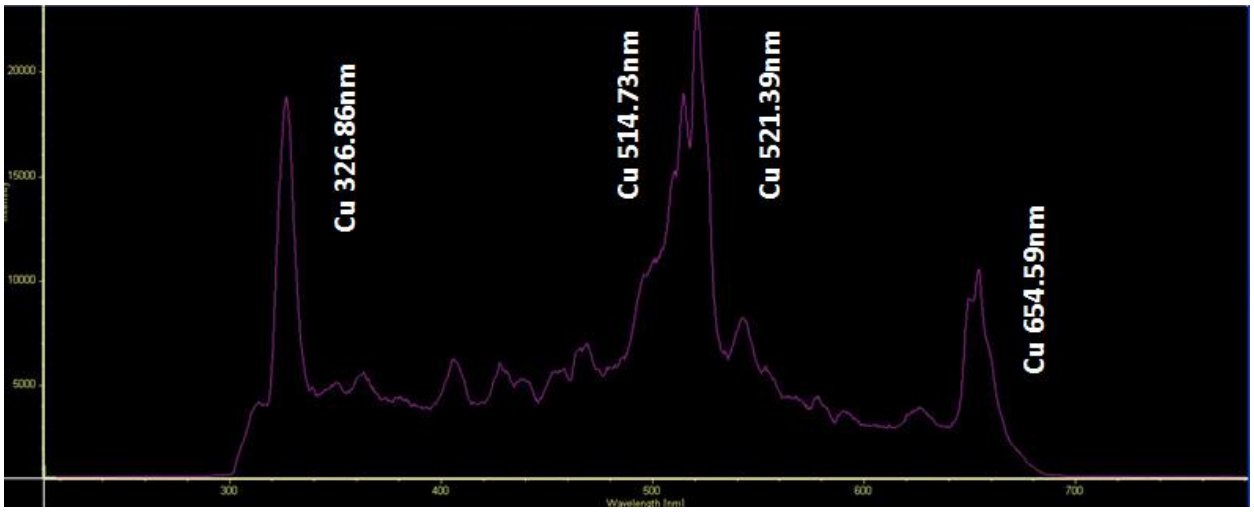

Figure 5-48: LIBS Spectra of Copper Sample

The next samples we had were Galvanized Steel and Black Steel. Figure 5-49 below shows the spectral range of a steel sample as obtained at the University of California, Irvine. Both Figure 5-50 and Figure 5-51 are very similar as they are both steel samples. Black steel shows peaks at 361.15, 374.05, 382.47, 523.61, and 549.68 nanometers whereas galvanized steel displayed three peaks at 379.10, 524.17 and 549.13 nanometers. In comparing them with the spectra shown in Figure 5-49, the peaks line up at the wavelength of 525nm. Both the black steel and galvanized steel samples show emissions that vary from three to four hundred nanometers in wavelength, they are much more intense than what was measured in the experiment at UCI. Utilizing the Peax Software, there were peaks located at wavelengths of 385.99, 371.99, 358.11, 374.55, 516.74 and 526.95 nanometers. These peaks reside within a few nanometers of those measured. Since it is known that these samples are not pure steel, the similar form of the spectra for the two samples shows that they are steel.

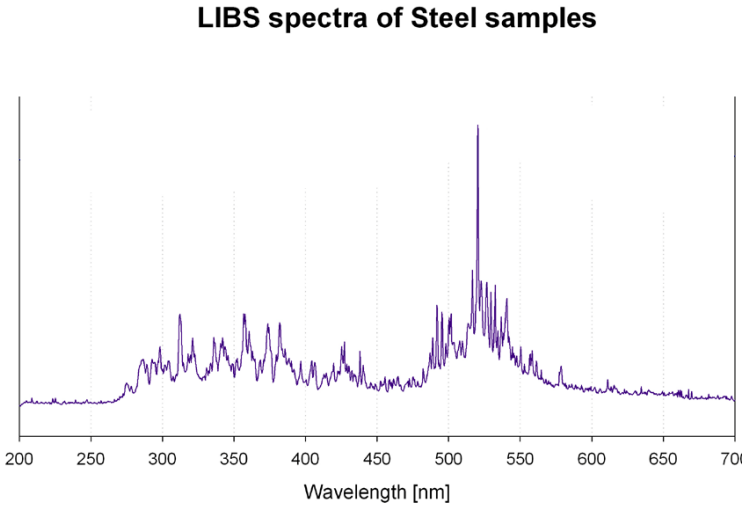

Figure 5-49: LIBS Spectra of Steel

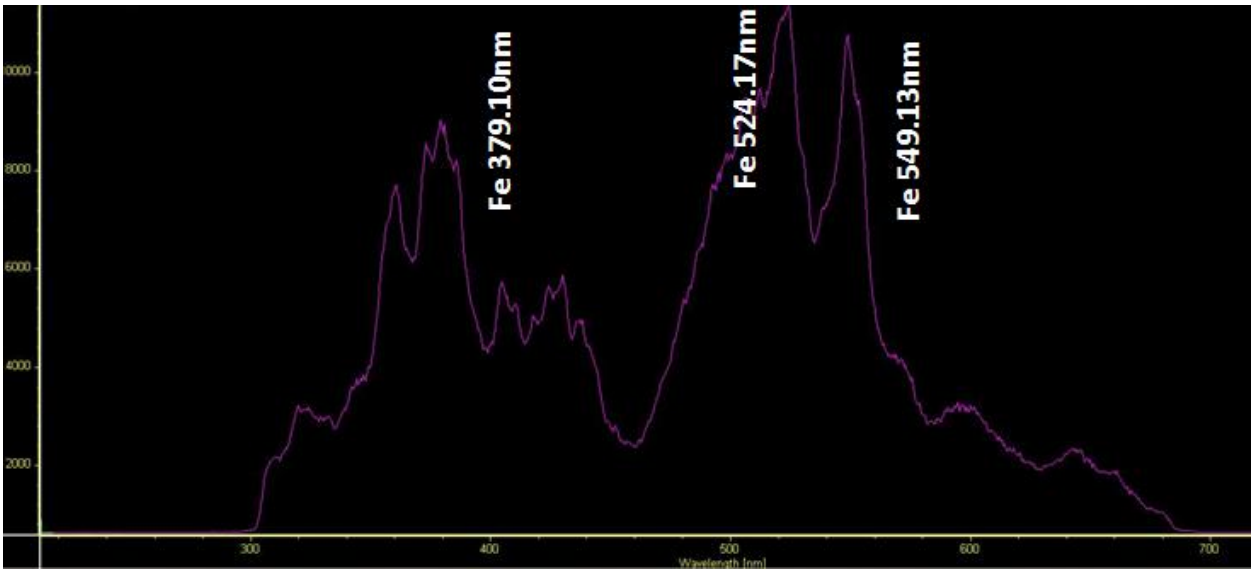

Figure 5-50: LIBS Spectra of Galvanized Steel Sample

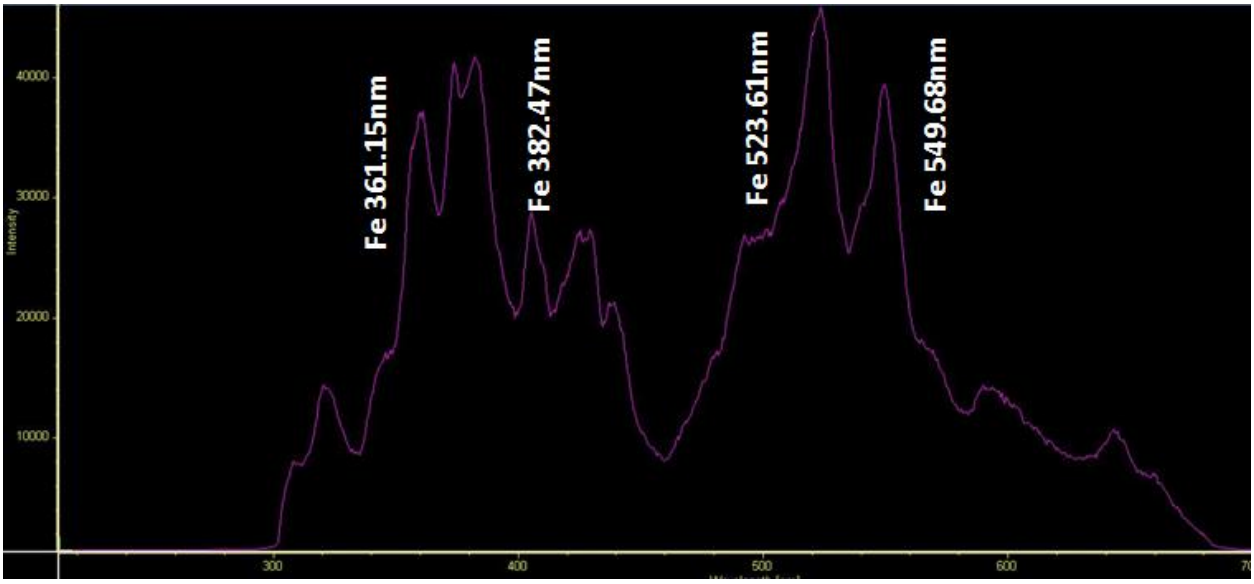

Figure 5-51: LIBS Spectra of Black Steel Sample

Finally, the thermal spray sample that was explained in experiment eight was tested for its spectra. Although the exact composition of this proprietary sample is not known, we were told that there was an abundance of aluminum present. Figure 5-52 below shows the known LIBS Spectra for Aluminum and Figure 5-53 is the measured spectra of the thermal spray sample. Although the thermal spray sample did not have as many peaks as the known aluminum spectrum, the peaks at 396.74 and 618.97 nanometers were very similar to the Peax values of 618.36 and 396.15 nanometers.

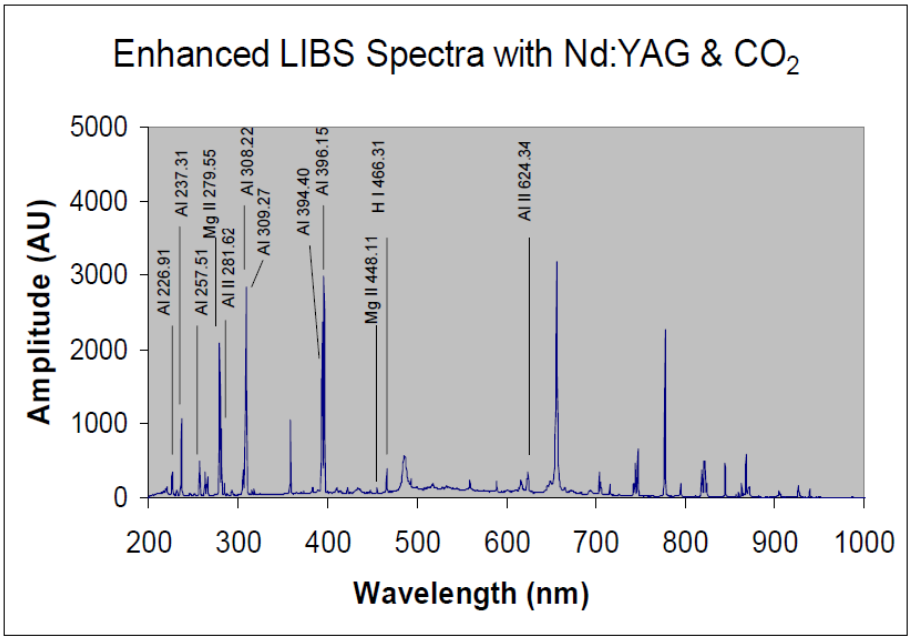

Figure 5-52: LIBS Spectra of Aluminum

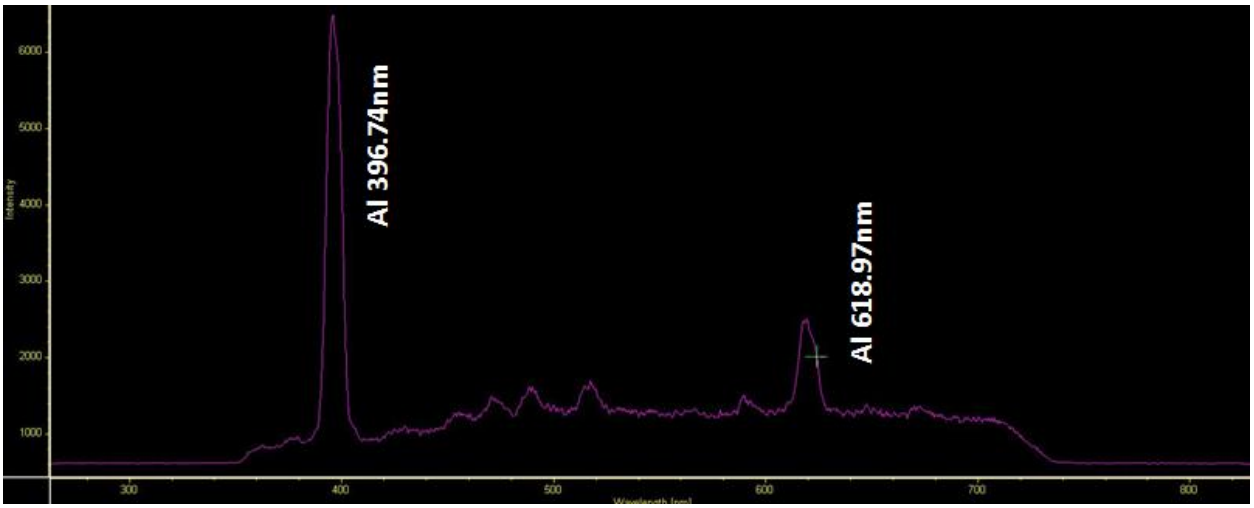

Figure 5-53: LIBS Spectra of Thermal Spray Sample

For a number of peaks, the database provided two peaks of similar wavelengths, however; the measured value yielded a single peak that resided between the known peaks. This was caused by a coarse grating being used and the peaks were absorbed into one another.

5.6 Visualization of Ablation Plume by Ablation Induced Plasma Emission Imaging and the Resulting Pattern Quality

This experiment was an analysis of plasma generation on a cylindrical surface. To perform this experiment, the addition of a magnified camera was required. This camera was mounted directly over the laser-material interaction point in order to capture images of plasma generation. Figure shows an overall view of the experimental setup. The camera was mounted to a manual two axis stage to enable camera to be focused in the correct location. The experiment setup is shown below in Figure 5-55.

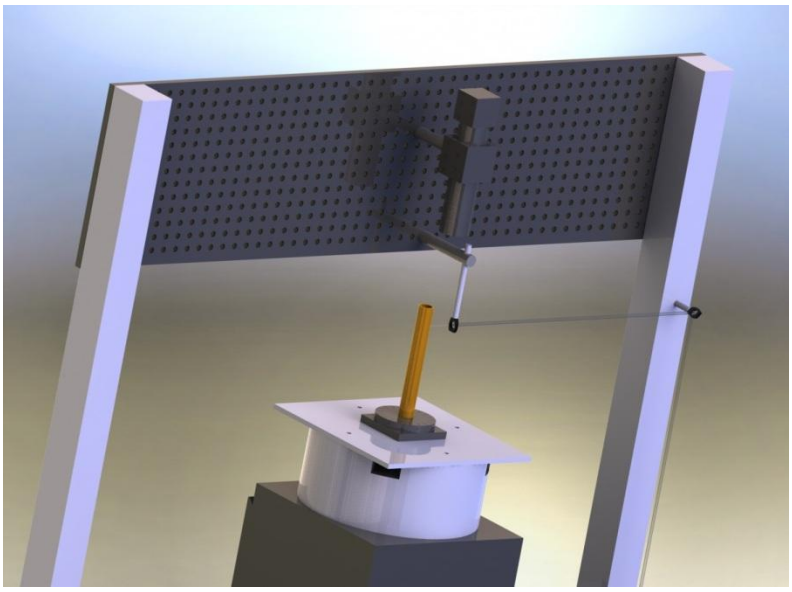

Figure 5-54: Camera Viewpoint

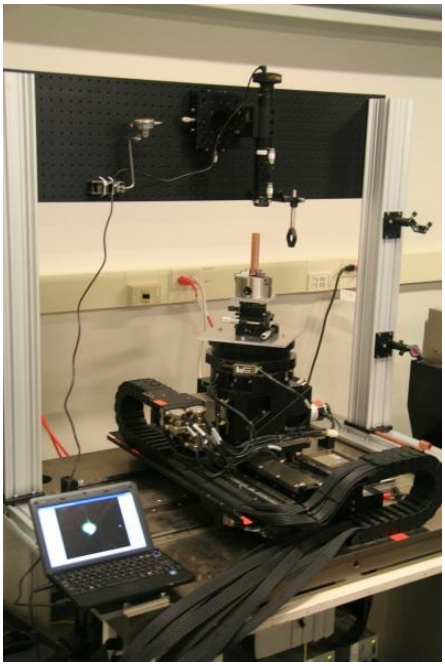

Figure 5-55: Plasma Generation Setup

This experiment was designed to measure the angle of plasma generation based on the incident angle of the processing laser. A copper surface was machined at a variety of angles to determine the direction of plasma generation. Figure 5-56 through Figure 5-59 illustrate the incident beam locations for the four performed trials.

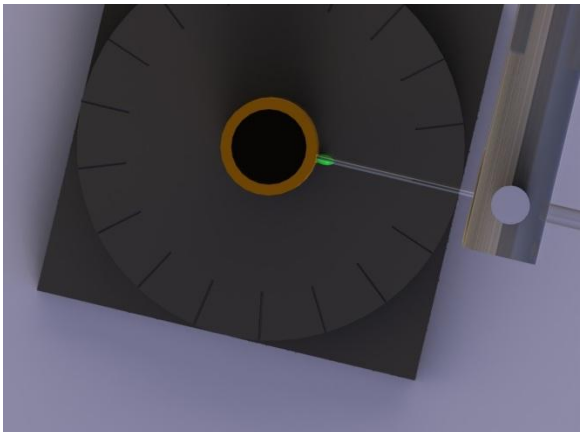

Figure 5-56: Trial 1 Beam Location

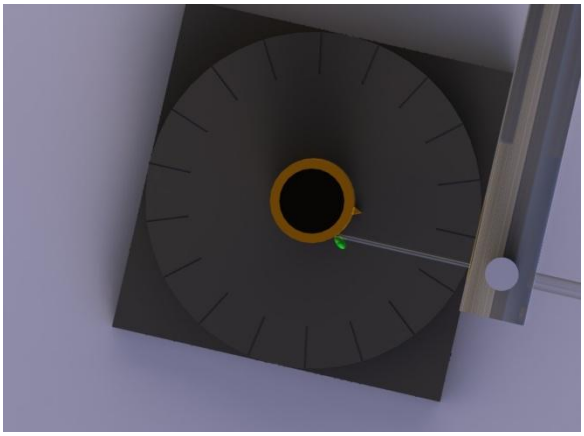

Figure 5-58: Trial 3 Beam Location

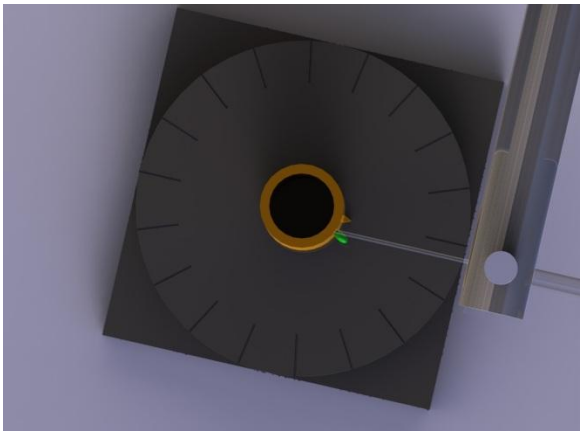

Figure 5-57: Trial 2 Beam Location

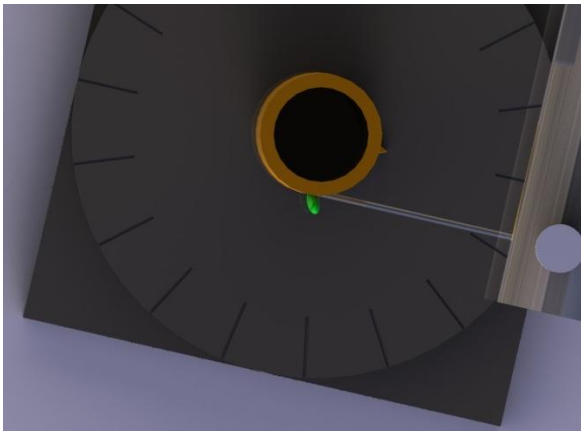

Figure 5-59: Trial 4 Beam Location

Trial one impacted the copper cylinder at a near right angle. Figure 5-61show that the direction of plasma generation is in the same direction as the incident beam. Essentially, the plasma is being generated in a direction normal to the surface of impact. Figure 5-61through Figure 5-64on the following pages show the results for the four trials in a number of images.

In trial two, Figure 5-62corroborates the results shown in Trial 1. Based on the direction of the incident beam, the plasma would be generated normal to the surface of impact. The results are similar in trial three where Figure 5-63shows the plasma generated at a reflected angle. The same results are shown for Trial 4 in Figure 5-64.

Upon Further investigation, the beam could be seen in some images. However, since the beam is Infrared this was in need of explanation. As plasma is generated, it expands in all directions as it cools. As it expands toward the direction of the incident laser, the beam will react with the expanding plasma and reheat the material plume. This will generate another instance of green emission.

This reheating along the laser trace can be used to explain the varying angles of plasma generation. Images in which the laser trace is less visible will result in a larger plume being generated as shown in Figure. This minor interaction with the plasma allows maximum energy to be directed onto the surface which results in a higher temperature and expanding plasma plume.

Figure 5-60 below demonstrates the visual conventions used to explain the trial results. The incident laser beam is represented by an arrow, and the tangential surface is represented by a line. The laser ablation plume is visualized through emission from a plasma state plume. This emission is dominated by an approximate wavelength of 520 nanometers. This is the atomic transition peak for copper and this wavelength corresponds to green light.

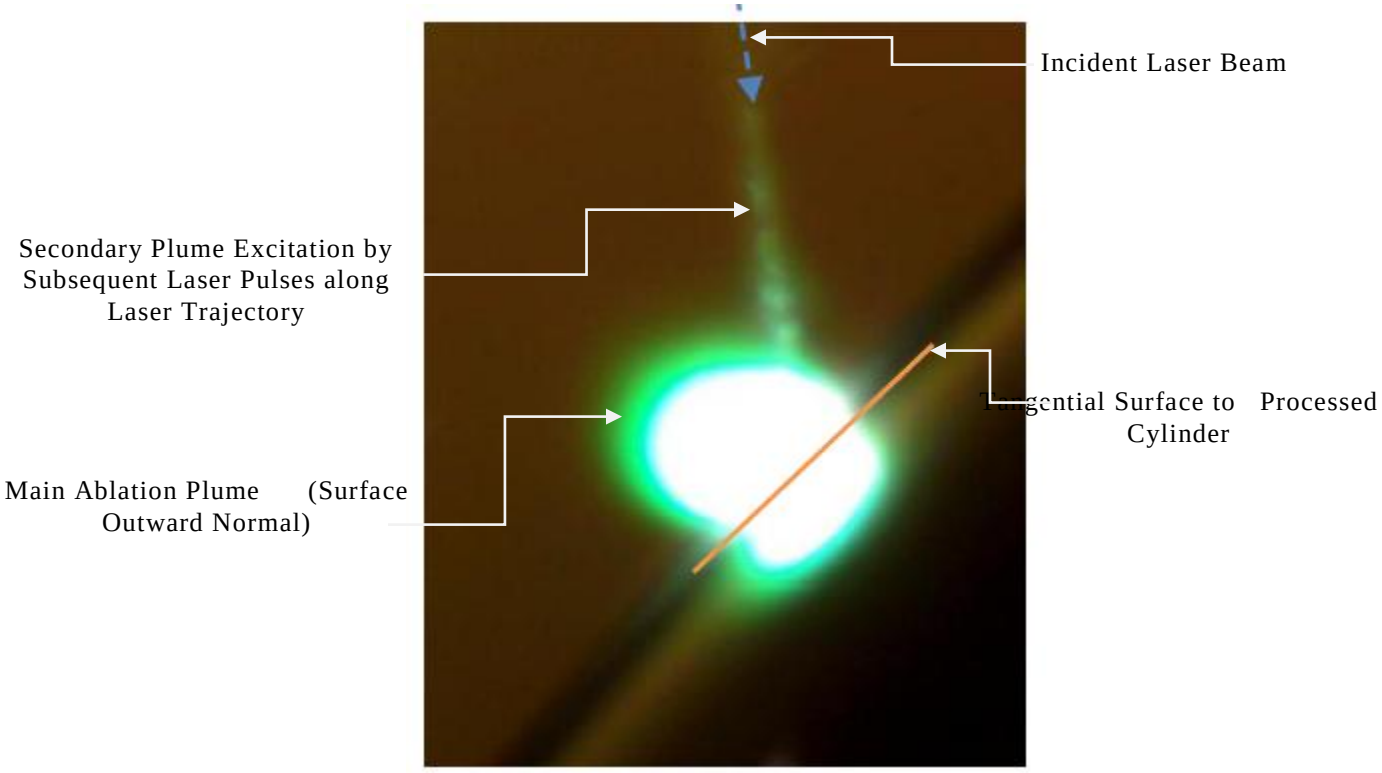

Figure 5-60: Plasma Generation Explanation

Trial 1 impacts the surface at a normal incidence. At this point the laser-plasma interaction is increased which results in a worsening of machining quality. As the trials progress, the laser reflection from the sample increases to a maximum in Trial 4, which

corresponds with an increase in wasted energy. With further analysis, this data can be used to optimize machining efficiency with respect to machining volume and laser power in addition to overall machining quality. Figure 5-61 though Figure 5-64are all of the same scale for accurate visible comparisons of plasma generation.

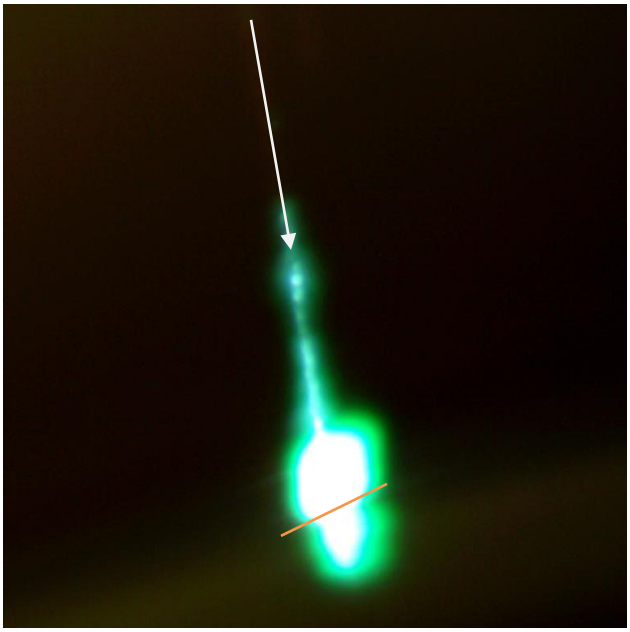

Figure 5-61: Generated Plasma Trial 1

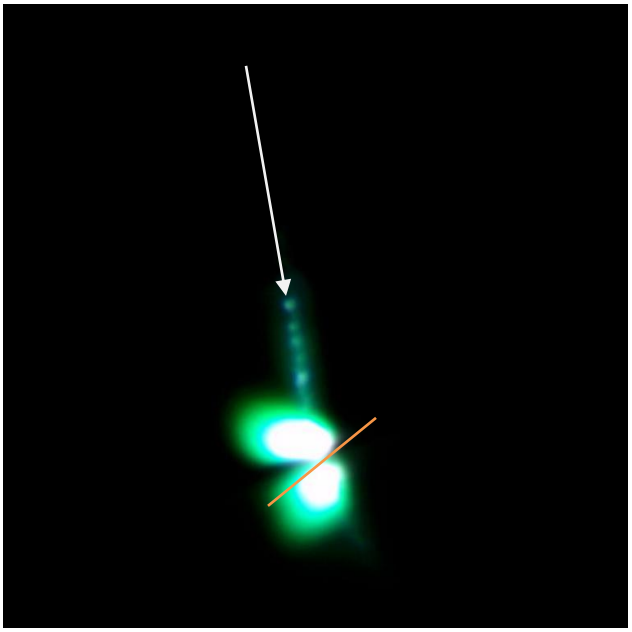

Figure 5-63: Generated Plasma Trial 3

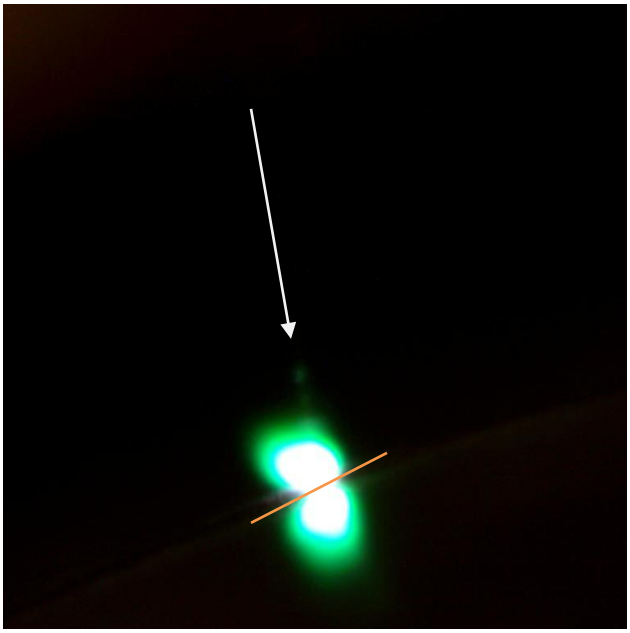

Figure 5-62: Generated Plasma Trial 2

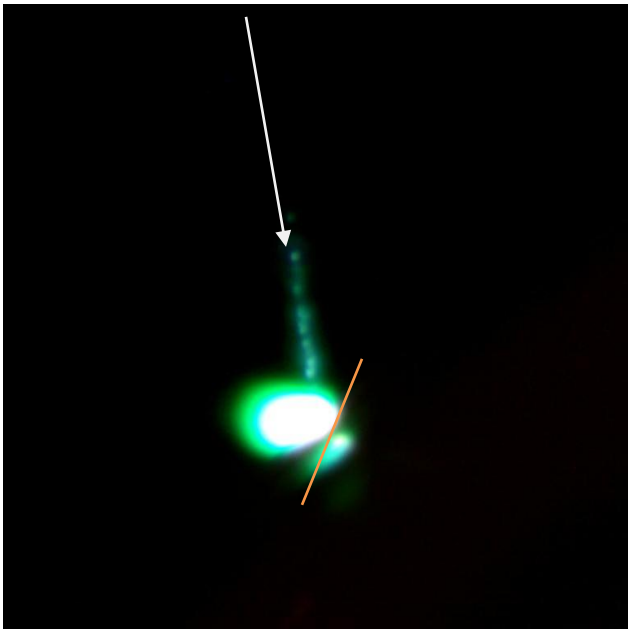

Figure 5-64: Generated Plasma Trial 4

5.7 Rapid Pattern Transfer Results by Subsequent Imprinting Processes

This experiment was designed to test the practicality of rolling the patterned cylinder across a flexible polymer to see if the pattern would be transferred. For this experiment, three patterns were made at a frequency of 70 kilohertz and varying the power between approximately 11 watts, 20 watts and 26 watts. The data is tabulated below in Figure 5-65. Figure 5-66 is a schematic of the feature transfer technique.

Pattern	Power [W]	Current [A]
1	10.82	38.0
2	20.08	39.4
3	25.60	40.5

Figure 5-65: Rolling Pattern Data

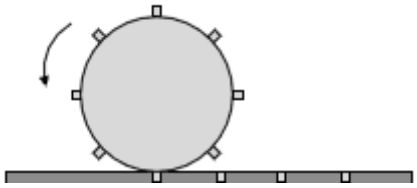

Figure 5-66: Pattern Transfer Technique[26]

Figure 5-67 is an image of the transferred patterns onto the flexible polymer.

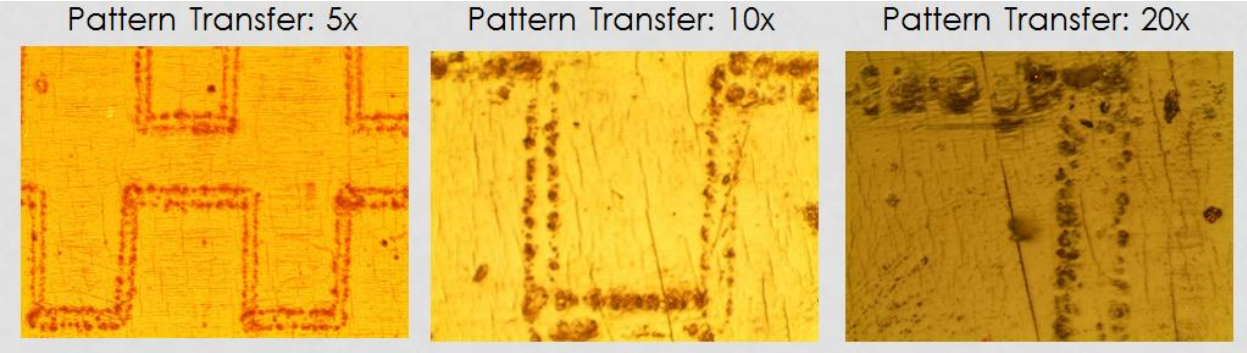

Figure 5-67: Transferred Patterns

Part of the pattern was indeed transferred, but it was not as expected. During the laser processing, a buildup of material was generated on either side of the beam path as shown in Figure. This build up was the feature that was transferred to the polymer. Computer models were generated to aid in the explanation process. Figure 5-68shows a processed linear pattern and Figure 5-69 shows the cross section of this pattern.

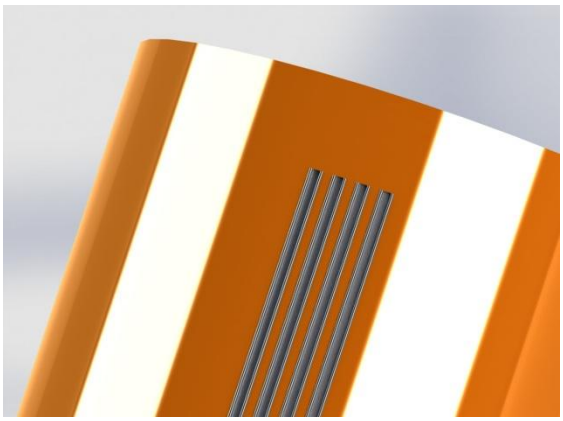

Figure 5-68: Processed Pattern

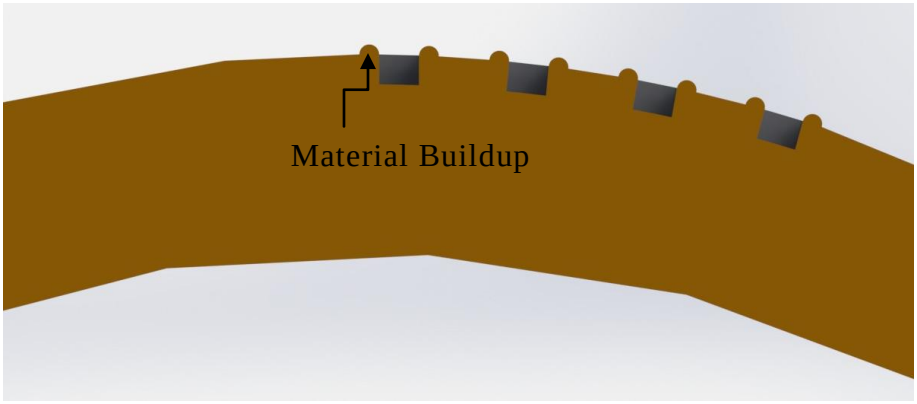

Figure 5-69: Cross Section of Processed Pattern Model

As this pattern was rolled onto the flexible polymer, the material buildup was transferred as shown in Figure 5-70 where the desired pattern was not transferred at all. This still produces the outline of the pattern but the correct feature was not transferred.

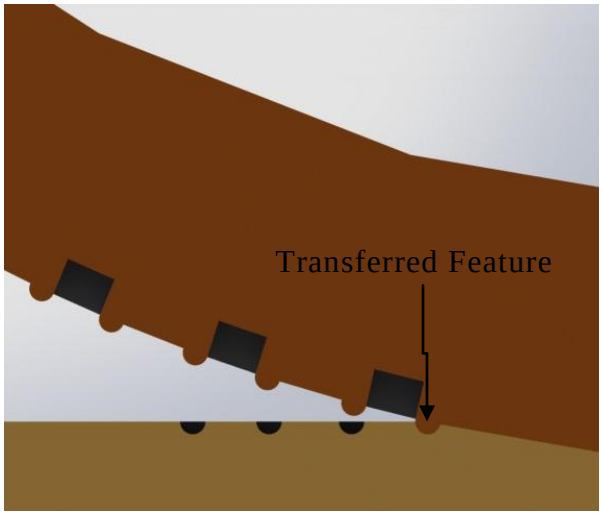

Figure 5-70: Pattern Transfer Model

Experiment five was performed in order to more readily examine a better feature transference. In looking at the higher magnifications, there are small copper particles visible within the material. For the higher powered features, the pattern was more visibly transferred to the polymer and remained after 24 hours.

This experiment arose from the shortcoming of experiment four. Since the only pattern that was transferred was caused by elevated features created during processing, it was desired to transfer a pattern that had the correct cross section. To accomplish this task, it was necessary to ablate a large amount of material from the cylindrical surface, while leaving small, unprocessed features that would then be used to indent the polymer.

Again, a computer model was generated to aid in the explanation of the experimental process. A large amount of material was ablated to decrease the surface height. In the center of the ablated materials, lines were left unprocessed. These lines would be the feature to be transferred as shown in Figure 5-72.

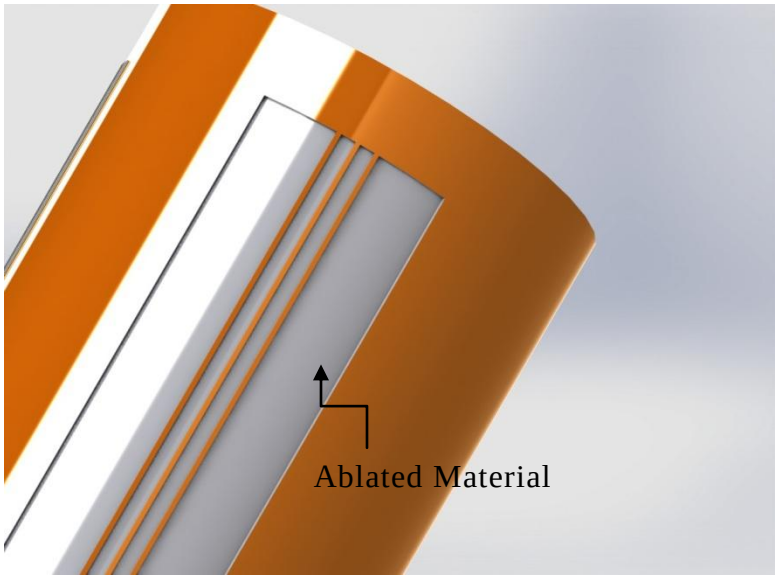

Figure 5-71: Processed Cylinder Model

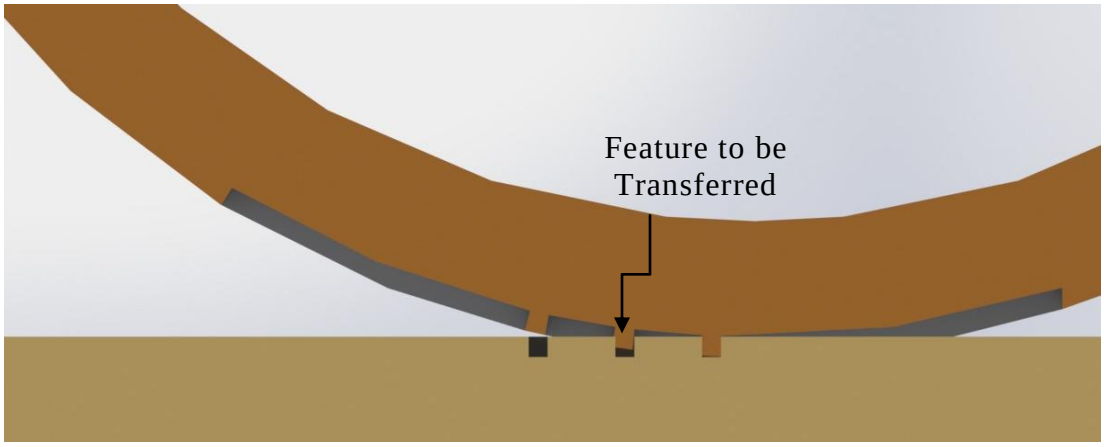

Figure 5-72: Feature Transference Model

Three lines were processed. Line one has a thickness of 0.05mm, Line two has a thickness of 0.1mm and line three has a thickness of 0.2mm. Since the surrounding area has been processed, it will reside at a lower level. Due to this fact, as the pattern is being transferred, the remaining line will be elevated, potentially allowing the pattern to be transferred more precisely.

The sample was heated to temperatures of 250and 350 degrees Fahrenheit prior to pattern transfer by means of a heat gun. The heat gun produced hot air which was not visible to the naked eye; the red flame in the figure is a visual aid only. Once heated, the same process outlined in Figure 5-66 will be followed to transfer the pattern. Coinciding with previous experiments, only the sharp remains of the ablated material was successfully patterned onto the polymer. None of the three patterned lines were sharp enough to puncture the surface causing the pattern to remain. Figure 5-73 shows the subsequent imprinting process. The image on the left is the processed cylinder whereas the right image in the transferred pattern.

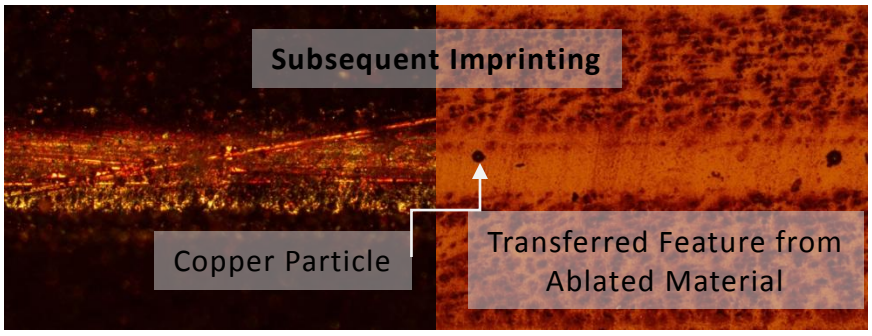

Figure 5-73: Subsequent Imprinting

6 Future Applications and Studies

This chapter considers future applications and studies for the various experimental results and concepts discussed. The future for cylindrical patterning is only just beginning. Currently, for much of the cylindrical rolling industry, the actual cylinder is not patterned itself. Instead, a flat flexible metal or polymer will be patterned and then adhered to the cylindrical surface. This step makes this process less desirable than a pattern that is correctly machined onto a cylinder. The potential for a loss of adhesion is always present and could severely damage any high speed operation if it were to come undone. Two prime examples of flat plates being formed around a cylinder are used in the processing of currency and the printing of newspapers.

On the smaller scale, micro and Nano-scale patterning is achieved via a step and repeat process. [27]Replacing this step and repeat process with a constant rolling device would drastically increase the speed of processing. Research into this area of study is currently being explored. [28], [29] Other techniques involve stepped rotating lithography and nickel plating as shown below in Figure 6-1. In this application, a photo resistive material is exposed around the circumference of the cylinder. This material is then developed, leaving a positive feature on the cylinder which is then electroplated. Stripping off the remaining photo-resistive elements yields a strong, positive pattern on the cylinder.

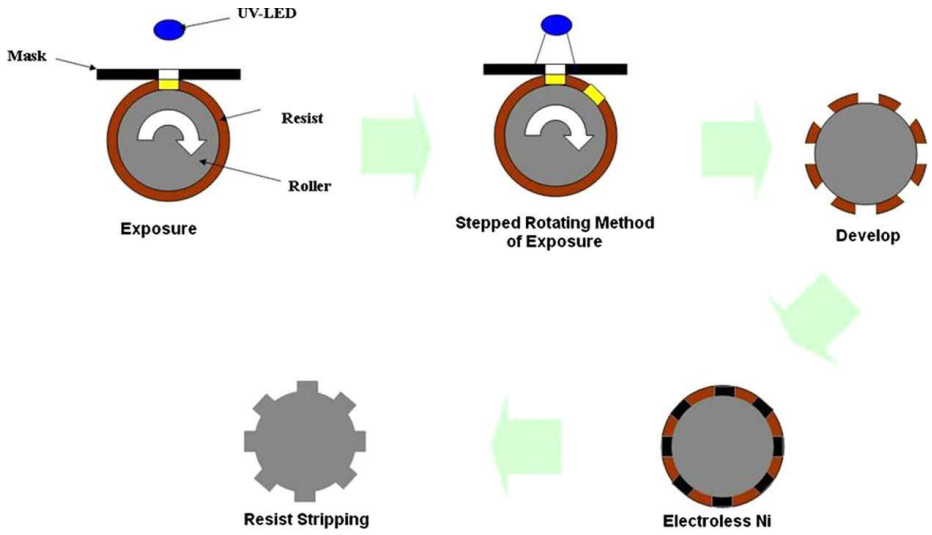

Figure 6-1: Fabrication Procedure via Stepped Rotating Lithography and Electroless Nickel Plating[30]

The rolling of micro scale features could allow for cheaper circuits, solar cells and various other implications in the electronics industry. Parametric analysis could determine what the ideal processing power, speed, and frequency would be for laser processing. Creating black copper on the surface of a cylinder would be ideal for use in evacuated tube solar collectors to more efficiently harvest the suns energy.

Surface patterning of cylinders can also better prepare the specimen for adhesion. The thermal spray sample will generally be applied to other surfaces. Pre-texturing of these samples could facilitate a stronger bond between the specimen and the applied coating. The patterning of the proprietary coating could have innumerable applications such as fuel cells, bio-fuel applications such as algae growth and various applications in thermo-electric devices.

Laser induced breakdown spectroscopy is an emerging technology that can determine a specimens composition with a laser strike. This can be used for many applications such as reverse engineering or material identification of a wide range of samples with a less destructive impact on the specimen. The largest use for LIBS is the determination of impurities within a material since the software has the ability to detect elements in the low

Finally, the fundamental knowledge that comes with understanding plasma generation has great implications. As experiments have shown, [23] the introduction of a compressed gas to force the created plasma buildup at the laser-material interaction point greatly increases the processing efficiency while decreasing the power required to achieve a specific result. In understanding the direction in which the plasma is generated could potentially remove the plasma from the equation by machining at an angle. This can also lead to Nano scale deposition in which another specimen is placed at a location in the direction the ablated material will flow.

The next step in this experiment would be to set up a shutter in conjunction with the imaging device. As the shutter is opened, the camera will snap an image that is at the exact moment the laser interacts with the material surface resulting in plasma generation. This would ensure there are no extraneous effects being generated from longer exposure times on the surface of the specimen.

7 Summary

This chapter summarizes the events of this thesis. Patterning of a cylindrical specimen has been known to be a difficult task, however, with the correct system; this process can be simplified to a typical two dimensional machining process. The parametric studies into various processing speeds, powers and frequencies depict results that can then be adapted to a particular application. Although manual intervention was required to fully pattern the circumference of a cylinder, with the correct upgrade to the rotational access, the scaling of the code is an effortless step to full scale patterning. Processing to the limits of the experimental setup proved the concept that it was possible and scaling the code up is a mere formality.

Some refinement of the rolling process would be necessary before large scale patterning can begin, but the experiments carried out was a general proof of concept that a pattern can be transferred from a laser machined, cylindrical surface, onto a flat, flexible polymer.

The processing of a sample with an unknown composition is also possible once parametric analysis has been carried out. This analysis derived the ideal system parameters for the patterning process and illustrated that a visible pattern could be machined onto the surface of the aforementioned compound without destroying its integrity.

It was also shown that the introduction of a compressed gas to the laser-material interaction location would result in the removal of plasma build up. This removal would increase the efficiency of the machining process and decrease the power required to obtain a specific result. However, in analyzing plasma generation on a more fundamental level, it is now evident that using the correct experimental setup and system parameters, plasma generation may be reoriented in a direction other than that of the incident laser beam. This would remove the additional cost of the compressed gas while still increasing the efficiency of the patterning process. Finally, laser induced breakdown spectroscopy was used to show that based on the spectral emission of a material, the elementary makeup of said material can be obtained.

References

[1]Narendra B dahotre, Sandip P. Harimkar: "Laser Fabrication and machining of Materials" [Book: Springer, Knoxville, 2008]
[2]Eichler, J., Eichler H. J.: :Laser, Bauformen, Strahlfuhrung, Anwendungen" [Book: Springer, Berlin, 6 Auflage 2006]
[3] Marshall, Gerald F.: "Handbook of Optical and Laser Scanning" [Book: Marcel Dekker, New York 2004]
[4] W. M. Steen: "Laser Material Processing" [Book: Springer, Knoxville, 1991]
[5] Duley, W. W.: "Laser processing and analysis of Materials" [Book: Springer, 1983
[6] Shane M. Eaton, Haiblin Zhang, Peter R. Herman, Fumiyo Yoshino, Lawrence Shah, James Bovatsek, Alan Y. Arai: " Heat accumulation effects in femtosecond laser-written waveguides with variable repletion rate" Optics Express Vol. 13 No. 12, June 2005
[7] C. Zhu, Y. G. Zhang, A. Z. Li, Y. L. Zheng, "Comparison of thermal characteristics of antimonide and phosphide MQW lasers" Semiconductor Science and Technology Vol. 20 No. 6, March 2005
[8]Laser Zentrum Hannover: "Microtechnology Presentation" [URL: http://www.laser-zentrumhannover.de/en/fields_of_work/material_processing/microtechnology/Microtechnology_LZH_2006-download.pdf]
[9]D. J. Hwang, H.J. Jeon, C.P. Grigoropolous, J. Yoo, R.E. Russo, Applied Physics Lett. 91, 251118 (2007)
[10]D. J. Hwang, H.J. Jeon, C.P. Grigoropolous, J. Yoo, R.E. Russo, Journal of Applied Physics, 104, 013110 (2008)
[11]Laser Induced Breakdown Spectroscopy, [URL: http://www.appliedspectra.com/technology/LIBS.html]
[12]R.E. Russo, X.L. Mao, H.C. Liu, J.H. Yoo, S.S. Mao: Appl. Phys. A 69 [Suppl.], S887–S894 (1999)
[13]Rockwell Automation MERS-50 Datasheet, [URL: http://www.rockwellautomation.com/anorad/downloads/pdf/MER-50RevA72128.pdf]
[14]Newport 420 Translational Stage [URL: http://eolsurplus.com/images/Newport420.jpg]
[15]Rockwell Automation RSLogix5000 Summary [URL: http://www.rockwellautomation.com/rockwellsoftware/design/rslogix5000/]
[16] Allen-Bradley Logix5000 Controllers System Reference, Publication 1756-QR107C-EN-P-June 2005
[17] Allen- Bradley Logix5000 Controller Design Consideration Reference Manual, Publication 1756-RM094B-EN-P-August 2005
[18] Allen-Bradley Logix5000 Controller Quick Start Guide, Publication 1756-QS001C-EN-P-May 2005
[19] Allen-Bradley Logix5000 Controllers Motion Instructions Reference Manual, Publication 1756-RM-007G-EN-P-May 2005
[20] Allen-Bradley ControlLogix Analog I/O Modules User Manual, Publication 1756-UM009B-EN-P-June 2003
[21]Axsys Technologies Advanced Information Systems, [URL: http://pdf.directindustry.com/pdf/axsys-technologies/lasertrac-autofocus/36088-64462.html]
[22]Matthew Quigley "Rapid Laser Scanning Based Surface Texturing for Energy Applications" May 2012
[23] D.J. Hwang, S.H. Ahn, C.P. Grigoropolous, H.K. Pahk: P2/P3 CIGS Scribing Improvement by Gas Injection
[24]Peax 2.0, Systematix: [URL: http://www.systematix.se/products/peax/]
[25]Salento University "Laser-Material Interaction" [URL: <http://www.fisica.unisalento.it/Int_Laser-Materia/page.php?page=research_activities/by_libs]
[26] Advanced Materials Processing Laboratory, Northwestern University: "Deformation-Based Texturing Methods" Journal of Manufacturing Science and Engineering Volume 133, Dec 2011
[27]Eung-sug Lee, Jun-ho Jeong, Young-sukSim, Ki-don Kim, Dae-geun Choi, Jun-hyuk Choi: "High-Throughput step-and-repeat UV-nanoimprint Lithography" Current Applied Physics March 2006
[28] Se Hyun Ahn, L. Jay Guo: "Large-Area Roll-to-Roll and Roll-To-Plate Nanoimprint lithography: a Step toward High-Throughput Applications of Continuous Nanoimprinting" American Chemical Society Vol. 3 No. 8, 2009
[29]SooYeon Park, KeeBong Choi, GeeHong Kim, JaeJong Lee: "Nanoscale patterning with the double-layered soft cylindrical stamps by means of UV-nanoimprint Lithography" Microelectric Engineering December 2008
[30] Tzu-Chien Huang, Jing-Tang Wu, Sen-Yeu Yang, Po-Hsun Huang, Shuo-Hung Chang: "Direct Fabrication of microstructures on metal roller using stepped rotating lithography and electroless nickel plating" Microelectronic Engineering 615-618, January 2009